DZNE
Deutsches Zentrum für
Neurodegenerative Erkrankungen
in der Helmholtz-Gemeinschaft

TECHNISCHE
UNIVERSITÄT
MÜNCHEN

How Stimulus-Responsive Extracellular Vesicle Release is Regulated and Associated to Lewy Body Disease

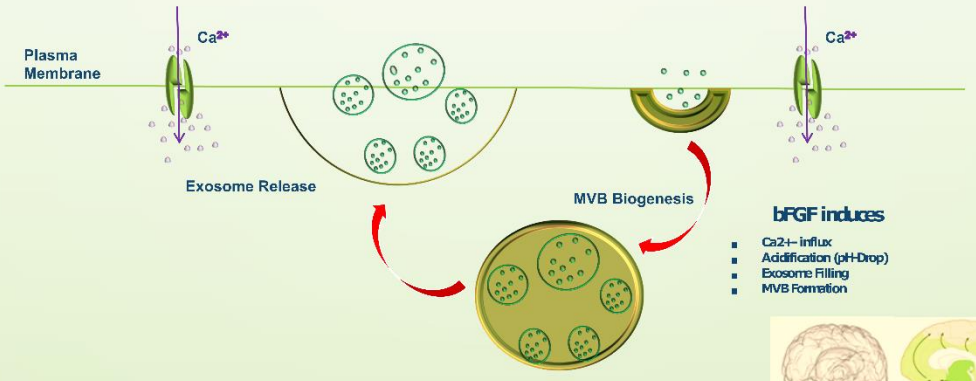

Rohit Kumar

Fakultät für Medizin der Technischen Universität München

How Stimulus-responsive Extracellular Vesicle Release is Regulated and Associated to Lewy body disease.

Rohit Kumar

Vollständiger Abdruck der von der Fakultät für Medizin der Technischen Universität München zur Erlangung des akademischen Grades eines Doktors der Naturwissenschaften (Dr. rer. nat.) genehmigten Dissertation.

Vorsitzende/-r: Prof. Dr. Mikael Simons

Prüfende/-r der Dissertation:

1. Prof. Dr. Paul Lingor

2. Prof. Dr. Andreas Bausch

Die Dissertation wurde am 14.09.2020 bei der Technischen Universität München eingereicht und durch die Fakultät für Medizin am 16.02.2021 angenommen.

Anhang I

Eidesstattliche Erklärung

Ich erkläre an Eides statt, dass ich die bei der Einrichtung,
Fakultät für Medizin der Technischen Universität München

der TUM zur Promotionsprüfung vorgelegte Arbeit mit dem Titel:

How Stimulus-responsive Extracellular Vesicle Release is Regulated and Associated to Lewy body disease.

in Fakultät für Medizin, Neurologischen Klinik der TUM und Lehrstuhl für Translationale Neurodegeneration am Deutschen Zentrum für Neurodegenerative Erkrankungen (DZNE), TUM Medical Graduate Center (MGC) unter der Anleitung und Betreuung durch: Technischen Universität München ohne sonstige Hilfe erstellt und bei der Abfassung nur die gemäß § 6 Ab. 6 und 7 Satz 2 angebotenen Hilfsmittel benutzt habe.

☒ Ich habe keine Organisation eingeschaltet, die gegen Entgelt Betreuerinnen und Betreuer für die Anfertigung von Dissertationen sucht, oder die mir obliegenden Pflichten hinsichtlich der Prüfungsleistungen für mich ganz oder teilweise erledigt.

☒ Ich habe die Dissertation in dieser oder ähnlicher Form in keinem anderen Prüfungsverfahren als Prüfungsleistung vorgelegt.

☐ Die vollständige Dissertation wurde in _____ veröffentlicht. Die promotionsführende Einrichtung

_____

hat der Veröffentlichung zugestimmt.

☒ Ich habe den angestrebten Doktorgrad noch nicht erworben und bin nicht in einem früheren Promotionsverfahren für den angestrebten Doktorgrad endgültig gescheitert.

☐ Ich habe bereits am _____ bei der Fakultät für _____

_____

der Hochschule _____

unter Vorlage einer Dissertation mit dem Thema _____

_____

die Zulassung zur Promotion beantragt mit dem Ergebnis: _____

_____

Die öffentlich zugängliche Promotionsordnung der TUM ist mir bekannt, insbesondere habe ich die Bedeutung von § 28 (Nichtigkeit der Promotion) und § 29 (Entzug des Doktorgrades) zur Kenntnis genommen. Ich bin mir der Konsequenzen einer falschen Eidesstattlichen Erklärung bewusst.

Mit der Aufnahme meiner personenbezogenen Daten in die Alumni-Datei bei der TUM bin ich

☒ einverstanden, ☐ nicht einverstanden.

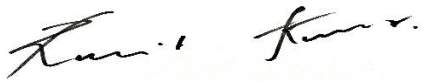

Rohit Kumar, München, Germany.

Declaration:

This thesis is written and compiled independently and with no other source or aid than quoted.

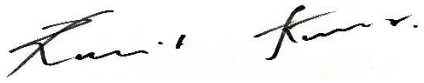

Rohit Kumar
München, Germany.

"That the death-response is an excitatory phenomenon, is seen from the fact that any circumstance which lowers physiological activity lowers the death-point also."

- (J.C. Bose, 1907)

"Until the characteristics of 1/f noise are better studied, then, it is difficult to separate out contributions from transport noise to those made by gating of channels."

- (E. Neher & C.F.Stevens, 1977)

***D**edicated to an honest and transparent scientist.*

Publications:

Aspects of this work are published in:

1. Kumar, R., et al., *Fibroblast Growth Factor 2-Mediated Regulation of Neuronal Exosome Release Depends on VAMP3/Cellubrevin in Hippocampal Neurons*. Advanced Science, 2020: p. 1902372.

2. Kumar, R., et al., *Basic Fibroblast Growth Factor 2-induced Proteome Changes Endorse Lewy Body Pathology in Hippocampal Neurons*. iScience, 2020: p. 101349.

Contents

List of Figures:

List of Tables:

Zusammenfassung

Hintergrund: Lewy-Körperchen-Erkrankungen wie die Demenz mit Lewy-Körperchen (LKs) und die Parkinson-Krankheit mit Demenz (PDD) sind durch das allmähliche Auftreten von LK im Gehrin gekennzeichnet. Daher ist ein Verständnis des molekularen und zellulären Mechanismus erforderlich, der die Bildung von LK begünstigt. LK finden sich in verschiedenen Zelltypen des Nervensystems. Der Hauptbestandteil dieser Aggregate ist das Protein Alpha-Synuclein (α-Syn). α-Syn wird zusammen mit anderen Biomaterialien in extrazellulären Vesikeln (EVs) freigesetzt. Diese Vesikel können Proteine über weite Strecken transportieren und haben somit Auswirkungen auf die Aussaat und Ausbreitung der Krankheitspathologie.

Methoden: Mithilfe von Patch-Clamp-Elektrophysiologie und simultaner molekularer Echtzeit-Bildgebung haben wir die Kinetik der EV-Freisetzung in Hippocampus-Neuronen bestimmt. Wir haben ein pH-sensitives, molekulares Tag entwickelt, das speziell auf Membranen von EVs vorkommt und diese Methode angewendet, um Stimulus-induzierte MVB-PM-Fusion zu untersuchen sowie deren Kinetik und Regulatoren solcher Fusionsereignisse zu bestimmen. Zusätzlich haben wir den EV-Gehalt durch Massenspektrometrie (MS) analysiert. Die MS-Ergebnisse wurden dann einer bioinformatischen Analyse unterzogen, um LBP-bezogene molekulare Wechselwirkungen zu identifizieren.

Ergebnisse: Unsere Ergebnisse zeigen die Unterscheide in der Freisetzung synaptischer Neurotransmitterim Vergleich zu der Freisetzung von EVs und legten nahe, dass es sich um eine relativ langsame Form der Kommunikation zwischen den zellulären Komponenten des Nervensystems handelt. Wir fanden heraus, dass die Rate von Fusionsereignissen mit Hochfrequenzstimulation (HFS) weiter verstärkt werden kann. Unsere Daten legen ferner nahe, dass die Stimulus-induzierte Fusion verstärkt wird, wenn sie durch eine Behandlung mit neurotrophen Faktoren (NTF) ergänzt wird, mit der höchsten Erfolgsrate bei mit basischem Fibroblastenwachstumsfaktor (bFGF) behandelten Neuronen. Zusätzlich haben wir bestätigt, dass die bFGF-verstärkte MVB-PM-Fusion und letztendlich die EV-Freisetzung teilweise über Tyrosinkinaseaktivität vermittelt wird und calcium-abhängig ist. Wir beobachteten eine Anreicherung des Vesikel-assoziierten Membranproteins 3 (VAMP3) / Cellubrevin in EVs aus bFGF-behandelten Zellen und stellten fest, dass diese Protein die EV-Freisetzung kontrolliert. Eine weitere Analyse sowohl des Zelllysats (CL) als auch des EV-Proteoms zeigte die durch bFGF induzierte differentielle Expression. Insgesamt wurden 5314 CL-Proteine und 2258 EV-Proteine mit einer signifikanten differentiellen Expression gefunden. Wir führten eine gewichtete Protein-Co-Expressions-Analyse (WPCNA) zusammen mit Ähnlichkeitsanalysen an diesen Proteinen durch, um die LBP-assoziierten Proteine spezifisch zu definieren. Dies hat zur Identifizierung molekularer Wechselwirkungen zwischen den LBP-verknüpften Rezeptoren, Ionenkanälen, RNA-bindenden Proteinen und α-Syn-Interaktionspartnern in verschiedenen Hirnregionen geführt.
Schlussfolgerung: Zusammenfassend unterstützen unsere Ergebnisse das Verständnis der EV-Freisetzung und ihrer NTF-vermittelten Regulation in gesunden Neuronen sowie bei der Lewy-Pathologie.

Abstract

Background: Lewy body (LB) disorders, such as dementia with LBs and Parkinson's disease with dementia (PDD) are characterized by their pathological hallmark, i.e., the gradual appearance of LBs. Therefore, a deep understanding of the molecular and cellular mechanism, favoring the formation of LBs is required, although these are not well understood at present. These proteinaceous inclusions are found in different cell types of the nervous system. The key constituent protein-component of such inclusions is the protein alpha-synuclein (α-Syn). α-Syn along with other bio-active material gets secreted as content of extracellular vesicles (EVs). These vesicles not only excrete bioactive material but are also able to transport it to distant sites, and therefore have implications for disease pathology seeding and spreading.
Methods: Using patch-clamp electrophysiology techniques along with simultaneous real-time molecular imaging, we determined the kinetics of EV-release in hippocampal neurons. We designed a pH-sensitive molecular tag, targeted specifically to membranes of EVs and applied this method to study stimulus-responsive MVB-PM fusion, in order to determine the kinetics, specific stimuli and regulators of such fusion events. In addition, we analyzed the EV-content by performing mass spectrometry (MS) analysis. The MS results were then subjected to a bioinformatic analysis to identify LBP-related molecular interactions.
Results: Our results clearly segregated synaptic neurotransmitter release from EV-release and suggested that it is a relatively slow form of communication among the cellular components of the nervous system. We found that the rate of fusion events can be amplified further with high-frequency-stimulation (HFS) but with an abate rate of success. Our data further suggest that stimulus responsive fusion is enhanced when supplemented by neurotrophic factor (NTF) treatment, with the highest success rate in basic fibroblast growth factor (bFGF)-treated neurons. In addition, we confirmed that bFGF-enhanced MVB-PM fusion and ultimately the EV-release is partially mediated via tyrosine kinase activity and is calcium dependent. We observed an enrichment of the vesicle-associated membrane protein 3 (VAMP3)/cellubrevin in bFGF-facilitated EVs and find the levels of this protein exerting a control over EV-release. The further analysis of both cell lysate (CL) and EV proteome delineated the differential expression induced by bFGF. A total number of 5314 CL-proteins and 2258 EV-proteins were found with a significant differential expression. We performed a weighted-protein-co-expression-analysis (WPCNA) along with similarity analyses on these proteins to specifically define the LBP-associated proteins. This has resulted in the identification of molecular interactions among the LBP linked receptors, ion-channels, RNA-binding proteins and α-Syn interaction partners in different brain regions.
Conclusion: In summary, our results support the understanding of EV release and its NTF-mediated regulation in healthy neurons as well as in LBP-associated conditions.

Foreword

Over the years the global burden of Lewy body diseases (LBDs) such as Parkinson's disease (PD) has increased and is predicted to increase in the coming years as a result of an aging society. [1]. It has been observed that the presence of Lewy bodies (LBs) is associated with declined cognition in patients with dementia e.g. in PD patients with dementia [2]. Clinically, the appearance of LBs is correlated with disease symptoms and stages indicating disease progression [3]. Therefore, a comprehensive understanding of the formation of such proteinaceous inclusions is required. Most of the postmortem studies from patients reveal the consequential aftermath of already formed inclusions but in order to develop comprehensive therapies for alive patients, it is important to understand the physiological environment that endorses such pathology. The main content of LBs are misfolded forms of pathological α-Syn which could travel from one part of the nervous system to another (e.g., the cellular components or from one brain region to another) propagating the disease pathology further and hence facilitating the progression of the disease. The specific populations of tiny vesicles known as exosomes carry such pathogenic forms of disease concomitant proteins and these vesicles appear to be associated with the clearance mechanism of α-Syn. Therefore, understanding the molecular mechanisms and the machinery responsible for their release and possible disease-linked interactions of the protein content carried in these vesicles would enhance the overall understanding of disease pathophysiology. Moreover, the biogenesis of exosomes is cell-type specific, so that the content carried by them could actually serve as the footprint of physiological changes that occur in response to certain triggers, thus allowing to determine the physiological state of degeneration-prone neurons. In the long run studies can be specifically focused on the effects of pathological proteins or compounds triggering the release of such vesicular populations which can then be analyzed for their contents. All in all, to make use of potentials of exosomes for diagnostic and therapeutic purposes one needs to first develop a basic understanding of them. Furthermore, the exosomal content internalization at recipient site after their release that could facilitate the seeding of the pathology in new cells or brain regions; for which it is evident that the actual story cues, right from the beginning of whole release cycle at the plasma membrane!

In such an endeavor it becomes important to understand the molecular factors controlling EV release. Such factors may operate through the receptors at plasma membrane to either induce MVB-generation or stimulus-induced plasma membrane fusion of the MVBs. In biochemical experiments a precise control over the temporal and spatial resolution of such triggers and their corresponding responses is overlooked, this contributes to a wide grey zone in the understanding of the true nature of any possible stimuli that

could lead to exosomal secretion or let alone the attempt of exploring the specific therapeutic potentials of such triggers.

The studies with unimolecular focus overpass the multi-variable associations of a neurophysiological environment, where multiple molecules are expected to be in action to result neural function or dysfunction. Investigating neuronal excitability provides insight to neuronal function in health and disease. Though restricted by the current availability of required technology, electrophysiology along with opto/chemo-genetic techniques allows us to exert a proper control and have a stringent experimental design to investigate stimulus-responsive EV-release in real time. Complimented by the state-of-art imaging techniques and astute computational analysis we can possibly one day understand the intricacies of nervous system function in a diseased state.

List of Abbreviations:

AD: Alzheimer disease
4-AP: 4-Aminopyridin
α-Syn: Alpha-synuclein
BAPTA-AM:1, 2-Bis (2-aminophenoxy) ethane-N, N, N', N'-tetraacetic acid tetrakis (acetoxymethyl ester)
BDNF: Brain derived neurotrophic factor
bFGF: Basic fibroblast growth factor
bFGFR: bFGF-receptor
BIC: Bicucullin
CAV1: Caveolin-1
CL: Cell lysate
C*m*: Membrane capacitance
CM: Co-expression module
CN: Composite Network
CNS: Central nervous system
DA: Dopaminergic neurons
DBS: Deep brain stimulation
DEPs: Differentially expressed proteins
DIV: Days *in vitro*
DLBs: Dementia with lewy bodies
DMEM: Dulbecco's modified eagle medium
EGTA: Ethylene glycol-bis (β-aminoethyl ether)-N, N, N′, N′-tetraacetic acid
EM: Electron microscopy
ENS: Enteric nervous system
ESCRT: Endosomal sorting complex required for transport
EV: Extracellular vesicle
EVs: Extracellular vesicles
FDR: False discovery rate
FGFs: Fibroblast growth factors
GDNF: Glial derived neurotrophic factor
GEN: Genistein
GFP: Green florescent protein
HBSS: Hank's Balanced Salt Solution
HEPES: 4-(2-hydroxyethyl)-1-piperazineethanesulfonic acid
HFS: High frequency stimulation
iLB: incidental Lewy body
KD: Knock down
KO: Knock-out
KEGG: Kyoto encyclopedia of genes and genomes
LB: Lewy bodies

LN: Lewy neurites
LBP: Lewy body pathophysiology
LFQ: Label-free quantification
LRBPs: LBP related RNA binding proteins
LUHMES: Lund human mesencephalic cells
M_{CL}: Cell-lysate modules
M_{EV}: Extracellular vesicle modules
MPTP: 1-Methyl-4-phenyl-1, 2, 3, 6-tetrahydropyridine
mRNA: messenger Ribonucleic acid
MS: Mass spectrometry
MVBs: Multivesicular bodies
NGF: Nerve growth factor
NSF: N-ethylmaleimide sensitive factor
NTF: Neurotrophic factor
NT-3: Neurotrophin-3
NTA: Nano-particle tracking analysis
PBS: Phosphate-buffered saline
PCA: Principal Component analysis
PD: Parkinson's disease
PDD: PD with dementia
PFA: Paraformaldehyde
PFF: α-Syn preformed fibrils
PM: Plasma membrane
PPi: Protein-protein interactions
RIPA buffer: Radio-immuno-precipitation-assay buffer
RNA: Ribonucleic acid
RRP: Readily releasable pool
siRNA: small interfering RNA
SN: Substance nigra
SNARE: SNAP receptor
SNAP: Soluble NSF attachment protein
SNc: Substantia par nigra compacta
sPD: sporadic parkinson's disease
TSG101: Tumor susceptibility 101
v-SNARE: Vesicle-SNARE
VAMP2: vesicle associated membrane protein 2
VAMP3: vesicle associated membrane protein 3
Veh: Vehicle
VPS: Vacuolar protein sorting
WGCNA: Weighted gene co-expression network analysis
WPCNA: Weighted protein co-expression network analysis
WT: Wild type

1. Introduction

1.1. Lewy bodies and Parkinson's disease

All forms of Parkinson's disease (PD), except juvenile-onset autosomal recessive forms, exhibit Lewy bodies (LBs) [4, 5]. Along with the gradual appearance of protein aggregates known as LBs, the characteristic feature of this progressive neurodegenerative disorder is the loss of dopaminergic neurons (DA) in the substantia nigra pars compacta (SNc) region of the brain [6]. As per Braak et al. LB-pathology (LBP) first starts either in the olfactory bulb (OB) or the dorsal motor nucleus of the vagus (DMV) in the caudal medulla because they presumed that axons in these areas extend to the body surface and are exposed to a pathogen or infectious agent that may cause LBP, which would be retrogradely transferred to neighboring neurons through synaptic connections reaching ultimately to the SNc and initiating the loss of neurons [7, 8]. It is further debatable whether or not LBs are a consequence of PD or vice versa because their gradual appearance does not correlate well with the Braak staging proposed for sporadic form of PD (sPD) e.g. PD cases with LBs confined to amygdala region or the dementia cases with LB (DLBs) where there is no proper staging available [3]. Hence, all conditions with LBs inevitably secure a place under the spectrum of LB-diseases. **Figure** 1 summarized the key PD pathology features.

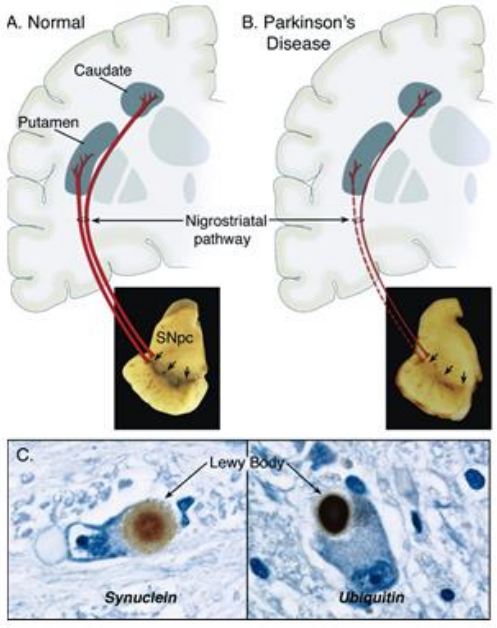

Figure 1. Parkinson's disease (PD) pathology: The characteristics of PD pathology are a loss of neurons in the substantia nigra pars compacta (SNc) and appearance of LBs. A) and B) depict the nigrostriatal pathways of healthy and PD patient with a characteristic loss of neurons in SNc region. C) The anatomical hallmark of PD pathology is a gradual appearance of Lewy bodies (LBs). These proteinaceous inclusions are comprised of proteins like Synuclein and Ubiquitin (Adapted from [6]).

1.2. Lewy bodies

In 1912, Fritz Jacob Heinrich Lewy first observed eosinophilic inclusion bodies (aggregates) in certain brain nuclei, that got the name LBs in his honor [9]. LBs have the protein α-Syn as their main component and have been heterogeneously spotted at diverse locations at cellular and organ levels e.g. found both intra- and extracellularly [10].

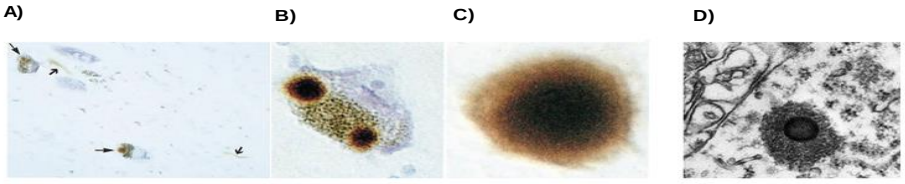

Figure 2. Lewy bodies (LBs) show a multifaceted diversity. Panel A) shows an alpha-synuclein (α-Syn) positive LB in PD patients. B) shows a neuronal intracellular α-Syn rich inclusions C) α-Syn-enriched extracellular inclusion in PD patients and D) depicts a cytoplasmic inclusion in a rotenone mouse model. (A-C are adapted from [10]; D adapted from [11]).

Therefore, it is central to examine the factors responsible for the onset of LB formation, seeding and further propagation to reveal their pathophysiological functions. These inclusions vary in terms of their composition, sizes, shapes, numbers, and their sensitivity to antibodies in a given incidental observation per sample (**Figure 2**). Initially, α-Syn has been proposed to be the central component of LBs from the strong immunostaining results in brainstem and cortical samples from both sPD and DLB cases and hence, the term "synucleiopathies" also sometimes resonates under the spectrum of LB-disease [10]. Furthermore, environmental factors such as exposure to chemicals are found associated to the formation of the proteinaceous inclusions in PD patients [12]. These chemical associations have led the way to, many attempts to create research models for experimentation and diagnostics. **Figure 2D** shows a LB in the rotenone model [11]. However, there are discrepancies involved in developing such research models because all the models do not depict the characteristic feature of LB formation e.g. 1-Methyl-4-phenyl-1,2,3,6-tetrahydropyridine (MPTP)-based models show the characteristic loss of SNc neurons but no LB formation [13, 14] .

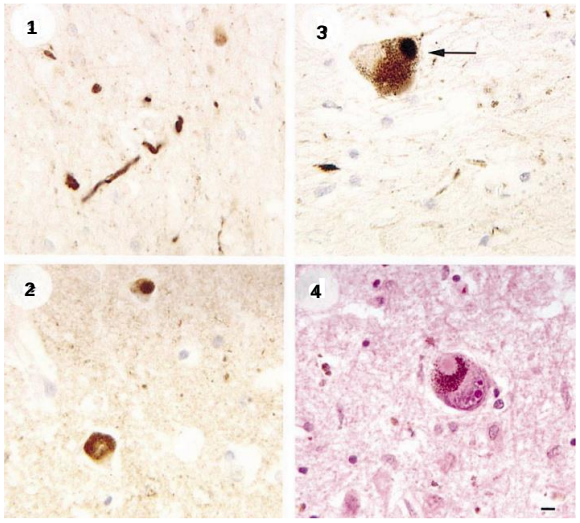

Figure 3. LBs appearance in various components of the nervous system accounts for LB pathology spread. 1) α-Syn positive Lewy neurites found in SNc neurons of PD patients 2) Two α-synuclein-positive LBs in the cingulate cortex 3) PD α-Syn positive Lewy body (arrow) in a pigmented nerve cell of the SNc 4) Haematoxylin adenosine-stained SNc tissue with a pigmented nerve cell containing a LB. (Adapted from [10]).

Some of the key assertions about LB formation and their further transformation to structures like Lewy neurites (LN) are drawn from the possibilities of structural modifications of its key component α-Syn. Three isoforms of Synuclein were first discovered in *Torpedo californica* using antibody based detection of sizes 17.5, 18.5 and 20 kDa; out of these synuclein forms, the isoform alpha at 17.5 KDa was most prevalent [15]. The structural prediction of this protein from cDNA analysis rejected the idea that the protein has an enzymatic function and therefore restrained to observe its roles either as structural or regulatory component in a physiological setting[15]. α-Syn is a 140 amino acid-long protein and is found in soluble and membrane bound states [16]. It has been observed that native α-Syn exists as an unstructured monomeric form which retains the tendency to aggregate in a time-dependent manner, possibly as a consequence of physiological factors [17]. It has been found that the higher order multimeric forms (e.g. α-helical form) of α-Syn exists more rapidly in a membrane bound state such as bound to vesicle membranes [18]. Promotion of multimeric aggregation further depends on the composition of vesicle membranes as studies suggest that these aggregations are regulated via the presence of unsaturated fatty acid in vesicle membrane [19, 20]. Moreover it has been confirmed now through *in vivo* studies that the multimeric forms of α-Syn are toxic in nature and might be able to disrupt the membranes [21]. Besides, membrane-bound α-Syn multimeric forms are found to disrupt the regular vesicular function such as vesicle trafficking and membrane transport etc. therefore, proposes its role as a stabilizer for proper vesicular interactions [22]. These tightly membrane-bound oligomeric (multimeric) forms can then further permeabilize the vesicular membrane and hence can propagate to other neurons or cells in its proto-

fibrillary or fibrillary form [23]. Such filamentous forms of LBs are consequently observed in PD pathology as LN and can be detected through their immuno-reactivity using antibodies as multiple aggregations in brain regions (**Figure** 3).

1.3. Lewy body pathology and Hippocampus

The hippocampus is mainly involved and responsible for memory function [24, 25]. But neuronal degeneration in the hippocampal CA2/3-region is associated with LB-pathology and the neurites of these regions with LBs appears to be different than the ones found in Alzheimer disease (AD) pathology [26]. PD patients with dementia (PDD) show a correlation with presence of LBs and LNs in the hippocampal CA2 region, thus highlighting the importance of the hippocampus in LBP [27, 28]. Immunohistochemistry-based studies confirm a sparse, restricted distribution of LN in the CA2 region for normal PD cases but a sever LB/LN distribution extends to other hippocampal regions and selectively cause the loss of cholinergic neuronal activity via α-Syn aggregation [29]. Furthermore, the presence of all Synuclein strains (α, β and γ) in the PD hippocampus with axonal pathology strengthen the possibility of Synuclein's role as key precursor molecule for aggregation led LB-formation [30]. The role of LBP in PDD is also emphasized by the findings of co-localization of LNs with cholinergic fibers in the CA2-subfield [31]. Moreover, outcomes of neuropathological investigations indicate that α-Syn could be more liable for the memory-related impairment along with a major role of the CA1-region even though CA2 is the most affected region during PDD [32]. Therefore, understanding of LBP in the hippocampus might be more pertinent to resolve the pathophysiology of memory retrieval impairment in PD.

1.4. Lewy body pathology propagation and extracellular vesicles

The successive appearance of LBs in various CNS and ENS regions acts as precursors for the progression of such a pathology and many attempts were made to correctly describe the stages of LB pathology [33-35]. The presence of LBs in transplanted fetal mesencephalic dopaminergic and nigral neurons, many years after the surgery advocate their transmission from the host neurons [36, 37]. The neural transmission of LBs was experimentally demonstrated in animal models via the formation and propagation of LB/LN after introducing extracted PD/LB-α-Syn from patients either subcutaneously, or via the gut or the olfactory bulb [38-40]. The missing LB-formation in the absence of α-Syn demonstrated a central role of this protein in LB propagation [41]. Moreover, single nigral or cerebral inoculations of α-Syn can initiate a progressive neurodegeneration [42-44].

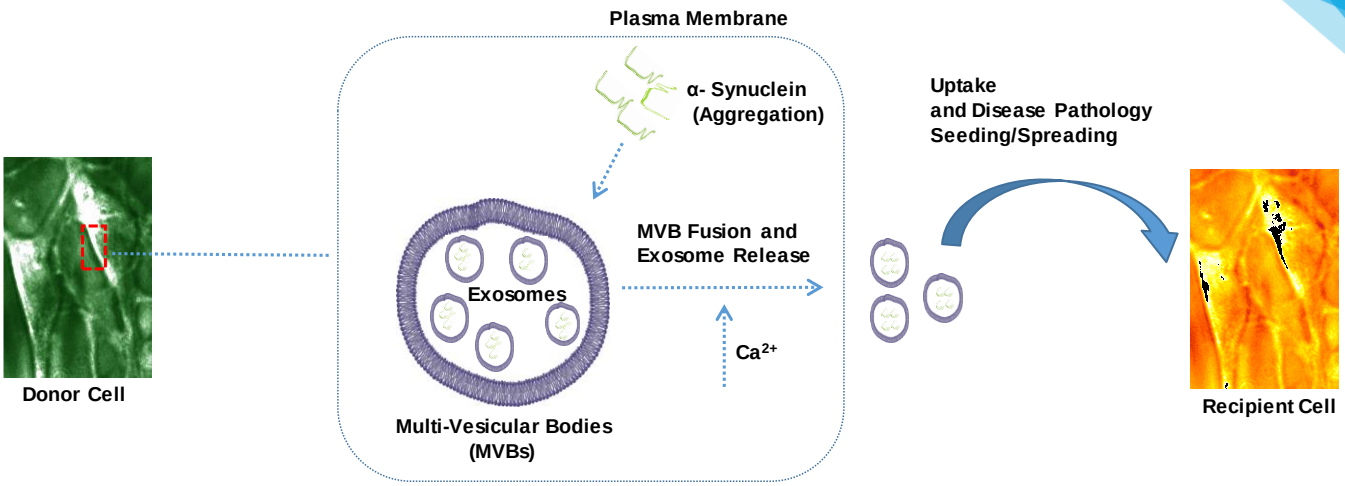

Figure 4. Spreading model of LB pathology. Diagram illustrating a donor-recipient model for an exchange of pathological proteins and their aggregates in vesicular bodies. The misfolded proteins or components of proteinaceous inclusions get transferred from one neuron to another, when vesicular bodies get released to the extracellular environments e.g., during an event like MVB-PM fusion. Such events can be stimulated via external triggers.

Aforementioned findings may establish α-Syn as a pioneer molecule for LB-formation which might be governed by various strains of this protein [45], although the trans-neuronal transfer of pathology was vaguely explained in these studies. It has been shown that extra-cellular vesicles (EVs), such as exosomes, facilitate intercellular communications[46]. Studies, reporting α-Syn aggregation after receiving extracted exosomes from patients of DLBs has proposed a donor-recipient model of disease propagation [47]. This model suggests that a recipient cell could get inoculated by a pathological precursor molecule and disease progression could then begin at a new sight (**Figure 4**). The pathology progression could then also be accompanied by the cell's intrinsic autonomous physiological state or by other molecular protagonists [48]. PD patients are reported with differential exosomal populations where, the expression levels of associated vesicular proteins were found to be characteristically distinct [49]. The fact that exosomes can speed-up the α-Syn aggregation affirms their role not only in spreading but also for seeding of the LB pathology [50]. Post-translational modifications guide the α-Syn sequestering to exosomes by interacting with members of the endosomal sorting complex required for transport (ESCRT) [51]. It has been shown that α-Syn can disrupt ESCRT function and enhance the extracellular release of the exosomes [52, 53] .

1.5. Extracellular vesicles

G-force sedimentation based experiments indicated two sets of vesicular populations which are now termed as ectosomes and exosomes[54]. Ectosomes are directly budding out of the plasma membrane into the extracellular space, whereas exosomes are of endosomal origin and gets released after the fusion of MVBs to the PM; these vesicles were first observed in a reticulocytes (**Figure 5A**; adapted from [55]). MVBs are present in almost all cell types and release exosomes to the extra cellular environment [56]; hippocampal MVBs are shown in **Figure 5B**.

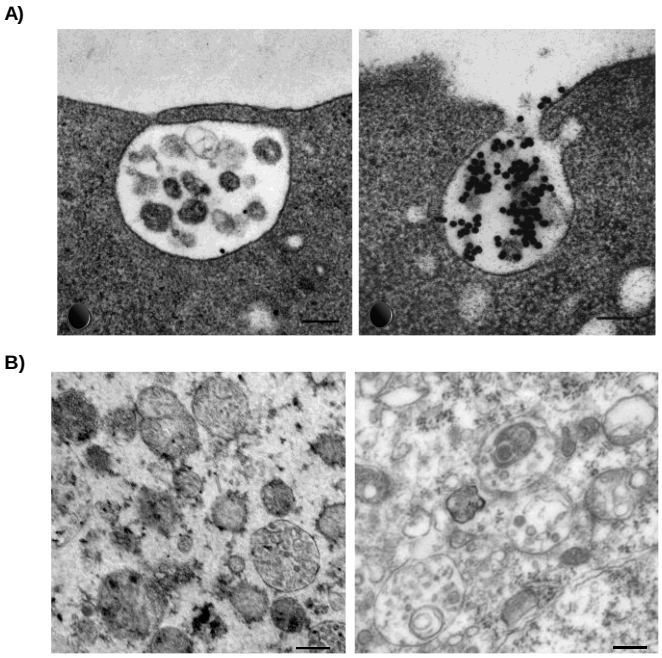

Figure 5. Neuronal multivesicular bodies and exosomes. A) Photomicrograph from electron microscopy (EM) illustrating an MVB filled with tiny vesicular bodies fusing to the plasma membrane (PM) and excreting exosomes to the extracellular space; bar 100nm (adapted from [55]) B) Photomicrograph from EM of hippocampal neurons showing multivesicular bodies (MVBs); bar 250nm.

Exosomes are the unimembraneous bodies of size ranged between ≈ 30 to 200 nm and can be visualized with florescent microscopy by labeling vesicle-specific molecular markers. Certain tetraspanin molecules such as CD9, CD63 and CD81 are specifically enriched in exosomes, thus establishing them as putative biomarkers [57, 58]. These tetraspanins get sorted to exosomes via ESCRT at the early endosome formation of intra-luminal vesicle (ILV) secretion [59]. In addition, the tetraspanin CD63 has been implicated in the ESCRT-independent formation of ILVs in some cell types [60]. The ESCRT is formed by three sub-complexes namely ESCRT-I, ESCRT-II and ESCRT-III [61]. ESCRT-I is a heterotetrameric complex comprised of TSG101 as a key component along with VPS28, VPS37 and MVB12 [62]. This sub-complex physically interacts with ESCRT-II, which is also heterotetrameric having VPS36, VPS22

and two copies of VPS25 as its components [63]. Sub complex-III is comprised of VPS2, VPS20, VPS24 and Snf7 subunits and assembled on endosomes [64]. ESCRT-III acts as a membrane scission complex promoting MVB formation and maturation via inward budding of the tiny vesicular bodies [61, 65]. Apart from their roles in exosome secretion, the components of ESCRT sub complexes are also assumed to take part in the regulation of neurite pruning, morphogenesis of the dendritic arbor and synaptic plasticity via maintenance of neuronal postsynaptic structures by yet to be defined mechanisms [66-68]. These complicated assemblies and features of the secretion pathway are likely to guide the fate of exosomal composition, shape, size and functional heterogeneity when released to the extracellular space via MVB-PM fusion [69]. Initially it was assumed that the fate of a MVB is to fuse with the lysosome, in order to operate autophagic functions of the cell. This view has been certainly challenged by the extracellular release of exosomes [69]. It has been reported that loss of ESCRT-III subunit Snf7 causes the accumulation of autophagosome which could lead to neurodegeneration [70].

The interactions of EVs with target cells corroborate their roles beyond their cells of origin, engaging in intercellular communication either by binding to targeted surfaces and spinning off cellular signals or via getting their content up-taken directly by the cells to modulate the intracellular environment of the target cell. The modus operandi of direct internalization of EV-content involves interactions with clathrin, lipid rafts, formation of caveolae, phagocytosis, and pinocytosis or direct membrane fusion (**Figure 6**). The exosomal-internalization ability is heterogeneous and varies between cell types and different species [71]. It seems logical from exosomal topology to assume that SNARE proteins may not be required for the internalization of EVs into the target cell [71]; however, this idea is too linear for the nonlinear intricacies of neuronal EV-physiology and overlooks possible scenarios such as the fading of small vesicles or pre-shredded SNAREs to inter-neuronal areas, and therefore needs further investigation.

The internalization of EV-content > 1µm in size is termed as phagocytosis. Smaller EVs are internalized via pinocytosis, which can be segregated into clathrin-dependent and -independent uptake from the presence of distinct clathrin-coated pits around the vesicular bodies [72, 73]. Experiments in HeLa cells suggests that EV-uptake can be clathrin independent and is mediated via lipid interactions [74]. Such a lipid raft-based EV-uptake is regulated by the raft associated protein caveolin-1 (CAV1) therefore, all in all suggesting multiple modes of EV uptake [75]. EV-uptake shows target specificity as EVs get taken up selectively based on the cell types [76]. For example, neuronal EVs, released in response to glutamate restricts their internalization only to neurons and depict cellular level preferences [77].

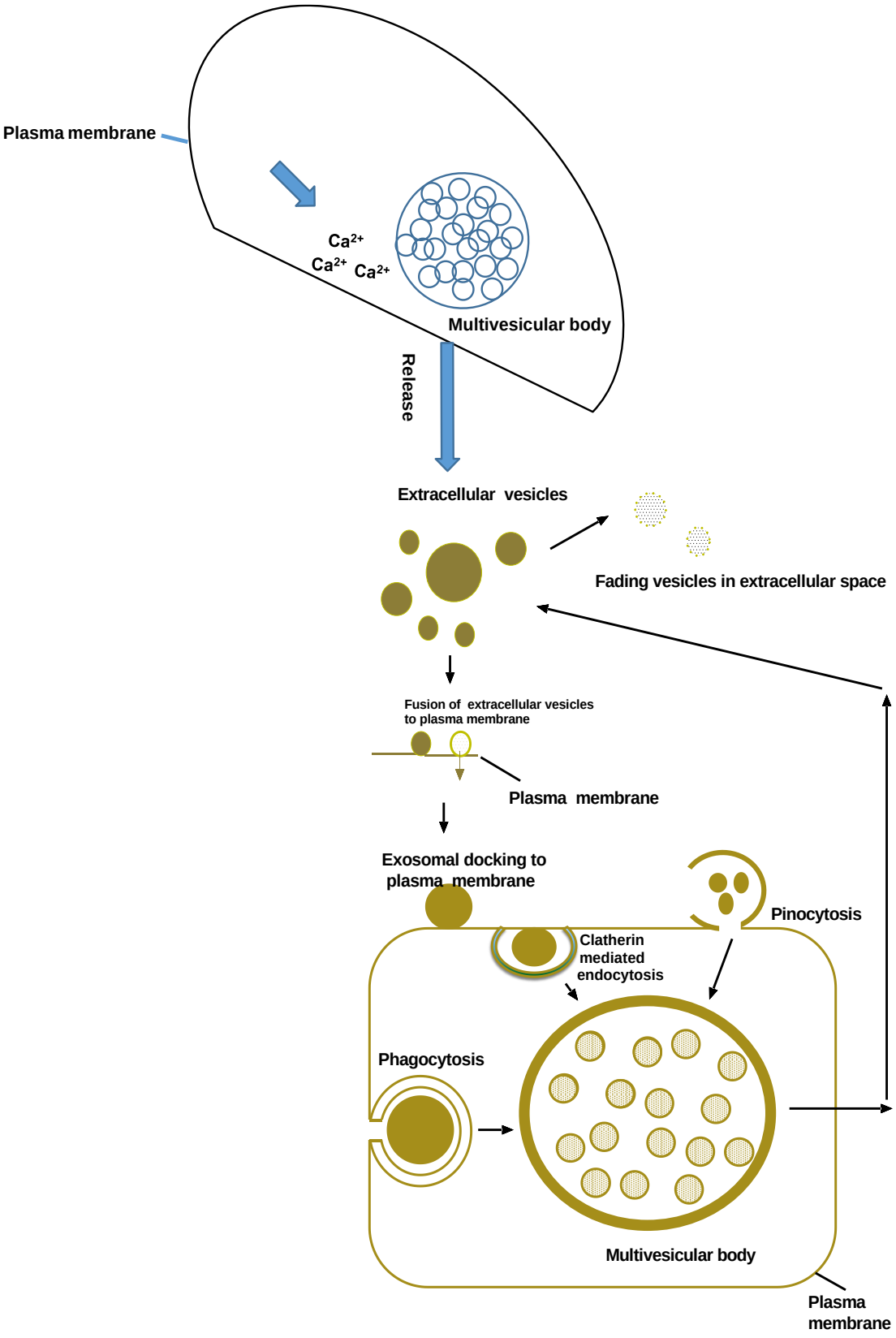

Figure 6. Extracellular vesicle secretion and interactions with target cells. The diagram depicts the intermediating steps of vesicle secretion and interactions.

Therefore, fusion specification and efficiencies of EVs required for uptake are controlled at the cells of their origin and may also be maintained via the physical factors such as pH in their respective microenvironments [78]. EVs are native nanoparticles in biological systems including the nervous system. These vesicles can cross the blood brain barrier, thus highlighting their therapeutic potential. Researches in this direction, got the momentum after a successful delivery of small interfering RNA (siRNA) embedded in exosomes leading to BACE1-knock-down in specific brain regions [79]. *In vivo* studies suggested that small EVs share a very heterogeneous kinetic bio-distribution once injected to the animals in an experimental setting and therefore, are likely to be involved in the regulation of local activity of various organs [80]. It has been shown that the differential compositions of EVs contributes to their heterogeneous kinetics [81] which has implications for the design of any EV-based delivery system. It has also been demonstrated in a PD-mouse model that intranasal ingestion of catalase-filled exosomes led to the prevention of SNc-neuronal loss [82]. The proposition that α-Syn aggregates internalize and get transported in exosomes [83] along with the idea of exploring the therapeutic potentials of EVs therefore nurtures the relevance of knowing the distribution, composition, kinetics, and regulators of these vesicular bodies.

1.6. Neurotrophic factors and Lewy body pathology

Neurotropic factors (NTF) in general are known for their protective effects such as growth and survival of neurons and therefore are investigated for their therapeutic potential in LB diseases [84, 85]. Ever since glial derived neurotrophic factor (GDNF) was found to be selectively protecting the degeneration of dopaminergic neurons (DA) the roles and therapeutic potential of NTF in PD-pathology are explored [86]. Immunohistochemical and mRNA expression studies in hippocampal region from PD and DLB-patients report their reduced abundance of the NTFs BDNF, GDNF, NGF and neurotropin-3 (NT-3) in activated microglia [87]. Conversely, systematic administration of GDNF protected from the loss of SNc neurons in a PD mouse model [88]. Besides these therapeutic aspects, alterations of NTF-levels in PD patients might have their roles in disease diagnostics. Results from the PD patient serum samples, however, showed mixed results with both increased and decreased levels of NTF [89, 90]. Furthermore, a segregation to a PD subtype level correlated reduced levels of BDNF to LBP but the results were limited by the low number of clinical subjects used in the study [89]. A systematic meta-analysis of clinical findings using intracerebral administration of NTF suggests that NTF do not improve the motor symptoms of PD-patients [91]. All in all, such discrepancies can be attributed to factors like disease stage (e.g. onset, late stages corresponding to the appearance of LBs etc.), physiological environment-dependent responses of neurons,

neuronal diversity or subject age used for the clinical studies or the age of animals used as a research model etc. Therefore, as of now, a comprehensive and concrete understanding of NTF's roles and its effects in LBP does not exist and needs further investigation.

1.7. Functional periphery of basic fibroblast growth factor

Fibroblast growth factors (FGFs) are a protein family comprised of 23 members and are involved in regulating cellular functions like cell shape, migration, proliferation, differentiation, and survival [92, 93]. Among those, acidic and basic fibroblast growth factor (bFGF) are more abundant and found both extra- or intracellularly, as they interact with their cognate receptors on the cell surface or regulate intracellular mechanisms when transported to cytosol or beyond [94]. The expression of bFGF is abundant in brain regions such as hippocampus or SN and is endogenously secreted by neurons as well as by glial cells [95-97]. In mice, bFGF deficiency is not lethal but impairs the precise development of the CNS and leads to a reduced abundance of parvalbumin-positive neurons in the hippocampal commissure [93]. The effects of bFGF are not restricted to one brain region or cell type, alongside parvalbumin-positive neurons, bFGF KO mice show a reduced number of cortical glutamatergic pyramidal neurons with a compact cell soma [98]. The specific effects of bFGF deficiency on glutamatergic neurons are associated with the regulation of locomotor activity which were found to be more susceptible to dopaminergic drugs thus suggesting a regulatory role for bFGF in glutamatergic and dopaminergic neurotransmission [99]. bFGF-deficient mice exhibit an approximate increase of 35% DA neurons as compare to the WT mice, which is suggestive of bFGF controlling the proliferation or development of SNc neurons [100]. In PD research models, immunohistochemical results suggest that dopaminergic neurons may exhibit a loss of bFGF prior to neurodegeneration [101]. Furthermore, it has been shown that bFGF levels in surviving SN neurons of PD-patients were found significantly decreased, thus suggesting its involvement in disease process [102].

FGFs carry out their pleiotropic effects through their receptor-mediated signaling which involves the activation of multiple downstream pathways where bFGF-receptors (bFGFR) can bind to multiple FGF-isoforms therefore exerting their functions by involving multifold molecular interaction underneath [103]. The bFGF mediated signaling is regulated via the presence of specific polysaccharide heparan-sulphate chains at the cell surface which are found to be interacting with both receptor and ligand and, therefore are critical in bFGF function [104]. In the SN, bFGF signaling is predominantly regulated via its binding to bFGFR isoforms i.e. 1IIIb, 1IIIc, 2IIIc and 3IIIc that are mainly expressed on glial cells [105]. In astrocytic cultures, agonists of dopamine receptors D1 and D2 were found to be capable of altering bFGF expression suggesting an intercellular crosslink [106]. It has been suggested that the secretion of bFGF

could happen rather unconventionally by direct shedding and is translocated to the PM and released directly to the extracellular space, thereby regulating the mechanisms of neighboring cells [94]. *In vitro* studies on astrocytes confirmed that bFGF influences the expression level of glial glutamate transporters and can thereby influence glutamate uptake activity which is further responsible for neuronal excitation [107, 108]. Besides, the extracellular presence of bFGF can promote the adhesive interactions between the components of the extracellular matrix and exerts cell to cell propagation of bFGF-signaling [109]. The bFGF propagating features are further supported by its alternative secretion in astrocytic exosomes and hence pledge the possibilities of their functions beyond the immediate vicinity of the release sites [110].

1.8. Aim and scope of the thesis

As described above, to understand the role of exosomes in seeding and spreading of LBP, it is important to understand the mechanisms of their release. Therefore, the key objectives undertaken here are to contribute to the understanding of the exosomal release processes in neurons and examine the possible implications of these findings for LBP. However, this thesis work embarks on many sub-assignments beneath its overall scope; the study also set out 1) to resolve the temporal kinetics of MVB-PM fusion events which are at the core of exosome release and were not studied before at a single-cell level in real-time 2) to identify the required stimuli (bioelectric, chemical and molecular) that regulate MVB-PM fusion events 3) to investigate the neurophysiological intricacies and changes induced by such stimuli 4) to develop a neuro-centric understanding of exosome-mediated interactions 5) to identify the exosome-mediated molecular architecture for LBP 6) to identify possible vulnerable precursor sites in LBP and 7) finally to offer a framework for future studies that would be contributing towards the better understanding of LBP. **Figure 7** depicts the broad overlapping interface of this study and highlights its possible contributions to understand LBP and neurodegeneration pathophysiology in general.

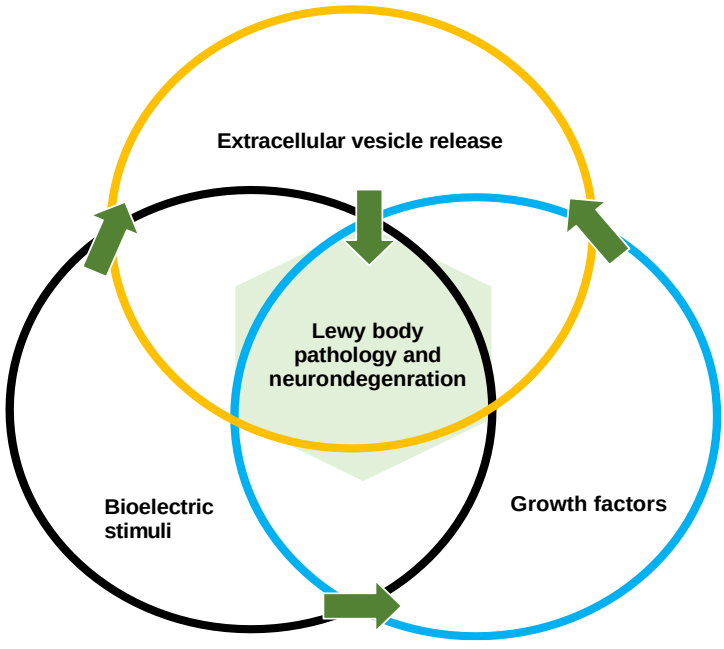

Figure 7. Thesis scope. Schematic illustrating the scope and interface of the thesis.

2. Methodology, methods, and materials

A brief account of experimental design is provided in this section.

2.1. Experimental design

To understand the physiological correlates of exosomal release, regulators, and their roles in Lewy body pathophysiology (LBP) we adopted patch-clamp electrophysiology in combination with imaging techniques in a time locked manner. For bulk assays we used nano-particle tracking analysis (NTA) along with biochemical methods. A system level network analysis was deployed to delineate the molecular level intricacies of LBP-significance from mass spectrometry (MS) data (publicly available in PRIDE data repository) obtained from neuronal cell lysate (CL) (Pride ID: PXD015969) and exosomal pellets (Pride ID: PXD014401) between the conditions examined from identified regulators.

2.1.1. Patch clamp electrophysiology

Over the time the technique has got manifested in multiple combinations but initially it was developed to run the diagnostics on electric properties of an ion channel by [111] and later on adapted to perform whole cell recordings. These recordings are performed by accomplishing a Giga-seal between neuronal membranes and a recording glass electrode, later subjecting to a strong suction pressure in order to acquire access to the intracellular environment [112]. The membrane potential (Vm) is kept constant usually at -70mV during voltage clamping and current flowing through the ion channels can be measured. Alternatively, the technique allows to manipulate the bioelectric properties of neuronal membranes by exerting brief depolarization pulses therefore providing a precise external control to deliver a stimulus of choice. This is established with the help of a computer-assisted control through a digitizer. An overview of rationales of using path-clamp technique for our experiments are shown in **Figure** 8 though a comprehensive account about the rationale of using this technique can be found in [113-116].

2.1.2. Cell Cultures

We used Lund human mesencephalic (LUHMES) cell cultures to obtain the initial insights to the exosome-release process while exerting bioelectric control using patch-clamp electrophysiology. The LUHMES cell cultures were prepared as described in [117] and primary rat hippocampal cultures were prepared as mentioned in [118] by following the regulations of local authorities and the animal welfare committee of the Ludwig Maximilian University Munich, Germany.

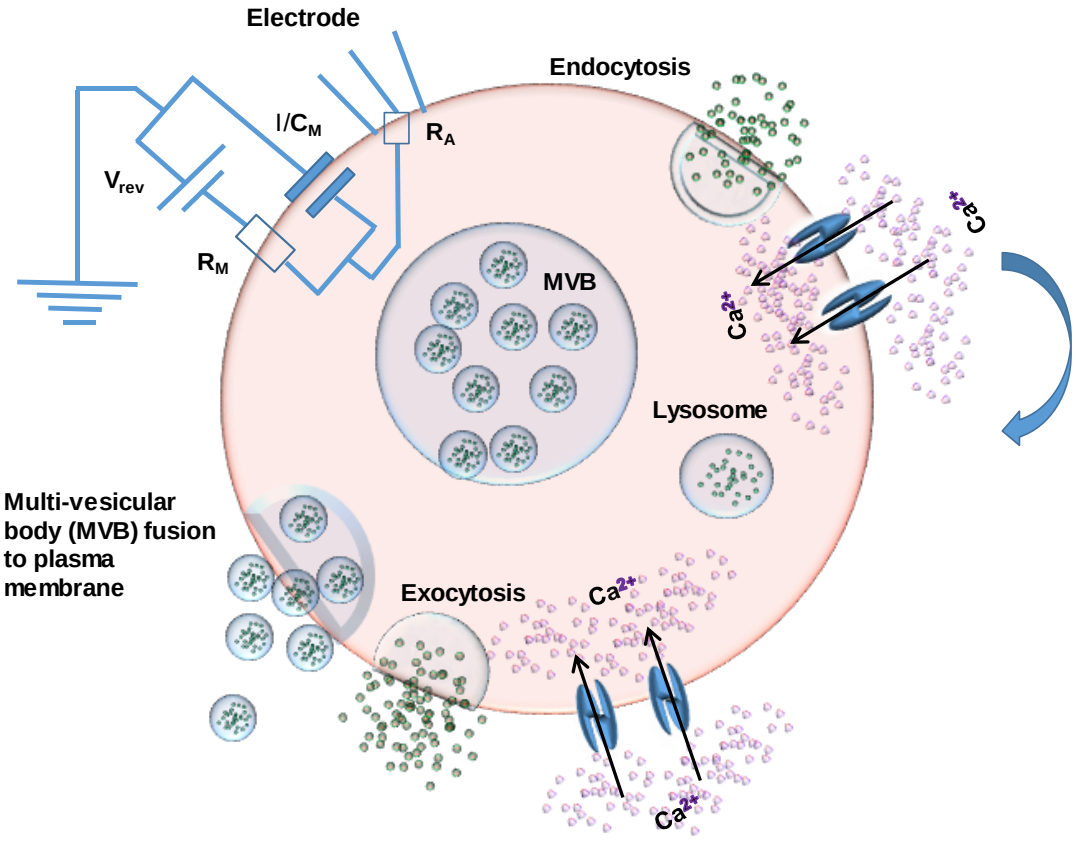

Figure 8. Overview of patch-clamp technique. Schematic illustrating a patched cell in the whole-cell configuration. This technique allows to study and control the regulation of cellular modulators such as ions (Ca^{2+} channels are shown) and ion-channels. Multiple ion channels are located on the PM and therefore any external trigger modulating the properties of these channels can be detected via patch-clamp recordings due to electric changes. Furthermore, the technique allows to record membrane fusion events as changes to membrane capacitance (C*m*) can be used as a measure of the PM surface area, which changes in response to EV release.

2.1.3. Exosome Labelling

In order to capture exosome release in a stimulus responsive manner using epifluorescent imaging we labelled exosome markers with florescent tags using lentiviral vector system as described in [118]. We used two different florescent tags fused to the exosomal biomarker CD63, which is a member of tetraspanin protein family and is expressed on the membranes of multivesicular bodies (MVBs) and exosomes [119]. Both tags (**Figure** 9), CD63-mCherry and CD63-pHluorin, can be used to capture an MVB-Plasma membrane (PM) fusion event, however pHluorin is a pH dependent green florescent protein (GFP) tag and therefore can track the changes associated to such physical factors in response to a bioelectric stimulus in a neurophysiological setting.

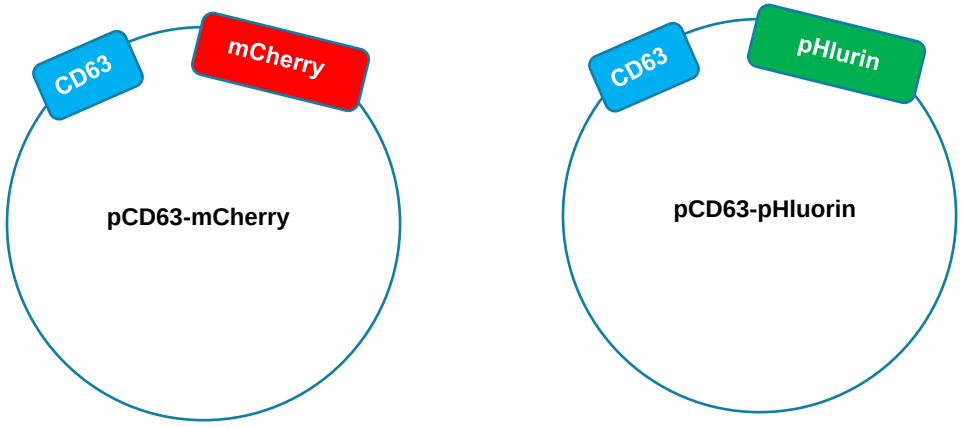

Figure 9. Schematic illustrating the plasmid map for CD63-pHluorin and CD63-mCherry.

2.1.4. Working model of the pHluorin tag

Most of the intracellular vesicles maintain a low acidic pH in their lumens[120]. The acidic pH in these compartments results from their H^+-ATPase activity during cellular buffering [121]. Hence a pH gradient is established across the membrane due to the pH difference which is also the case with MVBs. The higher extracellular pH therefore offers an opportunity to visualize the cellular activities involving pH-shift e.g., MVB-PM fusion event required to release the exosomes and EVs extracellularly and get exposed to higher pH. Miesenböck and coworkers used a histidine based combinatorial mutagenesis approach in combination with pH-dependent selection screen to find a pH-sensitive new GFP variant named pH-sensitive green fluorescent protein-based sensors (pHluorins) which when exposed to higher basic pH emits a green florescent signal [122]. We took advantage of these proteins in our experiments and targeted this tag to MVB membranes with the help of CD63 such that the florescent signal remains quenched in a proton dependent manner intracellularly (pH between ≈ 4.5-6) and similarly for exosomal membranes during their biogenesis via inward budding from MVBs (**Figure** 10A and B). These MVB when fuse to PM and get exposed to higher pH (≈ ≥ 7) or experience a pH shift because of the factors such as ion flux etc., will then emit a green florescent signal and marks MVB-PM fusion event (**Figure** 11). We further optimized the expression of our tag in hippocampal neurons by immunocytochemistry-based imaging (**Figure** 12A, B and C) and its functionality under physiological shifts created by the application of NH_4Cl (50mM) reaching to a maximal florescent signal intensity (**Figure** 12D, E and F).

2.1.5. A suitable bioelectric stimulus

To study the MVB-PM fusion in a stimulus responsive manner it was required to have a stimulus which can facilitate or orchestrate such an event. Intracellular calcium levels were previously shown to affect the rates of neurotransmitter release and hence their influence can be hypothesized for the fusion of such vesicular population [123]. Therefore, we assessed our neurons for calcium level manipulative tendencies using live-cell calcium imaging while applying the drugs capable of controlling the membrane bioelectric properties and beyond; findings of which were then applied to develop a stimulus usable during patch-clamp recording. Fluro-4-BAPTA-AM and Fura-2 preloaded neurons were optimized for a change in florescent signal intensity resulting after a calcium chelation-based reaction therefore, a shift in florescent signal could reflect a change to calcium levels. The application of 100µM Bicucullin (BIC), 2.5mM 4-aminopyridin (4-AP), 50mM KCL and subsequent application of 4-AP and 50mM KCl all have resulted in enhanced florescent signal (Figure 13).

2.1.5.1. 100 Hz

The physiological effects of above discussed compounds and results led a search for an "ideal" electric stimulus that could raise the calcium levels high enough and facilitate MVB-PM fusion. As reflected in **Figure** 14, various permutations of stimuli were tried out and simultaneous calcium level changes were measured as a change to florescent intensity during 0.05mM OGB-green dye filling of neurons with the help of patch pipette solution used in a patch-clamp recording. All the stimulus protocols were subsequently also tried in CD63-pHluorin expressing neurons (data not included) and assessed for MVB-PM fusion events. The stimulus protocol evaluation experiments initially demonstrated a slight-short term increase in neuronal calcium while switching the membrane potential to 0mV at 0.02Hz from holding membrane potential (V_{hold} = -70mV). A high frequency stimulation of 10Hz followed by a 40 and-50 Hz stimulus was successfully able to maintain an exponential rise in neuronal calcium with a very high success rate, which was not the case with other tested stimuli in our hands and in our experimental setup (**Figure** 14). Similar results were found with a single stimulus at 100 Hz (instead of subsequent 10-40-50 Hz stimuli) which when followed by a 2nd 100Hz stimulus helped maintaining the similar elevated neuronal calcium state. In **Figure** 15A a representative trace obtained after two subsequent 100Hz stimuli with an intermediate gap of three seconds is shown.

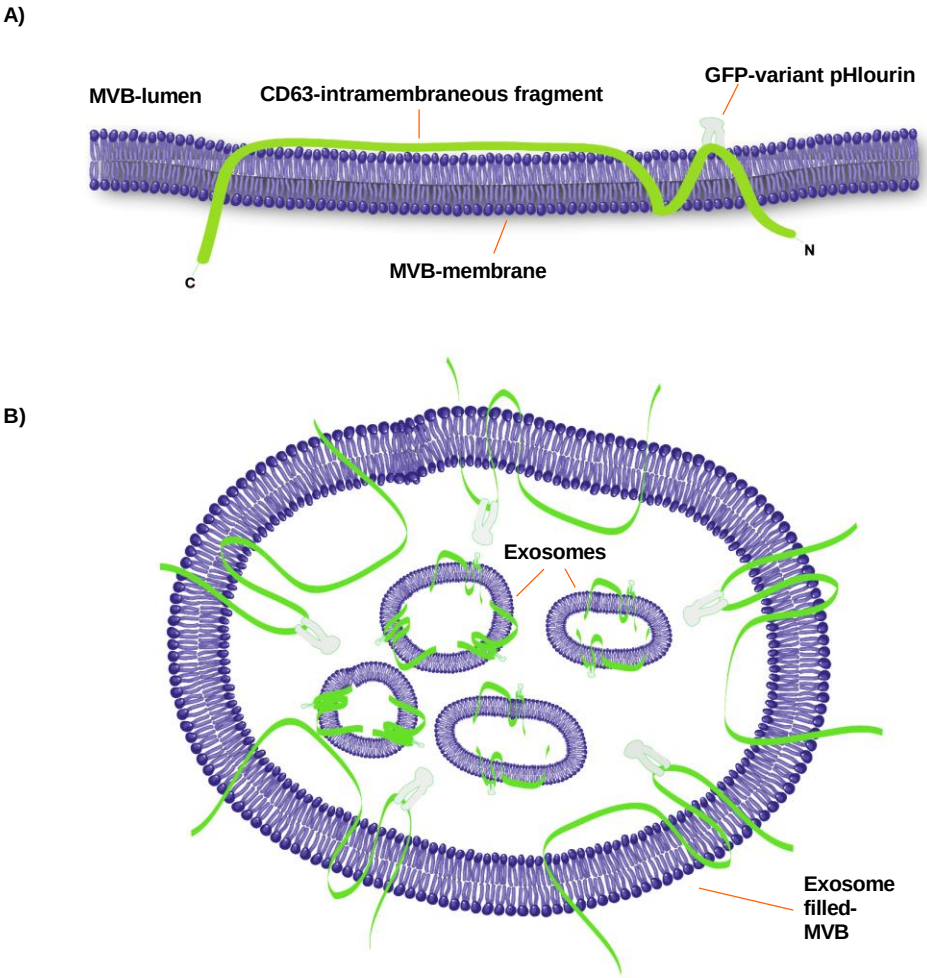

Figure 10. pHluorin: a pH-sensitive molecular marker for EVs. A) pHluorin is a variant of the green florescent protein (GFP) capable of sensing pH-changes. Diagram illustrating CD63-pHluorin tag on MVB membrane B) Representation of MVBs filled with exosomes and CD63-pHluourin tag embedded to their membrane in a native florescent signal quenched state.

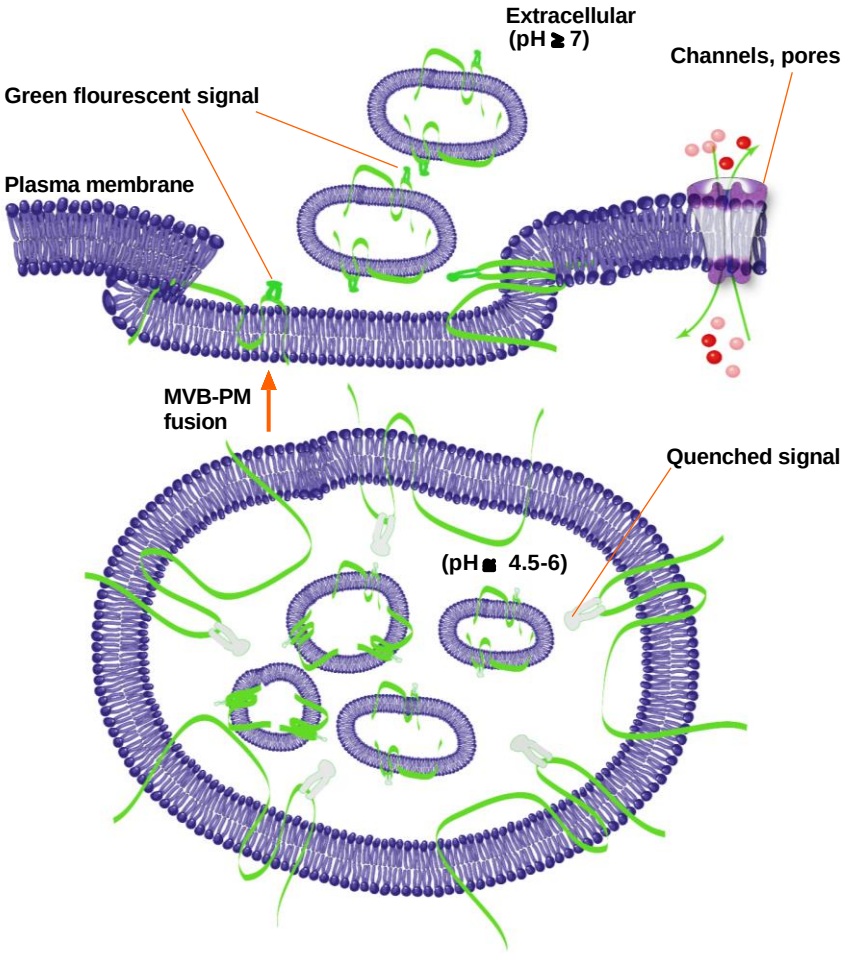

Figure 11. Working model of the florescent signal emitted by a CD63-pHluorin labeled MVB. The fluorescent signal of **pHluorin** remains quenched inside the MVB lumen where the pH is low (pH ≈ 4.5-6). When exposed to a higher pH (pH ≥7) e.g., during MVB-PM fusion, pHluorin emits a florescent signal and EV release can be visualized. Such shift may occur under the influence of an external triggers e.g., ion influx or efflux.

There was no significant difference between the inward currents after each stimulus (**Figure** 15B). A significant rise in neuronal calcium was observed in response to a single 100 Hz stimulus (**Figure** 15C and D; n=8). The effect of a 100 Hz stimulus to neuronal calcium level elevation was found rather network wide (global) in dissociated hippocampal neurons which were preloaded with Fluro-4-BAPTA-AM (**Figure** 16C and D; n=10). Therefore, based on these findings we began to investigate MVB-PM fusion events using 100 Hz stimulus.

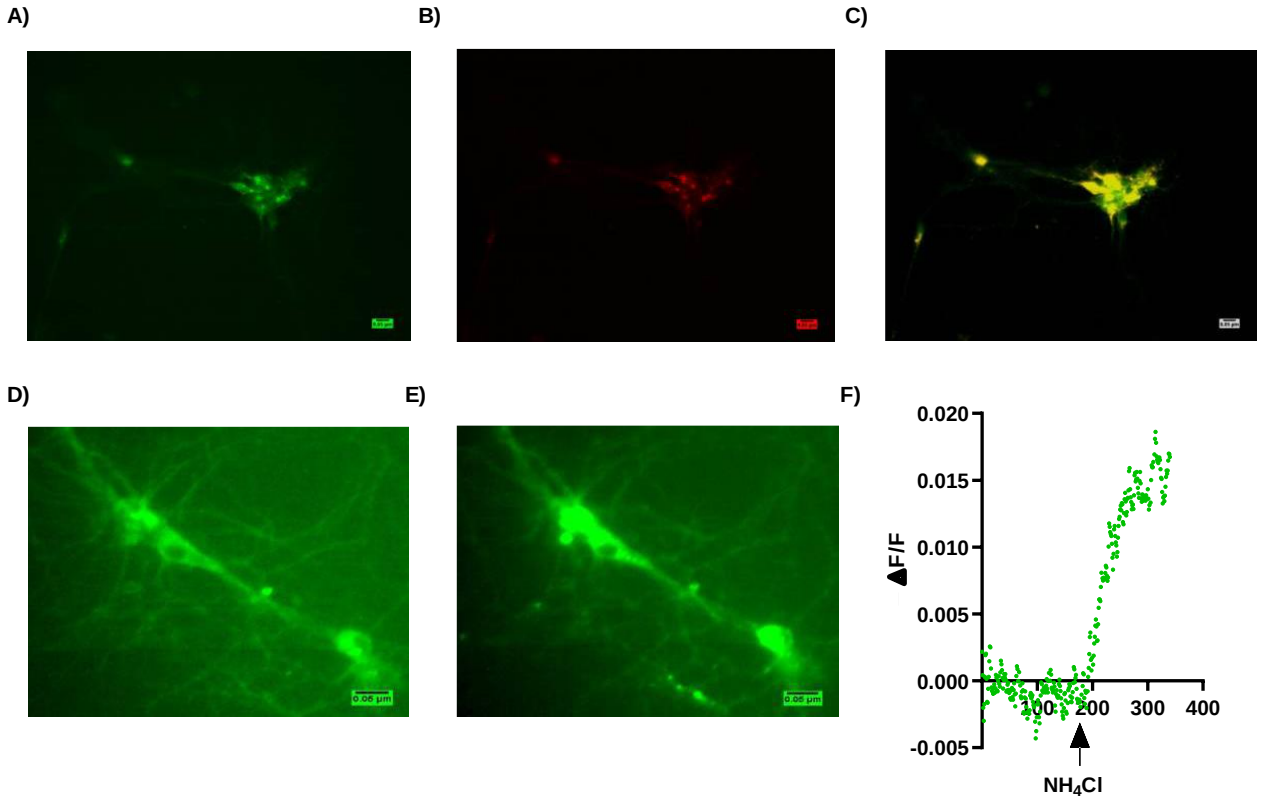

Figure 12. Optimization of MVB marker and pHluorin tag. A, B and C (GFP, Alexa 594 and merged channels respectively)) showing the CD63-tagged fluorescent labels D) live cell image of a hippocampal neuron before NH_4Cl application E) live cell image of a same hippocampal neuron after NH_4Cl application F) quantification of enhanced fluorescence after NH_4Cl application.

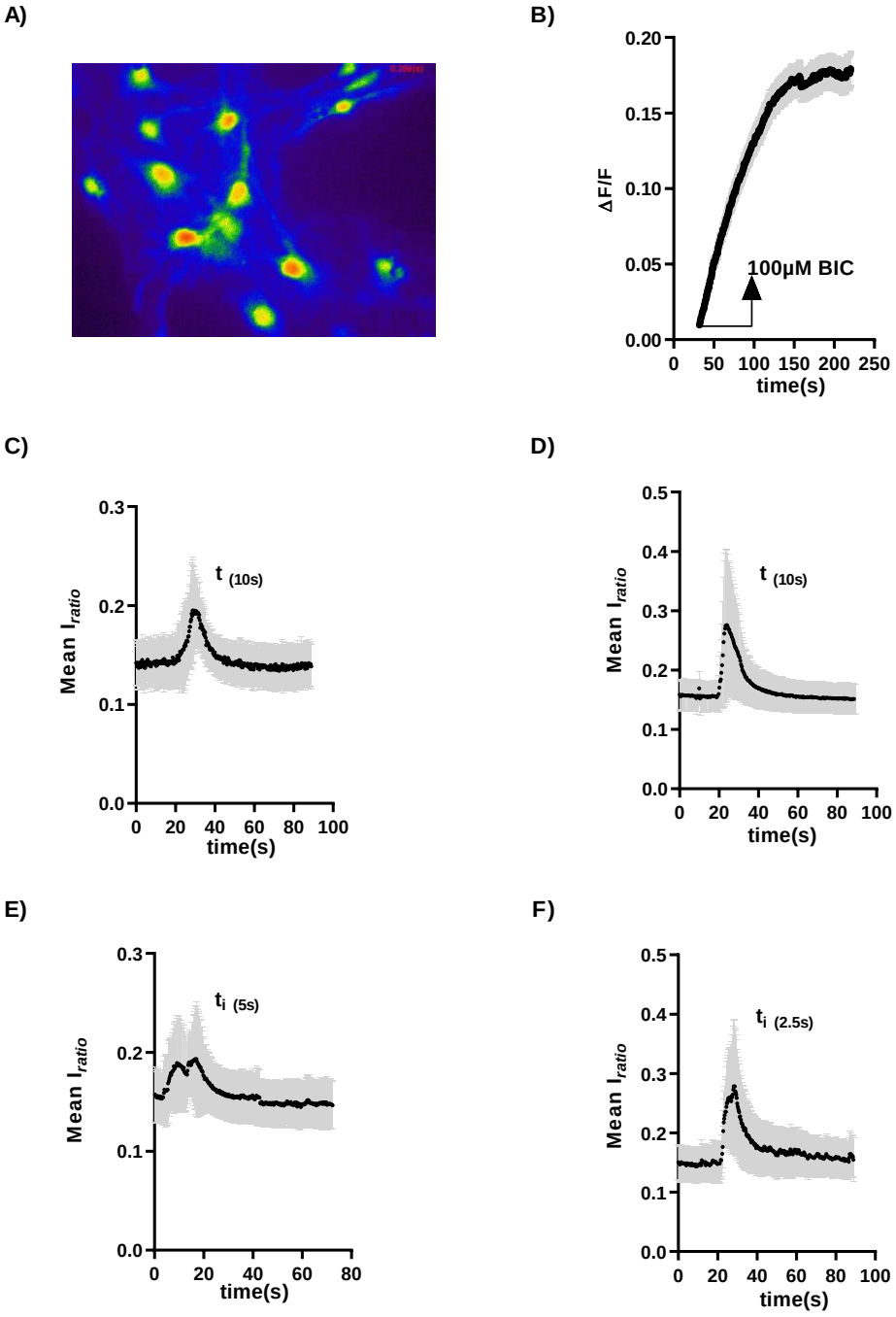

Figure 13. Assessment of the global calcium level in hippocampal neurons by calcium imaging. A) Application of 100μM Bicuculine to Fluo-4-BAPTA-AM preloaded hippocampal neurons confirms the rise in calcium B) quantification of fluorescent signal is shown in the plot (n=14) C) Enhanced calcium imaging signal in Fura-2 preloaded hippocampal neurons after application of 2.5 mM 4-AP (n= 25; drug application time(t)=10s)D) rise in calcium signal after depolarizing Fura-2 preloaded hippocampal neurons with 75mM KCl (n=18; t = 10s) E & F) Successive application of 2.5 mM 4-AP and 50mM KCl after a lag time between the drug application (t_i) of 5s (n=23) and 2.5s (n=16). Clearly segregated signal peaks are observed between the applications.

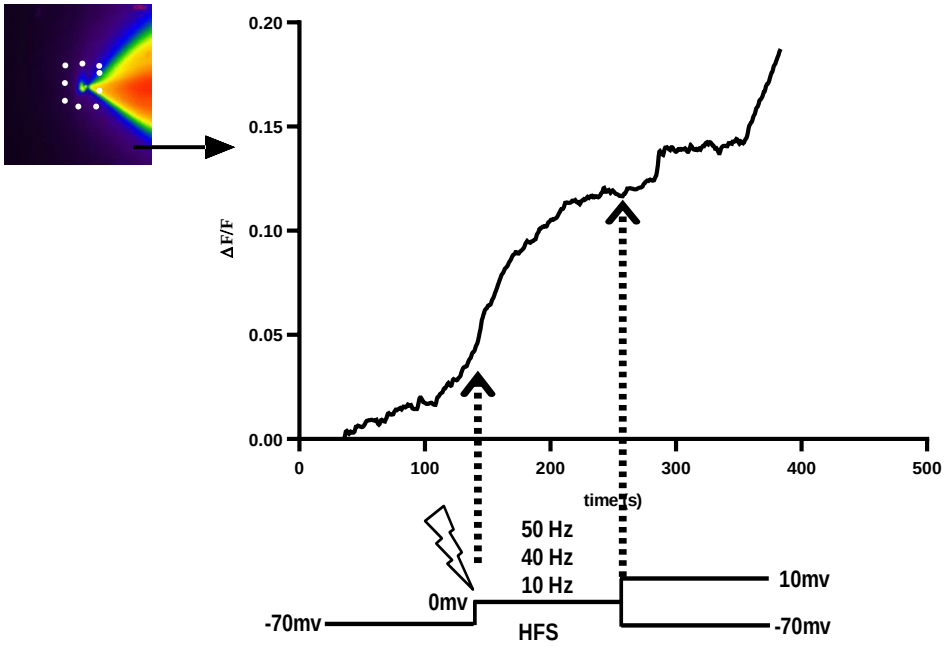

Figure 14. High Frequency Stimulation (HFS) induces a rise in intracellular calcium. High frequency stimulation (10-40-50 Hz) leads to an efficient and high intracellular calcium signal as confirmed by OGB (0.05mM) calcium imaging (n=5).

2.1.6. Nano-particle tracking analysis

We used nano-particle tracking analysis (NTA) to evaluate the EVs released in the culture medium from dissociated cultured-neurons in response to various treatments (i.e., mainly growth-factors treatments within the scope of this thesis). The culture medium was collected for treatment conditions and NTA was performed on these samples as described in [124-126] using a Nano-Sight LM10 equipment. NTA is a light scattering based method where particles in the path of a laser beam are visualized by collecting scattered light signal in a sequential (frame after frame) manner using a camera, which then is analyzed to determine the particle displacement from movement tracks, and from their velocities the particle sizes are calculated by using Stoke-Einstein equation:

In a two-dimensional system the particle displacement $[x, y]^2$ is;

$$[x, y]^2 = K_B T_{ts} / 3\pi\eta d_h \qquad (1)$$

Where K_B is the Boltzmann's constant, T is the temperature of particle solvent, t_s is the sampling time, η is viscosity of the particle medium and d_h represents the diameter. A more comprehensive view of the technique and various adjustable parameters of the technique are summarized in [124, 126].

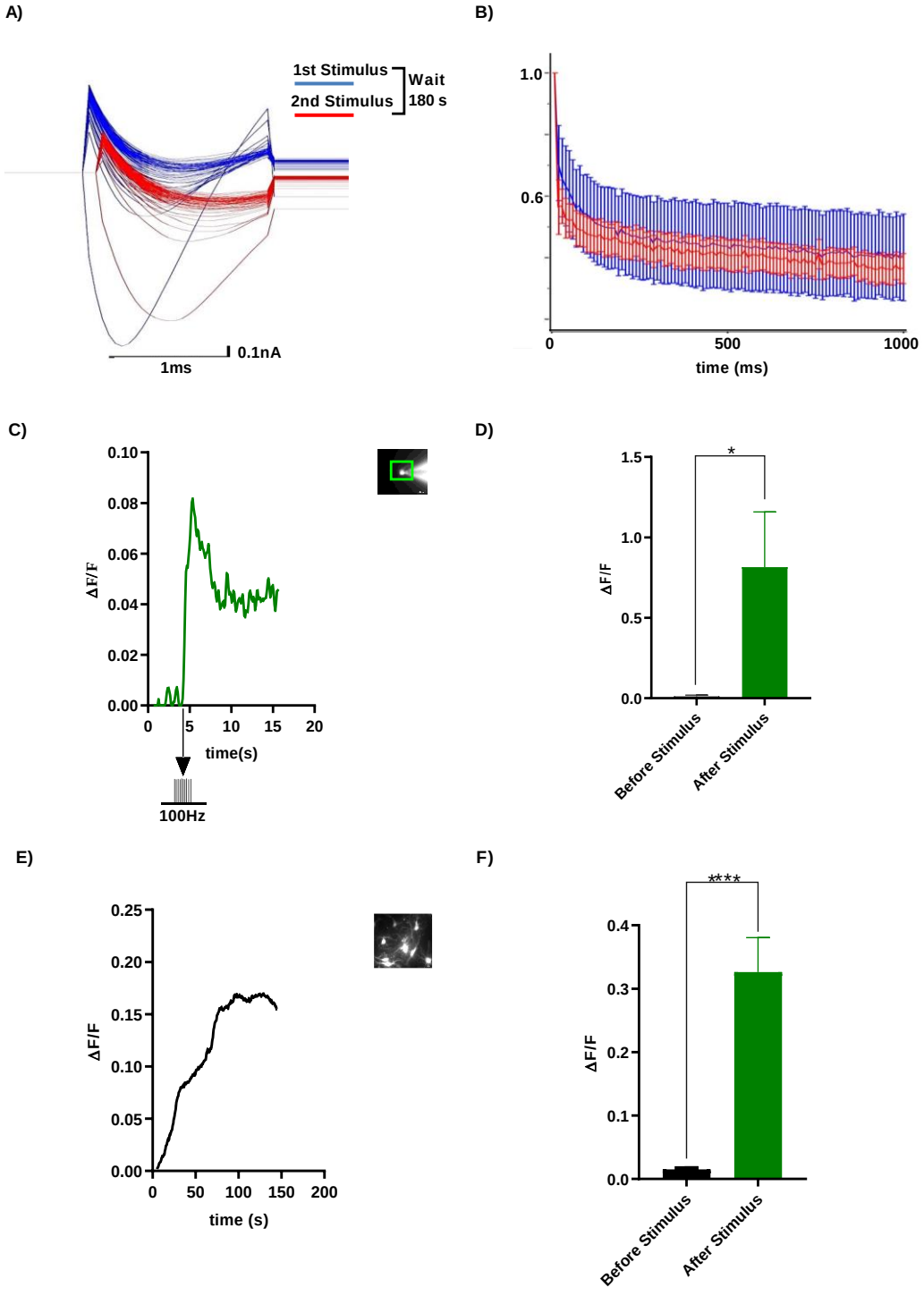

Figure 15. 100 Hz stimulus leads to a network-wide rise of intracellular calcium A) Representative traces after 1st and 2nd 100Hz stimulus in hippocampal neurons B) Normalized current trace after 1st and 2nd 100Hz stimuli (n=8) C) rise of calcium level after 100Hz stimulation in a OGB-green dye filled neuronal cell D) plot showing the enhanced calcium signal after 100 Hz stimulus, data is averaged from n=8 E) network wide rise in florescent signal of Fluro-4-BAPTA-AM preloaded neurons after 100Hz stimulus F) a significant rise in calcium concentration is assessed via the change in florescent signal after single 100Hz stimulus (n=10). Data are shown as mean ± SEM. For comparison, a two-tailed unpaired t-test was used in (D), and (F) and a paired t-test was used ****$p < 0.001$, *$p < 0.05$.

2.1.7. Weighted protein co-expression network analysis

To elaborate on underneath molecular grid responsible for neuro-exosomal response to a compound supplementing the occurrence of MVB-PM fusion events and ultimately the release of extracellular vesicles (EVs), we used systems level approach to the proteomics data acquired from mass spectrometry (MS) analysis of cell lysates (CL) and EVs-pallets. We developed co-expression network (CEN) using weighted protein co-expression network analysis (WPCNA) method. The development of a CEN using WPCNA depends on adjacency matrix (a_{ij}) which can be calculated from co-expression similarity (S_{ij}) among the nodes (*i* and *j*) and a thresh holding procedure is adapted to convert similarity to adjacency and nodal weights are assigned [127]. Following functions are included to develop a CEN in WPCNA:

Co-expression similarity (S_{ij}), defined as:

$$s_{ij} = |cor(x_i, x_j)| \tag{2}$$

Thresh holding (weighted nodal strength between 0 – 1(a soft-threshold setting)):

$$a_{ij} = \begin{cases} 1 & \text{if } s_{ij} \geq \tau; \\ 0 & \text{otherwise,} \end{cases} \tag{3}$$

Weighted network adjacency.

$$a_{ij} = s_{ij}^{\beta} \tag{4}$$

From these functions weighted network let the adjacency to get assigned, continuous values between 0 and 1; allowing to develop a network with weighted nodes. Such a network can then be used to identify the key proteins e.g., performing a centrality analysis on a curated network within the scope of MS-data

obtained for specific treatments. The functional association of key identified proteins can also be studied further beyond the restrictions of a treatment case by using publically available archives e.g. STRING database [128].

2.2. Material and methods

The full details on methods are provided in the publications enclosed for this thesis. Other protocols those are not included in published methods mentioned in these sections. A full list of materials and resources used can be found in (Table.1).

2.2. Materials

2.2.1. Chemicals used for electrophysiology

Patch-pipette solution (in mM)

136 mM KCl, 17.8 mM Hepes, 1 mM EGTA, 0.6 mM MgCl2, 4 mM NaATP, 0.3 mM Na2GTP, 15 mM creatine phosphate,and 5 U/mL phosphocreatine kinase, 315–320 mOsmol/L, pH 7.4.

Patch-pipette solution for LUHMES cells (in mM)

90 mM K+-gluconate, 40 mM KCl, 1 mM MgCl2, 10 mM NaCl, 10 mM EGTA, 4 mM Mg-ATP/ATP sodium hydrate, 10 mM HEPES, 10 mM KOH .

Extracellular solution (in mM)

140 mM NaCl, 2.4 mM KCl, 10 mM Hepes, 10 mM glucose, 4 mM CaCl2 and 4 mM MgCl2, 320 mOsmol/L, pH 7.4.

2.2.2. Miscellaneous

300 mM TTX, 0.05 mM Oregon Green 488 BAPTA-1 AM, 100µM Bicuculine, 1mM Fura-2, 4µM Fluro-4-BAPTA-AM, 10mM TEA, 2.5mM 4-AP, 50mM KCl, 50 ng/mL bFGF, 1 µM BAPTA-AM, 50 µM Genistein, 25 ng/ml BDNF, 50 ng/ml NGF, 50 mM NH_4Cl.

2.2.3. LUHMES cell culture

LUHMES cell cultures were prepared as described in [129]. In brief, LUHMES cells were maintained in poly-L-lysin (0.1 mg/mL)-coated Nunc flasks in DMEM-growth medium containing 1% N2-suppliment. For experiments cells were collected via a trypsin digestion and then seeded on double-coated (poly-L-

lysin (0.1 mg/mL) and fibronectin coating) glass coverslips. After a minimum of 6-8 hours in growth medium, the medium was changed to differentiation medium, and the cells were maintained for days while frequently changing the medium every 2-3 days until the day recordings were performed.

Main reagents used

Growth medium: DMEM/F12, 0.04 µg/mL bFGF, 1% N2-supplement.

Differentiation medium: DMEM/F12, 2 ng/mL glial cell-derived neurotrophic factor, 0.49 mg/mL dibutyryl cyclic AMP, 1% N2-supplement and 1 µg/mL tetracycline.

2.2.4. Calcium imaging fura-2 loading experiments

In brief, neurons were cultured on glass bottom dishes and loaded with 1mM Fura 2-AM diluted in DMSO solution. After removal of culture medium 0.5 ml of the Fura 2-AM working solution in HEPES was added to the cells and incubated for 20 minutes. Cells were then washed with HEPES buffer and incubated with the same for 1hour. After incubation, the cells were used for calcium imaging. The excitation spectrum was monitored at 380 nm (calcium free) and 340 (calcium complex) with a fixed emission at 510 nm.

Reagents used

1 mM Fura 2-AM/DMSO (1 mg Fura 2-AM in 1 ml DMSO), Hanks balanced salt solution (HBSS), HEPES buffer saline (20 mM HEPES, 115 mM NaCl, 5.4 mM KCl, 1.8 mM CaCl2, 0.8 mM MgCl2, 13.8 mM glucose, pH 7.4).

2.2.5. Immunocytochemistry for imaging

In brief, the culture medium was removed and neurons growing on a glass coverslip were washed with 1X-Phosphate buffer saline (PBS). After washing, they were fixed with 4% PFA solution for five minutes. Subsequently after fixation, the cells were washed 3x with PBS and then incubated with permeabilization solution (1% BSA in PBS with 0.1% Triton X-100) for another five minutes. The permeabilization solution was then exchanged by a one-hour long incubation step with blocking solution (5% BSA in PBS). After the removal of the blocking solution, the samples were incubated overnight at 4°C with primary (1^{st}) antibody (dilution used 1:200) without shaking. After incubation, the samples were washed 3 x 5 min. with PBS and then incubated with the secondary (2^{nd}) antibody for one hour at room temperature. The dilution used for the 2^{nd} antibody was 1:500 in blocking solution without shaking. The cells were washed

again 3 x 5 min. and the coverslips were transferred to the glass slides and sealed. The samples were stored in dark at 4°C until followed by imaging.

2.2.6. Other materials and resources:

Table 1: lists all the materials and resources used during the experiments.

Reagent/ Resource/ Software	Source	IDENTIFIER/VERSION
Leica DMI6000 B microscope	https://www.leica-microsystems.com/products/light-microscopes/p/leica-dmi6000-b/	
Leica Application Suite X (LAS X)	https://www.leica-microsystems.com/products/microscope-software/p/leica-las-x-ls/	LAS_X_Core_3.7.2
Glass Bottom Dish 35 mm	https://ibidi.com/labware/185-glass-bottom-dish-35-mm.html	81218-200
CCD Camera	https://www.hamamatsu.com/jp/en/product/cameras/ccd-cameras/	
ValveLink8.2 perfusion system	https://www.autom8.com/perfusion-systems-overview/valvelink8-2-controller/	
ImageJ	https://imagej.net/Fiji/Downloads	
Glass coverslips (German Glass)	Thermo-Fischer-scientific	
Nitric acid 65%	Sigma	1004561000
Poly-D-Lysin	Thermo-Fischer-scientific	A3890401
Poly-L-lysine	Sigma-Aldrich	P8920
DMEM	Sigma-Aldrich	
GDNF	R&D Systems	
Dibutyryl cyclic AMP	Sigma-Aldrich	D0260
Tetracycline	Sigma-Aldrich	T7660
N2-supplement	Life Technologies	17502001
Fibronectin	Sigma-Aldrich	F1141
Nunc-flasks	Thermo-Fischer-scientific	156367, 156499
Olympus BX51 microscope	Olympus	
HEKA EPC 10 USB amplifier	HEKA Electronics	
Patchmaster 10 software	HEKA Electronics	
Axograph X	Axograph	V 1.6.5
ExiBlue Camera	QImaging	
µManager	https://micro-manager.org/	V1.4

NanoSight LM10	Malvern Panalytical	
NanoSight NTA software	Malvern Panalytical	V3.2
Prism 7	Graph Pad	
4% PFA	Sigma	1004960700
heatmap3	https://www.r-project.org/nosvn/pandoc/heatmap3.html	R version 3.0.2
KEGG: Kyoto Encyclopedia of Genes and Genomes	https://www.genome.jp/kegg/?sess=ebfe2ad23e021e38540f798c803dd061	
Patch pipette glass	World Precision Instruments	
Micropipette Puller	Shutter Instruments	P1000
Faraday Cage	HEKA	
Micromanipulators	Luigs & Neumann	
Anti-vibration table	Newport	
Pipette holder	HEKA	
Headstage	HEKA	Red-star
Maxquant software	https://maxquant.net/maxquant/	V 1.6.1.0
UniProt database	https://www.uniprot.org	V 2019_10
R software	https://www.r-project.org	V 3.5.1
WGCNA	https://horvath.genetics.ucla.edu/html/CoexpressionNetwork/Rpackages/WGCNA/	
CINNA R package	https://cran.r-project.org/web/packages	V 1.1.53
Scatter plot3D R Package	https://cran.r-project.org/web/packages/scatterplot3d/index.html	V 0.3-41
Factoextra R Package	https://cran.r-project.org/web/packages/factoextra/index.html	V 1.0.7
PreprocessCore R package	https://www.bioconductor.org/packages/release/bioc/html/preprocessCore.html	V 1.50.0
ggplot2 R package	https://cran.r-project.org/web/packages/ggplot2/index.html	V 3.3.1
Vennuelar R package	https://cran.r-project.org/web/packages/venneuler/index.html	V 1.1-0
Biomart R package	http://bioconductor.org/packages/release/bioc/html/biomaRt.html	V 2.38.0

DisGeNet Database	https://www.disgenet.org	V 7.0
Rat Genome Database	https://rgd.mcw.edu/rgdweb/homepage/	V 20
hRBPome Database	http://caps.ncbs.res.in/hrbpome/	V 1.0
Channelpedia Database	https://channelpedia.epfl.ch	V 1.0
Human protein atlas Database	https://www.proteinatlas.org	V 19.3
STRING Database	https://string-db.org	V 11
Cytoscape	https://cytoscape.org	V 3.7.1
Metascape	https://metascape.org/gp/index.html#/main/step1	V 1.0
Easy nLC 1000	Thermo Scientific	LC 120
Easy nLC 1200	Thermo Scientific	LC 140
Q-Exactive	Thermo Scientific	
Q-Exactive HF	Thermo Scientific	
Perseus	https://maxquant.net/perseus/	Version 1.5.8.5
SP3 digestion	Sielaff, M., et al., Evaluation of FASP, SP3, and iST Protocols for Proteomic Sample Preparation in the Low Microgram Range. J Proteome Res, 2017. 16(11): p. 4060-4072.	
Protein lobind Tubes 0.5 mL	Eppendorf	0030108094
Protein lobind Tubes 1.5 mL	Eppendorf	0030108116
30 cm × 75 µm fused silica emitter	New Objective	FS-360-75-8-N-5-C30
ReproSil-Pur 120 C18-AQ	Dr. Maisch GmbH	r119.aq.0003
Tris	Millipore	648310-M
NaCl	Supelco	1.06404
Triton X-100	Sigma Aldrich	T8787
EDTA	Sigma Aldrich	E9884
Sodium Deoxycholate	Sigma Aldrich	30970
Benzonase	Millipore	E1014
MgCl2	Sigma Aldrich	M3634
Dithiothreitol	Sigma Aldrich	D5545
Iodoacetamide	Sigma Aldrich	I1149
SpeedBeads™ magnetic carboxylate modified particles	GE Healthcare	45152105050250

SpeedBeads™ magnetic carboxylate modified particles	GE Healthcare	65152105050250
LysC	Promega	V1671
Trypsin	Promega	V5111
Ethanol	Supelco	1.11727.2500
H2O + 0.1% formic acid	Biosolve	0023244101BS
Acetonnitrile + 0.1% formic acid	Biosolve	0001934101BS
Acetonitrile	Biosolve	01204101
bFGF	Peprotech	100-18B
anti-GFP	GeneTex	GTX113617
anti-Alix/AIP1	Merck	ABC40
anti-CD81	Santa Cruz Biotechnology	sc-166029
rabbit anti-rat EEA1	Cell Signaling Technology	C8R1
Neurobasal media	Invitrogen	
MLA-80 rotor	Beckmann	
TLA-55 rotor	Beckmann	
SW55Ti rotor	Beckmann	
TLA 110 rotor	Beckmann	
Phosphate buffer saline	Thermo-Fischer-scientific	10010023
RIPA Buffer	Thermo-Fischer-scientific	89900

3. Results

3.1. Abundant α-Syn expression and exosomal release

3.1.1.α-Syn overexpression results in an elongated morphology in LUHMES cells

A shift in somatic volume is observed for α-Syn over-expressing LUHMES cells (**Figure** 16A and B) as compared to WT LUHMES cells (**Figure** 16A). α-Syn over-expression resulted in a significant increase in the surface area (≈ mean area = 2.8 x 10^{-8} a.u.: n=15) as compared to WT cells (≈ mean area = 1.2 x 10^{-8} a.u.: n=15) (**Figure 16C).** The elongated morphological appearance of α-Syn-overexpressing cells is also evident from decreased somatic circularity (≈ to 1/2) as compared to the WT cells (**Figure** 16D). No change was found in the somatic solidity between WT and SNCA overexpressing LUHMES cells, thus suggesting that the overall quality of plasma membrane was uncompromised since the solidity is a ratiomeric measure between surface area and convex hull of the surface (data not included).

Using patch-clamp electrophysiology, it has been long established that the plasma membrane (PM) of a cell behaves closely like a parallel plate capacitor and increases in the surface area of plates corresponds to an increase in membrane capacitance (C*m*) and vice versa [130]. Therefore, a higher C*m* would correspond to a fusion of vesicular bodies.

3.1.2. α-Syn overexpression resulted in enhanced secretion of extracellular vesicles in LUHMES cells

In a follow-up experiment to our observation of elongated morphology in α-Syn over-expressing LUHMES cells, we began to investigate the media collected from GFP and α-Syn overexpressing cells. We subjected these samples to NTA analysis and found a higher particle concentration (≈2.3 x 10^{6} particle/milliliter) for α-Syn overexpressing cells (**Figure17A**). The concentration of particles was elevated roughly twofold, and most of the particles were of a size ranging between 50-150 nm. The size range for exosomes is similar to the observed sizes therefore, evident for a proportional conclusion of enhanced extracellular vesicle (EV) release in α-Syn overexpression conditions.

3.1.3. Exosome release in LUHMES cells is calcium dependent

The change in C*m* is a direct function of change in membrane surface area therefore, whole-cell voltage clamp was used to measure the current and capacitance changes across the cell membrane. Higher C*m* values were recorded for α-Syn overexpressing cells; approximately a two-fold increase in C*m* (**Figure** 17B).

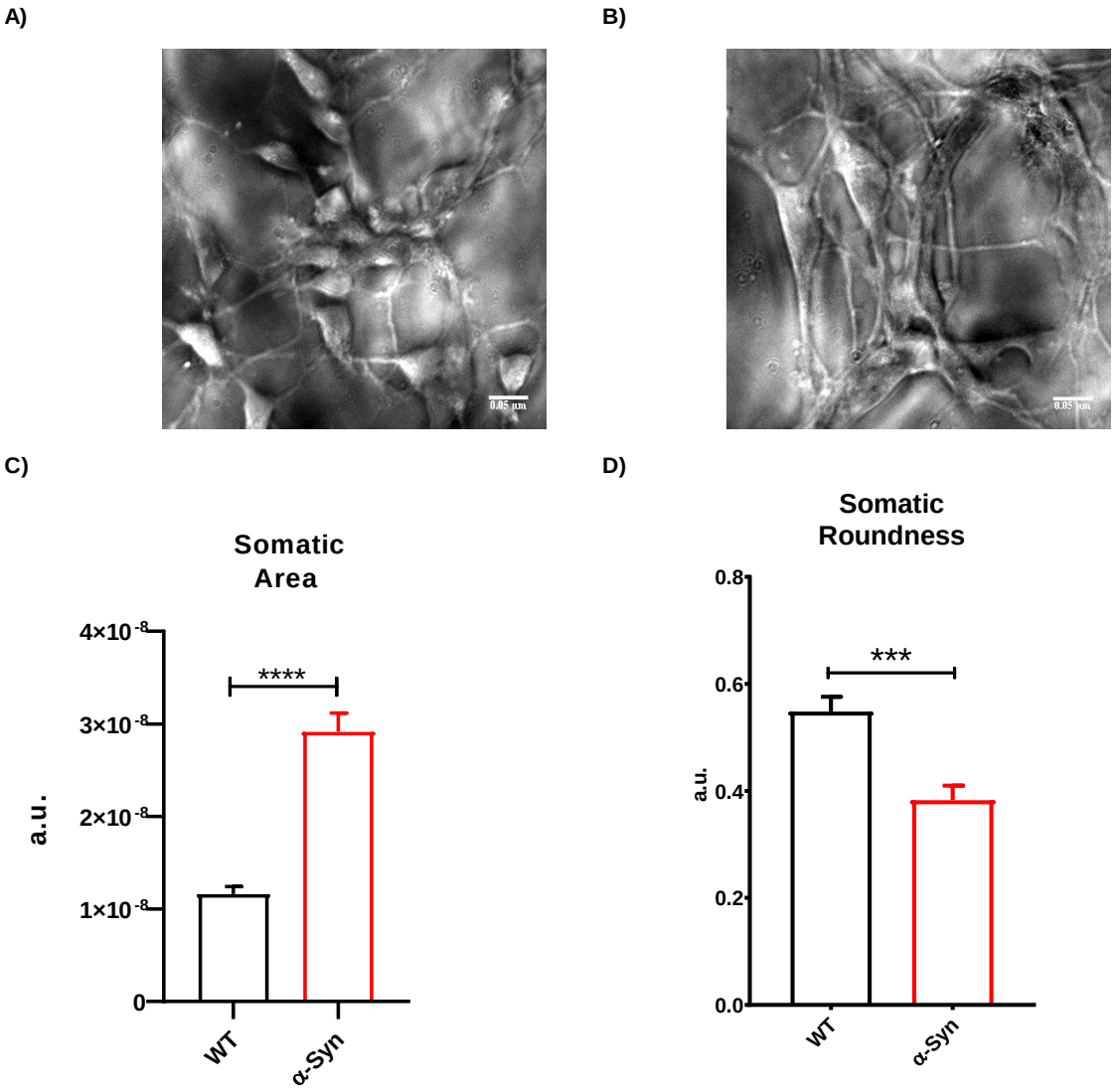

Figure 16. α-Syn overexpression induces significant changes to LUHMES cell morphology. A) Wild type (WT) LUHMES cells with round somas B) α-Syn overexpressing LUHMES cells with characteristic somatic-elongation C & D) quantification of the morphological changes in α-Syn overexpressing LUHMES cells in terms of the somatic area (N=15/condition) and the somatic roundness (N=15/condition). The elongated morphology of LUHMES cells correlates with a significantly enhanced surface area and a significantly decreased somatic roundness. Data are shown as mean ± SEM. For comparison, a two-tailed unpaired t-test was used in (C), and (D) and a paired t-test was used ***p < 0.001.

We further inducted these cells with external electric stimuli of voltage (V*m*= -10mV), (τ =50 ms) to facilitate an increase in the cytosolic calcium concentration via inward calcium current (I_{ca}). I_{ca} was isolated by applying 1µM TTX and 10mM TEA in the extra-cellular solution (ECS) in the presence of cesium gluconate to abolish sodium (I_{Na}) and potassium (I_k) currents. In a time-locked manner, we made I_{ca} and C*m* recordings in α-Syn overexpressing LUHMES cells (**Figure 17C**).

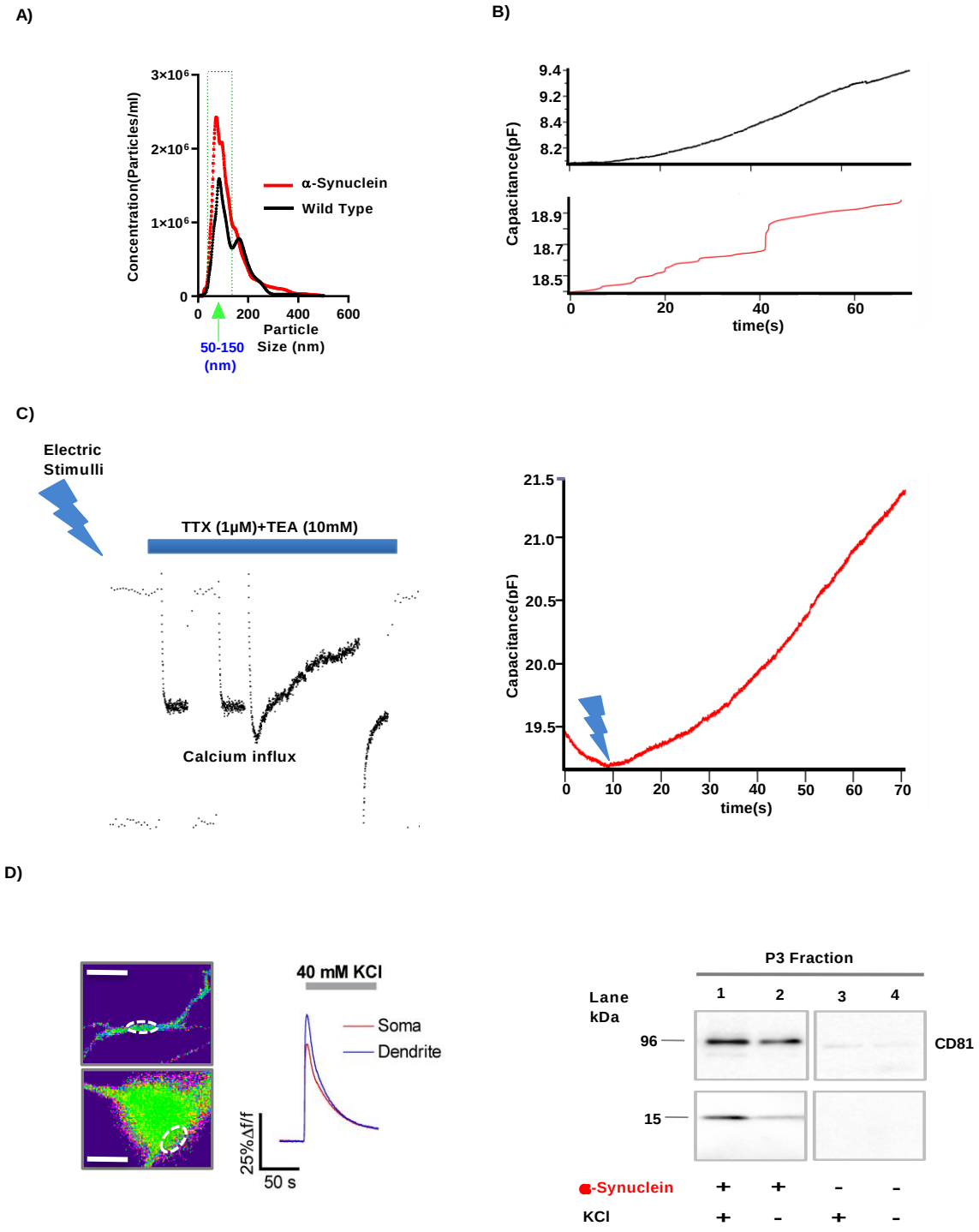

Figure 17. α-Syn overexpression enhance EV release. A) Nano-particle tracking analysis (NTA) of media collected from α-Syn (red) overexpressing and WT (black) LUHMES cells B) Shows the relatively higher C*m* observed in α-Syn overexpressing LUHMES cells as compare to the WT cells C) A calcium-dependent increase in C*m* is depicted and the calcium levels were elevated after electrical stimulation D) A rise in global calcium is observed in KCl mediated depolarization; the enhanced signal for exosomal marker was found in a Western-blot of exosomal fraction (first appeared in poster presentation [131]).

A linear immediate increase in the C*m* was observed in relation to I_{ca}. Each step-like increment corresponds to a fusion event with the step size corresponding to the presumed vesicle size. Many fusion events were seen for α-Syn overexpressing cells, indicating more intracellular vesicles were fused in response to a subsequent availability of calcium.

In addition, we depolarized the plasma membrane by applying 40mM KCl to induce a calcium influx, which was confirmed via simultaneous calcium imaging (**Figure 17D**). We further quantified the amount of exosomal markers and the abundance of α-Syn in exosomes by Western blot in WT and α-Syn over-expressing LUHMES cells. A strong band was observed in EV-enriched medium pellets from KCl-treated and α-Syn-transduced neurons, suggesting that more α-Syn was released via EVs, further facilitated by inward I_{ca} (**Figure 17D**).

Though α-Syn over-expressing LUHMES cells were found to have a higher C*m* (≈1.5-2 fold), the phenotype of increased C*m* is not coupled to an electric stimulus in a linear fashion as can be appreciated from the representative traces in **Figure 18A**. Moreover, we observed no spontaneous activity in LUHMES cells of age between 6-8 days *in vitro* (DIV) (**Figure 18B**), although some groups report spontaneous activity in older LUHMES cells [132]. Considering such physiological variance, we choose to perform electrophysiological investigation in primary hippocampal cultures.

3.1.4. α-Syn overexpression enhances extracellular vesicles in primary hippocampal neurons

The similar results as in LUHMES cells were reported by NTA experiments (N=5) performed with the media samples collected from WT-primary and α-Syn over-expressing hippocampal neurons. The abundance of particles between 50-150 nm size range, was significantly enhanced in hippocampal neurons overexpressing α-Syn (**Figure 19A** and **B**). We observed on average ≈ 5.8 x 10^6 particles/milliliter for WT as compared to α-Syn (≈ 7 x 10^6 particle/milliliter) transduced cells i.e., significantly enhanced ($p < 0.0001$). The size of the particles remained unchanged between the two conditions (**Figure 19C**). Such findings convinced us about the suitability of using the primary hippocampal neuronal cultures for further investigations and are a more established and relevant research model for our research objectives.

3.2. Calcium level and exosomal release

3.2.1. A relative slower rate of MVB-PM fusion

Our earlier experiments demonstrated (please refer to methods) that high frequency stimulation or biochemical depolarization of neuronal membranes elevate neuronal calcium levels (**Figure 13-15**).

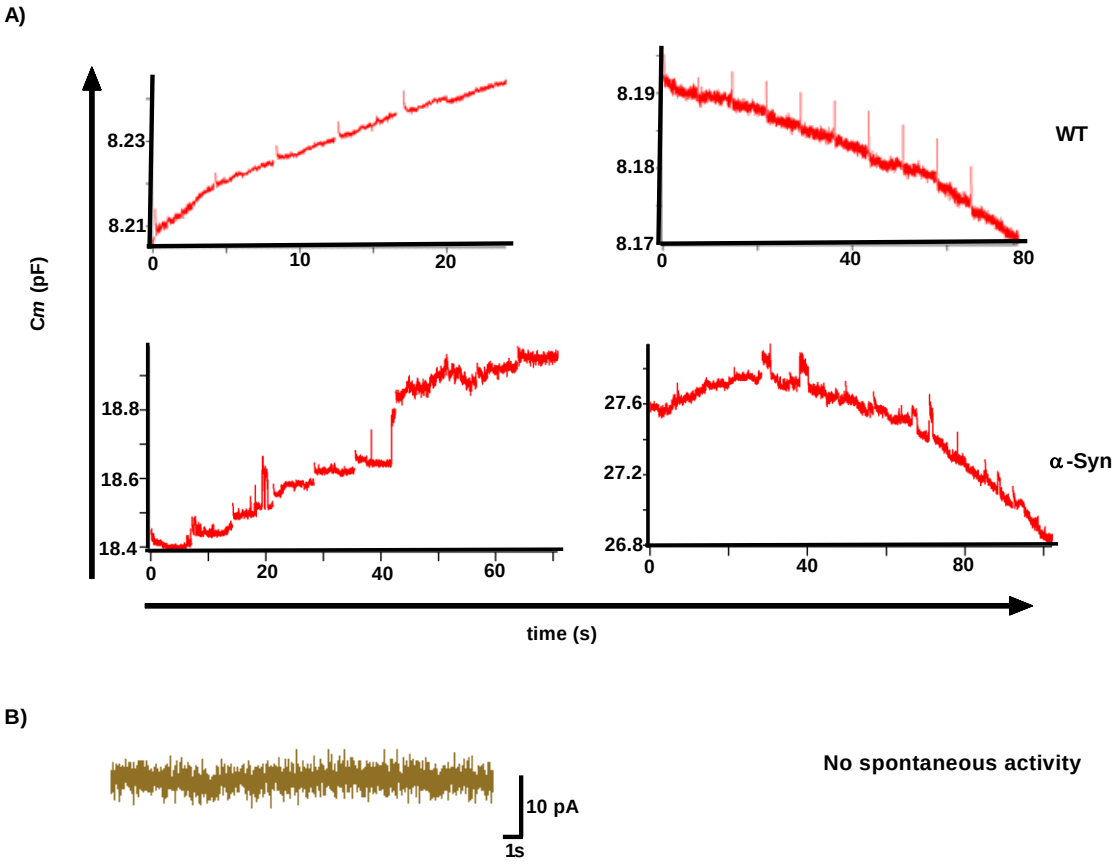

Figure 18. α-Syn overexpressing LUMES cells have a higher specific C*m* A) Representative traces showing a higher specific C*m* in α-Syn overexpressing LUMES cells (approximately twofold compared to the WT cells) and in response to an electrical stimulus both increased and decreased C*m* exists in LUHMES cells B) Representative trace showing no spontaneous activity in LUHMES cells of age DIV 6-8.

Therefore, we set out to investigate the effects of high calcium in real-time to determine the temporal kinetics of MVB-PM fusion which is overlooked in bulk, only biochemical analysis-based studies, and hence the findings from these studies cannot comprehensively address the physiological aftermath of a stimulus. To address this problem, we labeled exosome-filled MVBs by overexpressing CD63-mCherry (**Figure 9**) in primary hippocampal rat neurons at DIV3 (**Figure 20**). Between DIV9-14 these neurons were then used for the HFS experiments by jointly using patch-clamp electrophysiology and simultaneous imaging techniques in a time-locked arrangement.

As shown in **Figure 20A**, neurons with CD63-mCherry labeled MVBs possess illuminated granular structure across the cell but more visible at cell-soma. These neurons when subjected to a bioelectric stimulation exhibit a gradual disappearance of the granular structures that may be attributed to a demarcation of MVB-PM fusion event.

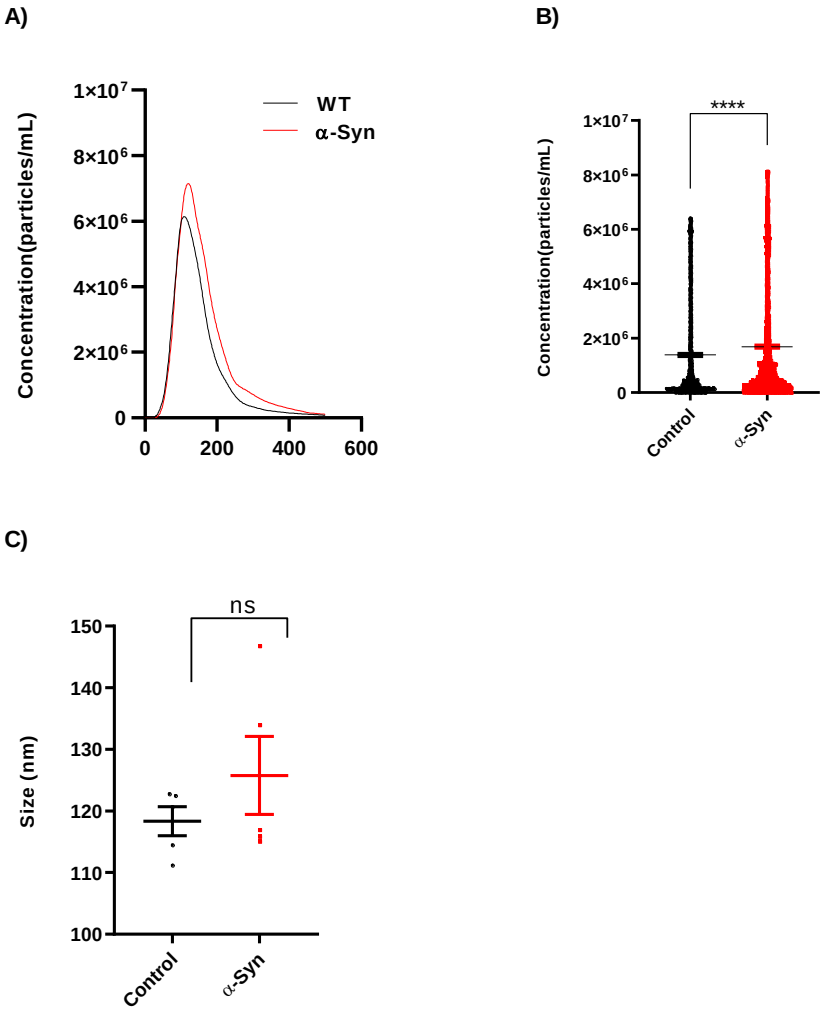

Figure 19. α-Syn overexpression in hippocampal neurons leads to an enhanced EV release. A and B) NTA analysis shows a higher concentration of EVs for the media samples collected from α-Syn overexpressing neurons as compared to WT neurons (n=5). C) Bar graph illustrating the average EV size observed for the particles in the culture medium collected for two conditions (n=5). Data are shown as mean ± SEM. For comparison, a two-tailed unpaired t-test was used in (B), and (C) and a paired t-test was used ****p < 0.0001.

These events were seen after an electric stimulus in due time, ranging from seconds to minutes (**Figure 20A** (at 64.425 seconds ≈30s after stimulus), **Figure 20B** (at 80.523 sec), and **Figure 20C** (at 111.725 sec)). The calibration of these events is then be done in a real-time florescent signal intensity map where each step decrease, will render to an MVB-PM fusion (**Figure 20D**) illustrating the temporal kinetics of such events. We observe a slower rate of MVB-PM fusion in comparison to neurotransmitter releasing vesicles as can be seen from the representative traces (**Figure 20E**, **F** and **G**) obtained after 10Hz, 40Hz and 50Hz, respectively. The post-synaptic responses generated after such stimulation because of

neurotransmitter release to synaptic cleft can be seen within a few milliseconds and can be assessed as the quantal size of the neurotransmitter-release corresponding to a postsynaptic response. The temporal kinetics in such events can be attributed to the immediate availability of readily releasable pool (RRP) of vesicles which is replenished at a relatively faster rate (from milliseconds to seconds) [133, 134]. Contrary to this, the rate of MVB-PM fusion is ranging from seconds to minutes and is much slower therefore, highlighting exosomes as a kinetically distinct vesicle population in rat hippocampal neurons.

3.2.2. HFS enhances MVB-PM fusion events with a subsided success rate

The CD63-mCherry construct can label MVBs but it does not provide much insight about the cell's physiological environment in response to an electric or biochemical stimulus. Therefore, we used another labeling construct to over-express CD63 fused to a pH sensitive GFP variant in hippocampal neurons, termed pHluorin (**Figure 21**). At first, we began to investigate these neurons at the holding potential of -70mV, corresponding to basal calcium levels. Up to several minutes, the fluorescent signal was almost stable as indicative by the CD63-pHluorin expressing neuron presented in Fig.20A at the time points 500ms and after 200 seconds. During a span of ≈ 3mins, we observed some random burst-like punctate (≈ 2 in 3-4 minutes), presumably MVB-PM fusion events (**Figure 21A**).

After subjecting the same neuron (panels **Figure 21B**) to a high calcium state through application of a HFS (a brief pulse of 100 Hz over 1s), we observed a series of more rapid fluorescent bursts (neuron shown in **Figure 21B** at 154 secs) as it is depicted by the florescence intensity plot in **Figure 21B**. However, this stimulus evoked response was only exhibited by a subset of neurons (n = 5/34 neurons, 14.7%). In stimulus-responsive neurons, the burst-like increase to pHluorin-fluorescence was found after an average interval of 38.51 sec (38.51 ± 12.54 sec) following the first HFS stimulus. Thus, we observed a similar slow rate in the range of seconds to minutes (t1/2 = 86.83 ± 0.6149 sec; n = 5) for MVB-PM fusion events consistent with the results from using CD63-mCherry. Recordings lasting for several minutes there was no overall significant decay in the fluorescent signal. Taken together we concluded that the success rate of stimulus-evoked MVB-PM fusion is subsided in hippocampal neurons and a long lag-time between an HFS, and an MVB-PM fusion event persists.

3.3. Growth factors and exosomal release

3.3.1. The effects of growth factors are restricted largely to intraneuronal physiological environment

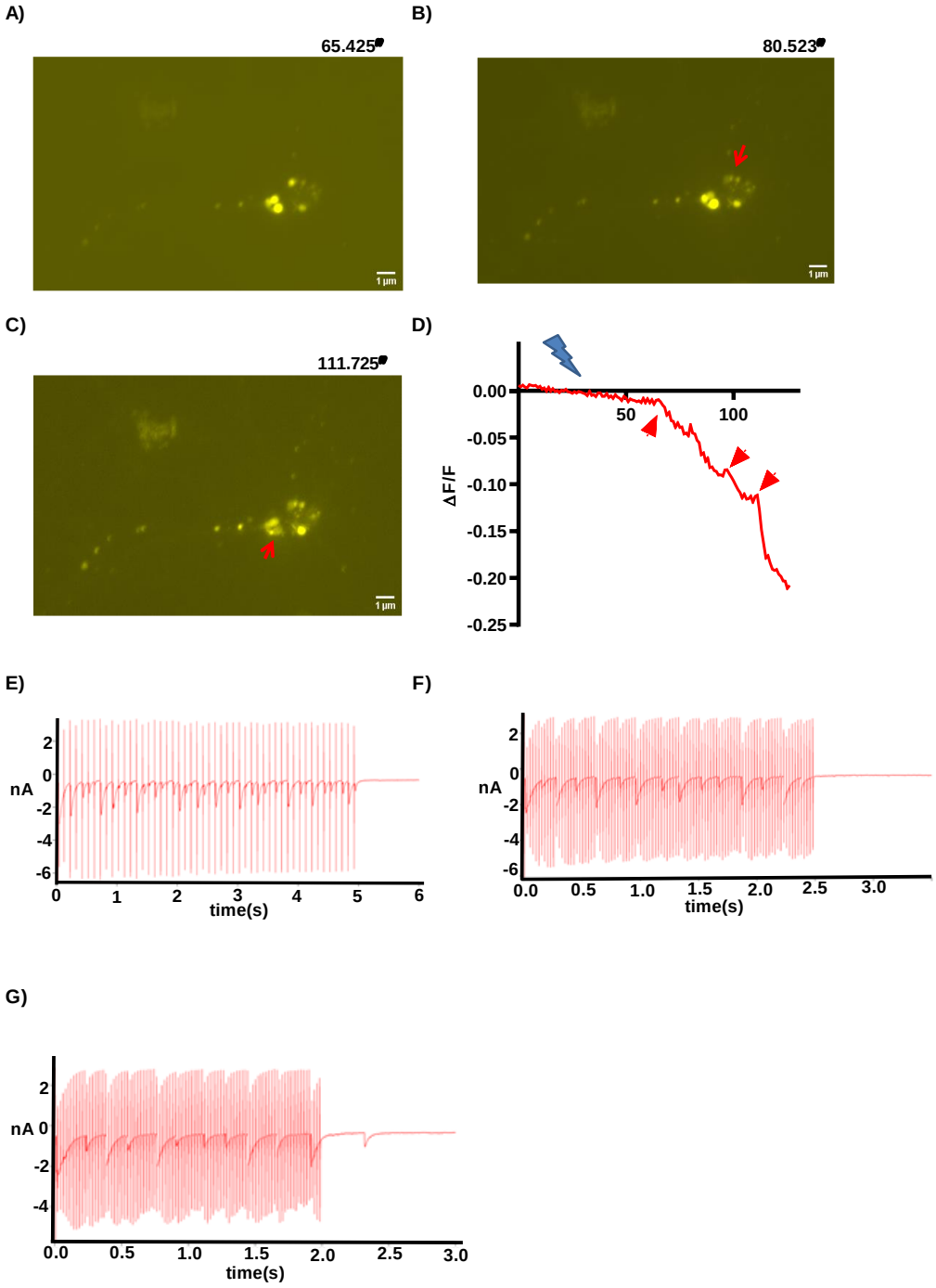

Figure 20. HFS leads to a slow release of CD63-mCherry positive EVs. A, B, C and D) As compared to neurotransmitter releasing vesicles a slower rate of release is observed (at 65.425 sec, 80.523 secs and 111.725 secs respectively) for the CD63 positive exosomes after an electric stimulation of neurons. EV release occurs in the range of seconds to minutes as indicated by the loss of fluorescent signal over time after electric stimulation. D) Florescent signal intensity plot showing fusion events; red arrows indicate an individual release event and the corresponding loss of fluorescent signal over time. E, F and G) Showing the representative voltage clamped current traces for 10 Hz, 40Hz and 50Hz respectively, with a relative faster rate of release of neurotransmitter releasing vesicles.

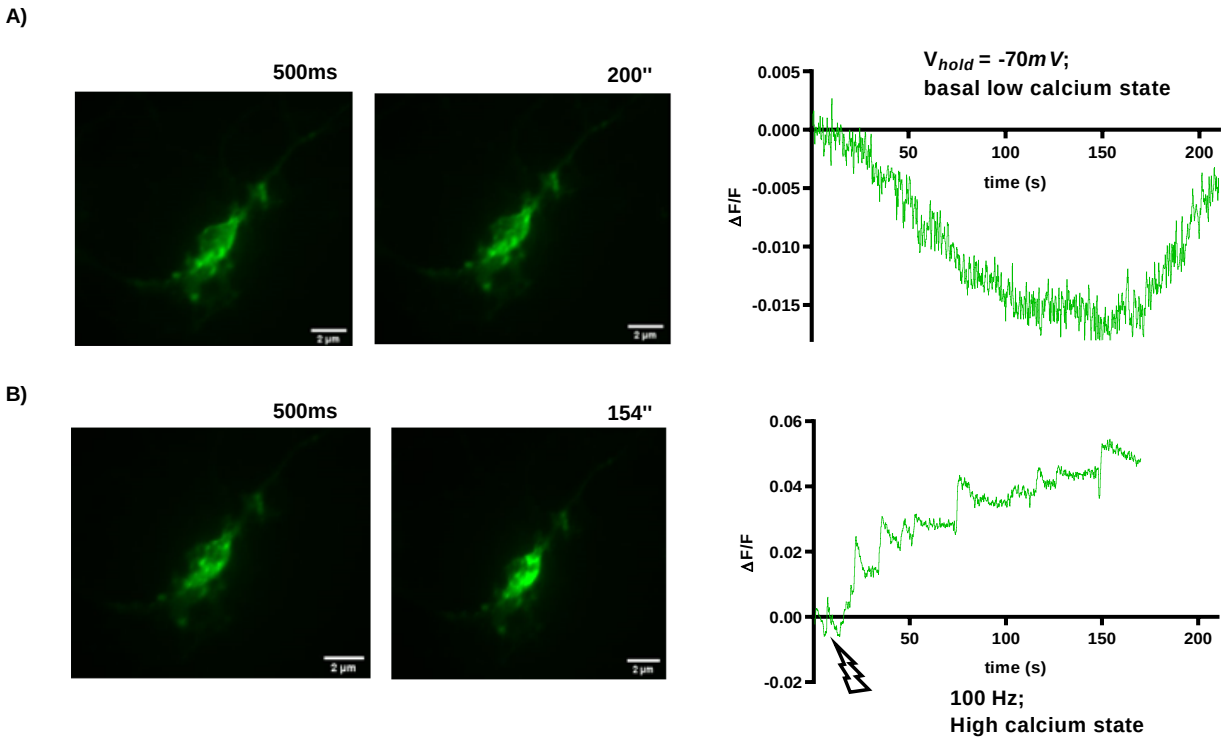

Figure 21. 100 Hz stimulation leads to an enhanced release of CD63-pHluorin positive EVs. A) No significant change in fluorescent signal was found at a V_{hold} = -70mV. Panels showing neuron at 500ms and 200 seconds. Changes to fluorescent signal over the time are depicted in the plot B) A 100 Hz stimulus given to the neuron induces a significant change to the fluorescent signal. Panels showing neuron at 500ms and 154 seconds after the 100 Hz stimulation. Plot illustrating the intensity changes to CD63-pHluorin florescence over the time.

The abate rate of success for HFS-evoked MVB-PM fusion motivated us to investigate regulators of exosome release. In this pursuit, we investigated the effect of many factors ranging from chemicals to biomolecules. However, in this thesis we only present the effects of growth factors on hippocampal neurons in context to the EV release. Among growth factor treatments, only neurons treated with bFGF (50ng/ml), BDNF (25ng/ml) and NGF (50ng/ml) showed a significant enhancement of CD63-pHluorin fluorescent signal in response to a HFS (**Figure 22**). Across the neuronal populations, 63.265% (n=49) of bFGF treated, -43.478% (n=23) of BDNF and 10.5% (n=19) of NGF treated neurons were found to exhibit enhanced signal intensities in response to electric stimulation. We further assessed these neurons for the effects of treatments on bioelectric activity and found regular firing patterns in accordance with the published literature [135]. The representative trace depicting spiking bursts in a growth factor treated, CD63-pHluorin overexpressing neurons is shown in **Figure 23A**, obtained under current-clamp. We found normal patterns of spontaneous synaptic activity in these neurons as depicted in a representative trace obtained under voltage clamp (**Figure 23B**). The current-voltage relationship analysis for stimuli ranging

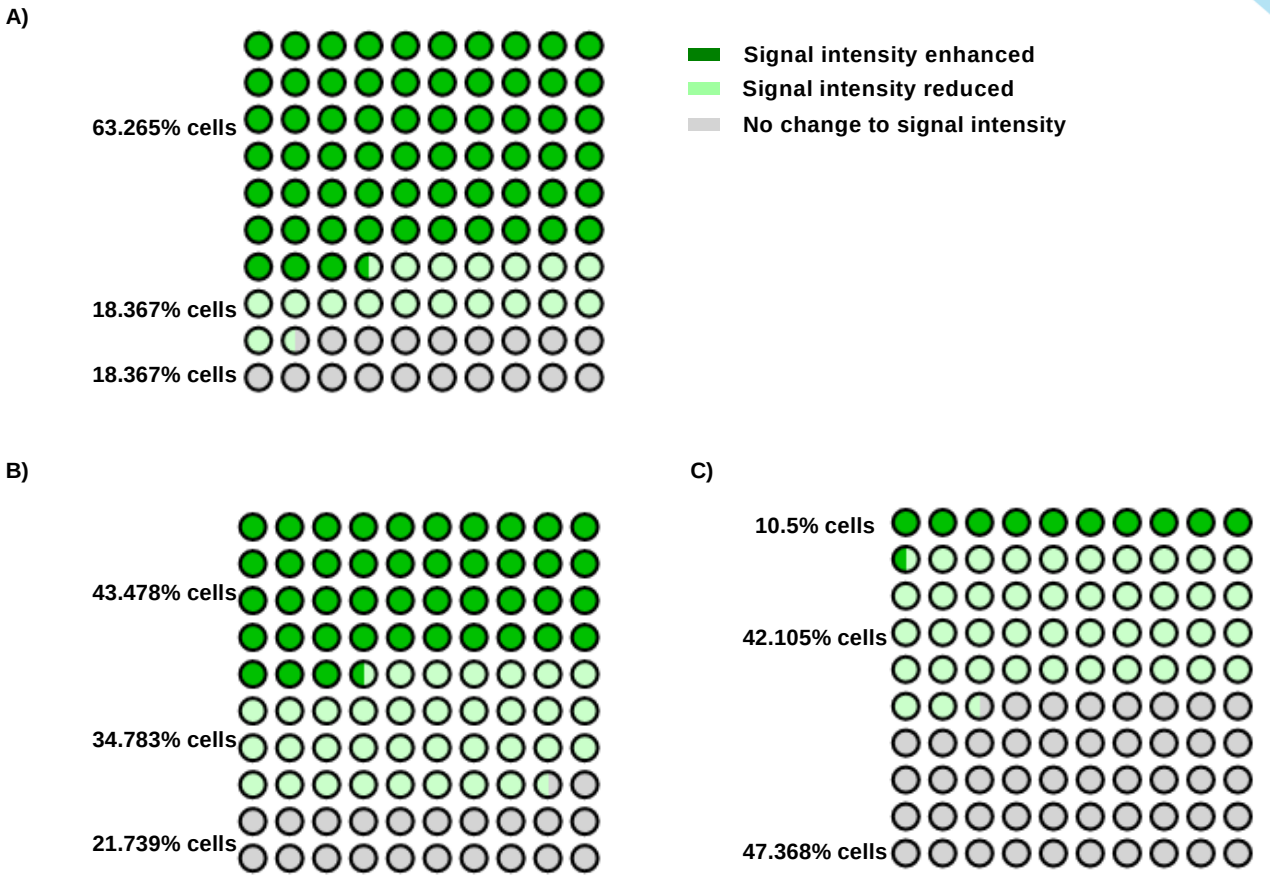

Figure 22. HFS stimulus-evoked MVB-PM fusion events are found in neurons in response to bFGF, BDNF and NGF application but with a higher rate for bFGF treatment. A) 63.265% of bFGF-treated neurons showed an enhanced CD63-pHluorin signal (n=49) B) A population of 43.478% BDNF treated neurons exhibited an enhanced CD63-pHluorin fluorescent signal (n=23), when subjected to HFS C) A relatively low rate of enhanced fluorescent signal of CD63-pHluorin, 10.5% was found for NGF treated neurons (n=19) in response to an HFS, indicating a low rate of stimulus-evoked MVB-PM fusion event.

from -50mV to 50 mV has reflected no significant alterations to the components of membrane contributing to bioelectric properties e.g. currents flowing across the membrane in these neurons (**Figure 23C**; WT (n=16), Veh (n=15), bFGF (n=11), BDNF (n=10) and NGF (n=13)), a separate further investigation is needed to illustrate the contributions of various individual channels to delineate the existence of such an equilibrium among the treatment conditions and is beyond the scope of this work. To perform NTA we have collected the culture media for the NTF treatment conditions from the neurons by maintaining similar culture conditions during the collection of respective samples. NTA results confirmed a significant increase in particle concentration across the three treatment conditions (**Figure A1.1**). We found no significant changes in particle size in response to the growth factor treatments. Conclusively, from the unaltered voltage current relationship, a high but not a 100% success rate of MVB-PM fusion events

among the treated neurons suggest that the main influence of growth factor treatment is intrinsic and is carried out mainly by preparing intracellular physiological conditions more favorable for enhanced availability of MVBs which can be released after a pulse of HFS.

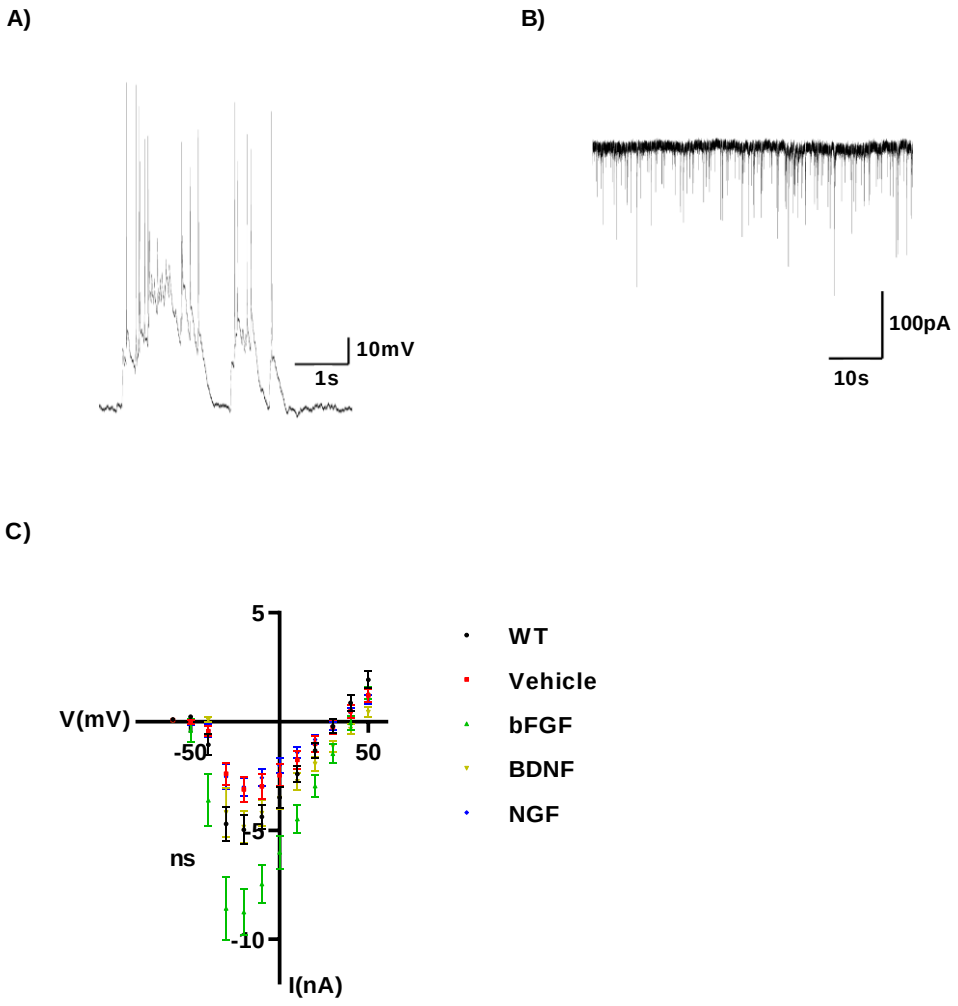

Figure 23. No significant current-voltage alterations were found among the various growth factor treatments. A) Representative current-clamp trace from a bFGF-treated CD63-pHluorin overexpressing neuron B) Trace showing normal spontaneous EPSCs in the same neuron C) I/V curves from bFGF (n=11), BDNF(n=10), NGF(n=13), CD63-pHluorin overexpressing (Veh) (n=15) and wild type (WT) (n=16) cells. No significant alterations were found in response to membrane depolarizing voltage command steps between -50mV to 50mV.

3.3.2. bFGF regulates exosomal release

Indicative from our electrophysiological results, we found the highest HFS-responsive neurons among the bFGF-treated population and therefore started to explore them further for EV release. Primary hippocampal cultures at DIV 9-14 were used for these experiments and two conditions were compared i.e., WT and bFGF-treated neurons (50 ng/ml). Exposed to an HFS, these neurons showed an enhanced

fluorescent signal in a time span of minutes with a half maximal time of $t_{1/2}$ = 117.8 ± 2.67 s; n = 17 (**Figure 24A** and **B**). At low basal calcium levels (i.e., V_{hold} = -70mV), we observed no change to the CD63-pHluorin signal intensity in WT and bFGF-treated conditions (**Figure 24B** and **C**). We found most of the bFGF-treated neurons 63.265% (n=49) exhibiting increased fluorescent signal at high calcium levels (i.e., HFS condition) (**Figure 24D**).

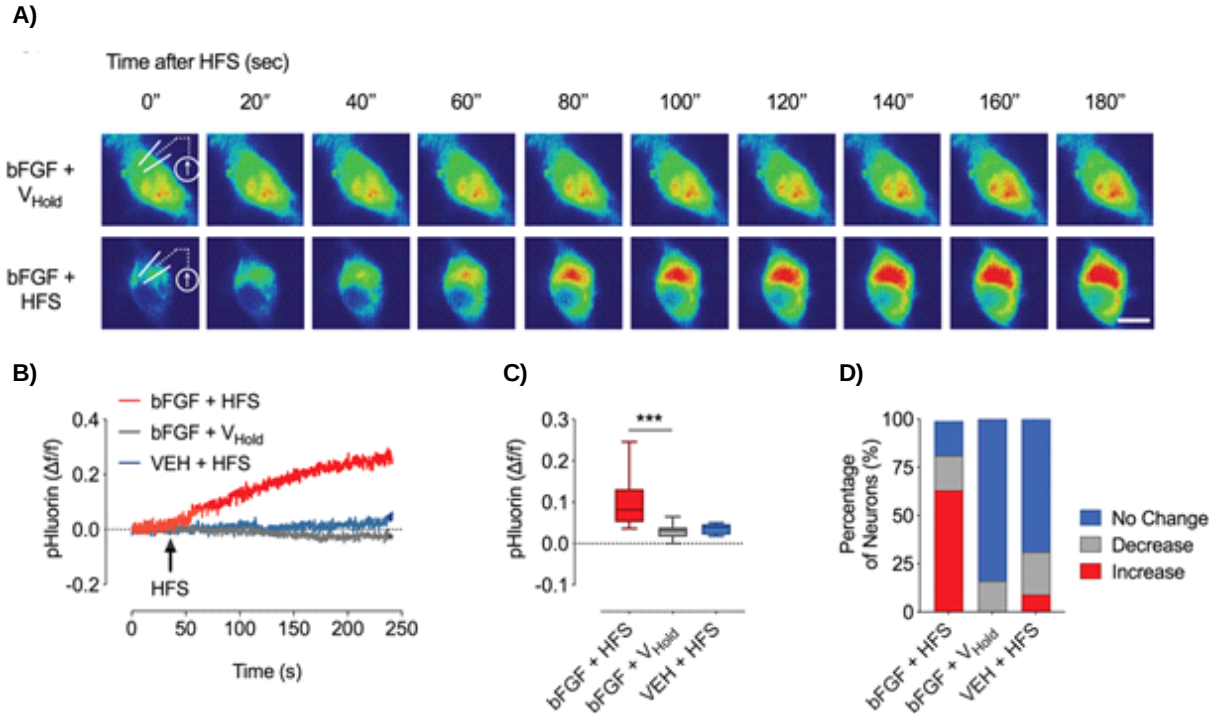

Figure 24. bFGF promotes HFS-evoked MVB-PM fusion events. A) The pseudo-colored panels illustrate an enhanced fluorescence signal in bFGF-treated neurons after HFS. B) Intensity signal profiling of an enhanced CD63-pHluorin fluorescence after HFS in VEH- and bFGF-treated neurons compared to unstimulated cells (V_{hold}). C) Box plot showing the average maximal fluorescence in response to a HFS (number of cells/conditions: bFGF + HFS vs bFGF V_{hold}; n = 17 and 10; p = 0.0007). D) Bar graph demonstrating the relative proportion of neurons that exhibited an increase or decrease of fluorescence or no change in response to a HFS in the same groups (number of cells/condition (bFGF + HFS; n (increase) = 31, n (decrease) = 9, n (no change) = 9 (n total = 49); bFGF + V_{hold}; n = n (increase) = 2, n (decrease) = 1, n (no change) = 7 (n total = 10); VEH + HFS; n = n (increase) = 1, n (decrease) = 1, n (no change) = 9 (n total = 11), respectively). Data are shown as mean ± SEM, a two-tailed unpaired t-test was used in (c). ***p < 0.001. (Published and adapted from [136]).

It is evident from the enhanced fluorescent signal, that bFGF-treated neurons encounter several MVB-PM fusion events at increasing rates but there is a possibility that the treatment reverses the pH (shifting to basic) in the MVB lumen, therefore illuminating the fluorescent tag. We resolved this by comparing the signal intensity of WT and bFGF-treated neurons by normalizing against a state of maximal signal intensity and found that bFGF maintains an acidic pH (data not shown please refer to [136] for details), suggesting that MVB-PM fusion causes the increase in fluorescence instead of a pH shift in the MVB-

lumen. Our confocal microscopy results showed bigger sized CD63-pHluorin puncta in bFGF treated neurons (n=10/condition) (**Figure 25A**). However, electron microscopy (EM) results recorded no significant difference in CD63-pHluorin positive MVBs (WT; n =16 and bFGF treated neurons; n = 21). Though a trend towards higher MVB number was observed and may require a bigger sample size for much clear assessment (**Figure 25B**).

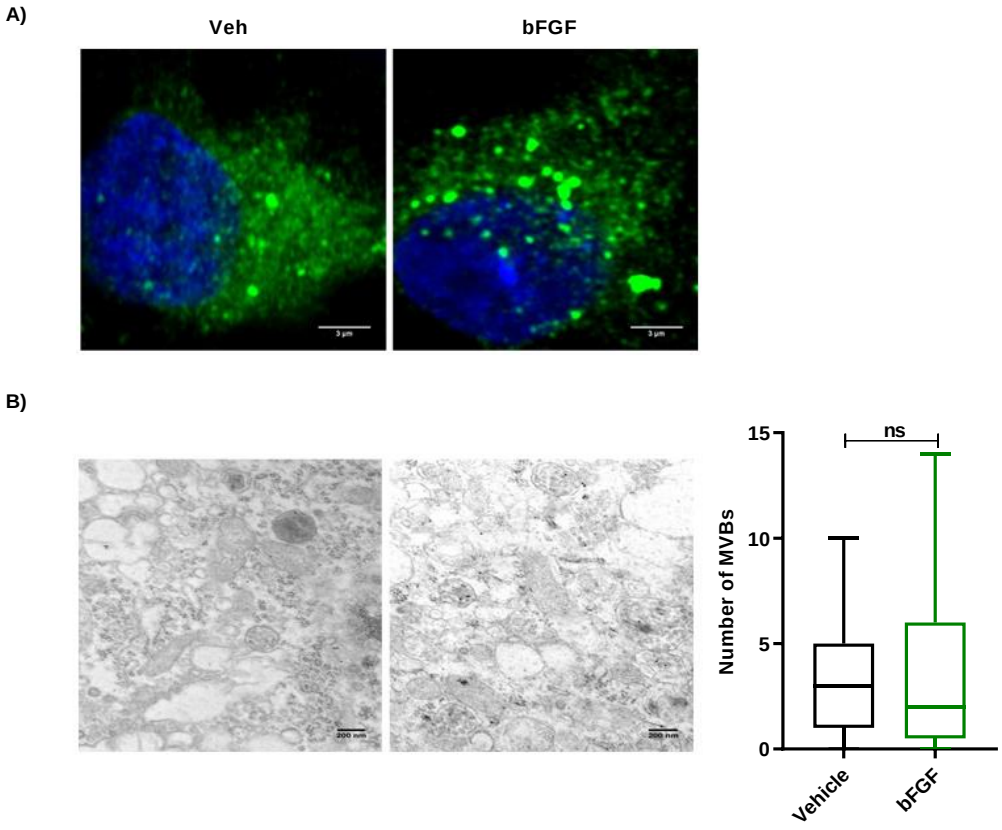

Figure 25. bFGF-treatment results in a trend of greater number of CD63-pHluorin puncta but no significant change to number of MVBs A) Confocal image showing more CD63-pHluorin positive punctate in bFGF-treated neurons (n=10) as compared to the vehicle (Veh) condition (n=10) B) Electron micrographs of Veh (n=16) and bFGF-treated neurons (n=21). No significant difference was found in the number of MVBs. Data are shown as mean ± SEM. For comparison, a two-tailed unpaired t-test was used in (A), and (B) and a paired t-test was used *$p < 0.05$.

The bFGF-induced release was further examined by NTA for which we collected the culture media from the neurons of similar age as for electrophysiology or imaging experiments after treatment with same bFGF-dose. We found a significant increase (n = 11 and 15 samples/condition; $p < 0.001$) for the particle concentration in bFGF-treated cells (**Figure 26A** and **B**). There was no significant difference in the average particle size (average particle size = 130.2 ± 3.15 nm) (**Figure 26C**). To answer the question how bFGF may mediate such an effect, we treated the neurons with Genistein (GEN) (50µM), which is an inhibitor of receptor tyrosine kinases-mediated activity. GEN treatment significantly reduced the number

of particles per milliliter in the media (**Figure 26D** and **E**), whereas we observed no significant effect to the size of the exosomes (**Figure 26F**). A long-term co-application of 1µM BAPTA normalized the effects of bFGF on EV release, suggesting a calcium dependency of such a release (**Figure 26G** and **H**) and had no effect on the size of EVs (**Figure 26I**). We further examined the EV-related biomarkers (Alix, CD81 and **pHluorin** (GFP)) in EV pallets obtained from VEH, bFGF and bFGF with a co-application of BAPTA (**Figure 26J**). The expression level quantification confirmed the NTA findings (**Figure 26K**). These results clearly established that a long-term treatment of neurons with bFGF leads to the enhanced EV release in a calcium dependent manner without affecting vesicle size.

3.3.3. SNARE proteins mediate bFGF regulated exosomal release

Concordant to the assertion that the bFGF led abundance of MVB membrane proteins would be replicated by the enriched EV membrane as well, from the logic of their biogenesis via inward budding has motivated us to perform mass spectrometry (MS) analysis. For each condition (bFGF and Veh; n=6) EV pellets were isolated and subjected to MS-analysis. In total, 2258 differentially expressed proteins (DEPs) were identified from our MS analysis (PRIDE data ID: PXD014401). These DEPs were further analyzed by adapting them to a pipeline as shown in **Figure 27A**. Principal component analysis (PCA) and hierarchical clustering analysis demonstrated a clear segregation among the treatment conditions and a DEP expression pattern (n=705; FDR<0.05) in terms of up/down-regulated proteins was reported respectively (**Figure 27B** and **C**). 441 proteins were found with a fold change of 1.5 or more and were significantly (p-value < 0.05) upregulated (n=235) or downregulated (n=206) after bFGF application (**Figure 27D**). A strong enrichment of the biological pathways “import into cell”, “vesicle mediated transport” and its regulation was found for these proteins (**Figure 27E**). The interactions of the candidate proteins were studied via a network analysis approach and a protein-protein interaction (PPi) network was developed (**Figure 27F**). Using hub-detection techniques, we identified 53 key proteins (**Figure 27G**). The hub proteins were detected from the network topological parameters via centrality analysis. The topological centrality measures 1) degree 2) stress 3) betweenness and 4) closeness were considered, resulting vesicle-SNAREs (v-SNAREs), vesicle associated membrane proteins 2 and 3 (VAMP2 and VAMP3) among the top hub proteins (**Figure 27G**). Notably, the abundance of these v-SNAREs was reciprocally influenced by bFGF

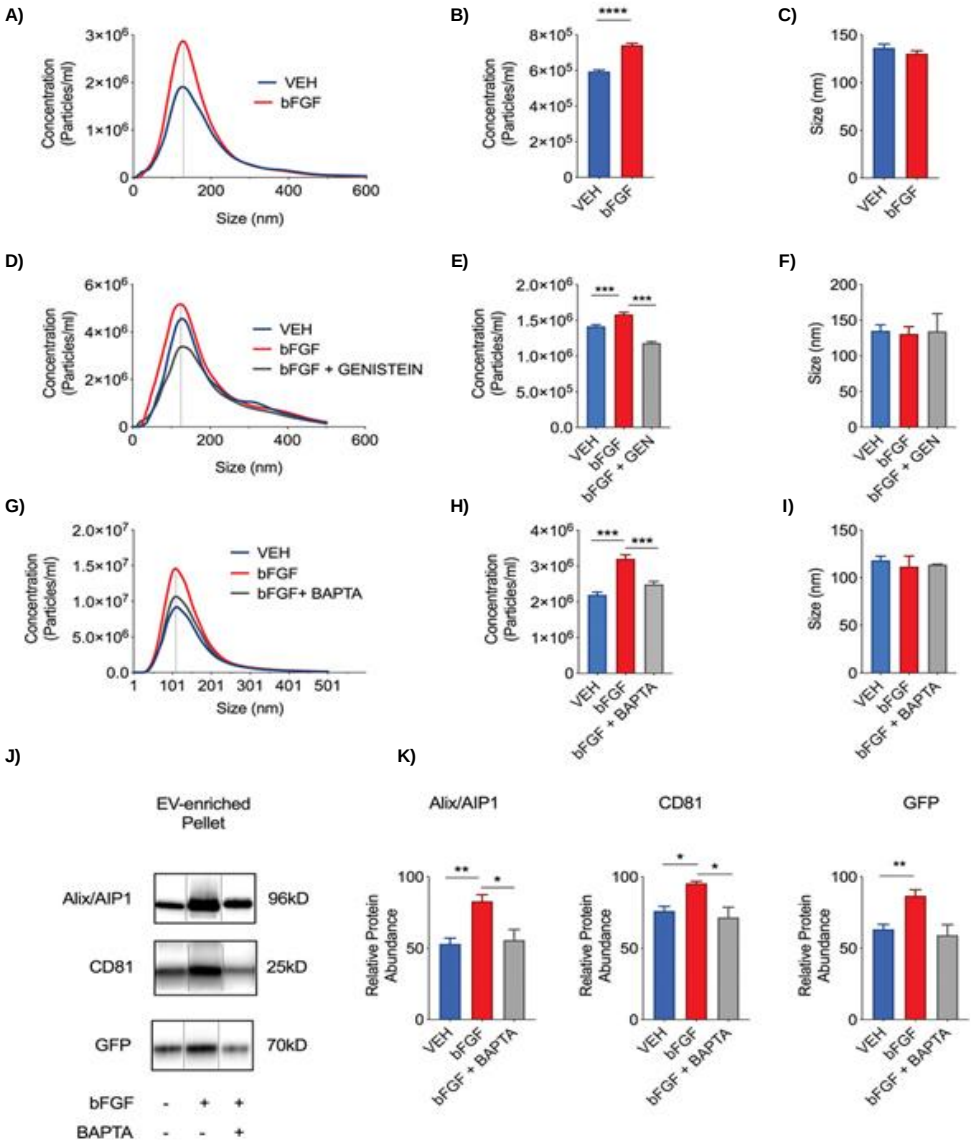

Fig.26. bFGF-treated cultured hippocampal neurons release EVs in a calcium and tyrosine kinase-dependent manner. A) Nanoparticle tracking analysis (NTA) showing the mean number of particles/ml vs particle size in the cell culture medium of bFGF- or vehicle (VEH) -treated hippocampal neurons. B) Bar plots demonstrating an increased particle number in bFGF-treated neurons (n = 11 and 15 samples/condition; $p < 0.001$). C) bFGF has no significant effect on the average particle size ($p = 0.2687$). D) NTA illustrating the number of particles/sizes in medium from bFGF or VEH-conditions with or without co-application of 50 µm genistein (GEN). E, F) GEN reduces the bFGF-induced increase in particle number but had no effect on the size of particles (n = 5 samples/condition; $p < 0.001$). G) NTA results illustrating the amount of particles/size in medium with or without co-application of 1 µm BAPTA-AM. H, I) BAPTA-AM normalized the bFGF-induced increase in particle number but had no effect on the size of particles (n = 3 samples/condition; $p < 0.001$). J) Western blot confirming the abundance of CD81, Alix/AIP1, and GFP in the EV-enriched pellet of cell culture medium from bFGF and VEH-treated cells with or without co-application of 1 µm BABPTA-AM. K) Bar plot quantifies an increase of CD81, Alix/AIP1, and GFP in the EV-enriched pellet of bFGF-treated neurons (VEH vs bFGF: n = 5; $p = 0.0006$ for CD81, $p = 0.0013$ for Alix/AIP1, $p = 0.0028$ for GFP). Co-application of BABPTA-AM normalized the bFGF-induced increase in these proteins in the EV-enriched pellet. Data are shown as mean ± SEM. For comparison, a two-tailed paired t-test was used in (B) and an unpaired t-test in (E, H, I) ***$p < 0.001$, **$p < 0.01$, *$p < 0.05$ (Published and adapted from [136]).

treatment, which was found to be interacting with other SNARE proteins and proteins involved in vesicle fusion machinery (**Figure 27H**).

3.3.4. VAMP3 regulates bFGF enhanced EV release

From the roles of v-SNAREs in controlling the cellular fusion machinery and their altered expression levels after bFGF treatment, we hypothesized about their role in controlling MVB-PM fusion events.

Therefore, we first assessed the levels of VAMP2 and VAMP3 in bFGF-treated neurons via Western blotting (**Figure 28A**) and found that VAMP2 levels were reduced in the cell lysate without a significant change to VAMP3 levels (**Figure 28B** and **C**). Similarly, we looked for their abundance in EV pellets and found VAMP3 specifically enriched to a significant level (**Figure 28D** and **E**). Therefore, we further decided to study the effect of VAMP3 on EV release. To do so, we applied siRNAs to knock down (KD) VAMP3 as confirmed via Western blot in **Figure 28 F** and **G**. We therefore assessed the abundance of EVs released to the culture medium in Veh and bFGF treated neurons with or without knocking down VAMP3. Culture media was collected from these conditions and NTA was performed. Our results showed fewer particles in the culture media from VAMP3-deficient cells (**Figure 28H** and **I**). We found that the size of particles remained unaffected in response to VAMP3 KD conditions (**Figure 28I**). Therefore, these results suggest that VAMP3 has a role in the molecular mechanisms prevailing bFGF-enhanced EV release. Furthermore, considering the reciprocal expression of VAMP2 and VAMP3 together with EV release, it can be speculated that these molecules can pave a way forward to distinctively identify various vesicle populations and their molecular signatures.

3.3.5. A spectrum of EV biomarkers is affected by bFGF treatment

The EV concentration in bFGF-treated VAMP3 KD neurons was found to be elevated as compared to the EV-concentration in the VAMP3 KD condition suggesting a partial regulation of EV release by VAMP3 (**Figure 28I**). Such variations may account for the enrichment of individual EV-proteins varying from vesicle to vesicle without affecting the number of EVs. Therefore, we assessed the expression levels of the top 100 Exocarta, EV-abundant proteins in our MS data (**Figure 29**). We found that bFGF treatment had a differential effect on the abundance of EV biomarkers suggesting a fold change of ≈ 10 to some of the candidates. The differential expression of EV-biomarker proteins may be due to the differential enrichment of these markers to different vesicle populations which needs further investigation.

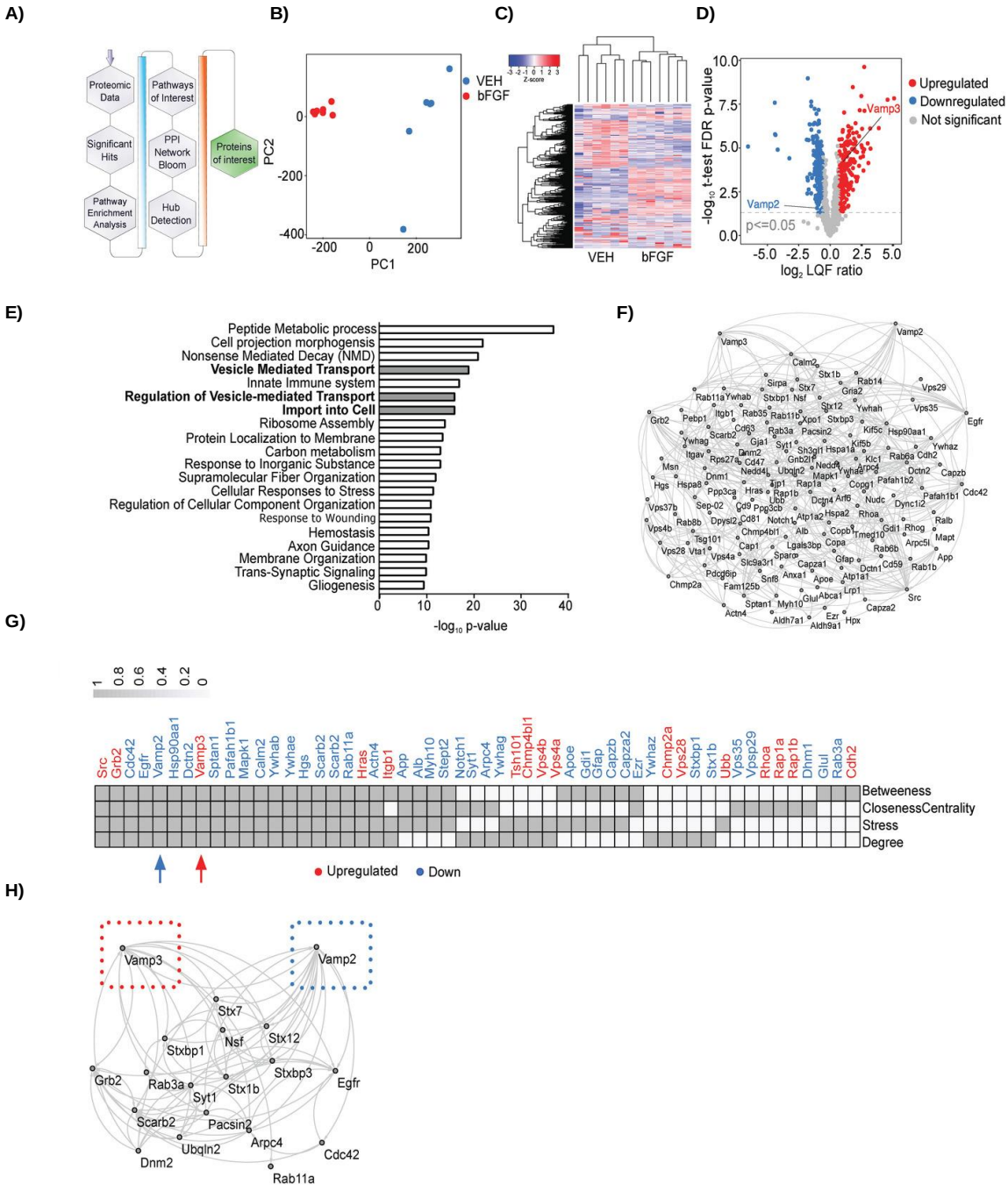

Figure 27. bFGF-evoked EV release is regulated via modulating the SNARE protein abundance. A) The workflow pipeline adapted to analyze proteomic data B) PCA showing clear segregation between the treatment conditions (bFGF vs VEH). C) Hierarchical clustering heat map showing the relative expression levels (z-score and log2-transformed LFQ protein intensities) of 705 differentially abundant proteins (FDR < 0.05) in EVs. Each column represents a replicate of either treatment condition, each row corresponds to a differentially abundant protein. D) Volcano plot (−log10 transformed p-value, −log10 (0.05) = 1.30) showing up (red) and down (blue) regulated statistically significant proteins. E) Bar diagram showing the significantly enriched biological pathways based on Gene Ontology, Reactome, and KEGG resources. F) Protein-protein interactions (PPi) network of abundant proteins G) Top 53 hub proteins based on four centrality measures of network topology. H) PPi network showing interaction partners of SNARE proteins; VAMP2 and VAMP3 (Published and adapted from [136]).

3.4. Growth factors and Lewy body pathophysiology

3.4.1. bFGF induces changes to the cell lysate and extracellular vesicle proteome

Studies show that components of LBs get sequestered in exosomes [51] and it is also known that growth factors trigger the common downstream molecular signaling pathways at plasma membrane. Therefore, we adapted to a system level approach to investigate the overall effect of bFGF on EV-release and its implications to LBP. We developed a pipeline to analyze the bFGF induced protein abundance and expression in our MS data for both CL-EV samples along with the molecular interactions between neuronal CL and released EV content relevant for LBP (**Figure 30A**). At least triplicates of biological samples were used to obtain MS datasets with a strong correlation coefficient ranging between ($r \sim 0.98$-1) denoting strong reproducibility among the samples (here, Pearson correlation results are not included but published in [137]). The samples were found clearly separable according to our PCA results with 86.8% of variance holding up to an individual component percentage of PC1=82.03%, PC2=3.47%, PC3=1.37% (**Figure 30B**). A similar segregation among the samples was also confirmed via Euclidian distance based hierarchical clustering ((**Figure 30B**). In total 5314 proteins were identified in the CL and 2258 proteins were identified in EVs, out of which 1660 CL and 650 were EV-significant DEPs. These proteins were then used to develop co-expression modules from data specific to our samples such that the bFGF-induced LBP-relevant interactions during the enhanced EV-release could be delineated.

3.4.2. Development of protein-protein interaction networks among co-expressing proteins and pruning their LBP associations

Sample-specific interaction networks were developed using a WPCNA method among the significant DEPs. Our CL-MS dataset yielded nine modules and EV-MS dataset analysis resulted in four modules, representing the direct interactions of co-expressed proteins (**Figure 31A**). CL modules M2-M8 (M_{CL2}, M_{CL8}) and EV modules M1, M2, M3 (M_{Ev1}, M_{Ev2}, M_{Ev3}) showed the maximum abundance of significant DEPs (**Figure 31B**). Since WPCNA represents modules as a weighted expression profile (Eigen protein) of co-expressed proteins, we therefore computed module eigen-protein values to test the expression pattern of individual modules. This resulted in M_{CL2}, M_{Ev2} and M_{Ev3} as the modules with most abundant DEPs as compared to M_{CL8} and M_{Ev1} (**Figure 31C**). The module preservation assay confirmed the modules with a Z-summary score > 10 as the most preserved co-expressed networks. The modules were then explored and mapped for PD-related proteins pertaining to LBP by intersecting the identified candidates from the published literature in a reverse-tracing manner. Modules M_{CL2}, M_{CL8} and M_{Ev1}, M_{Ev3} were found to be significantly (BH corrected P-value ≤ 0.05) enriched for LBP related proteins (**Figure 31D**).

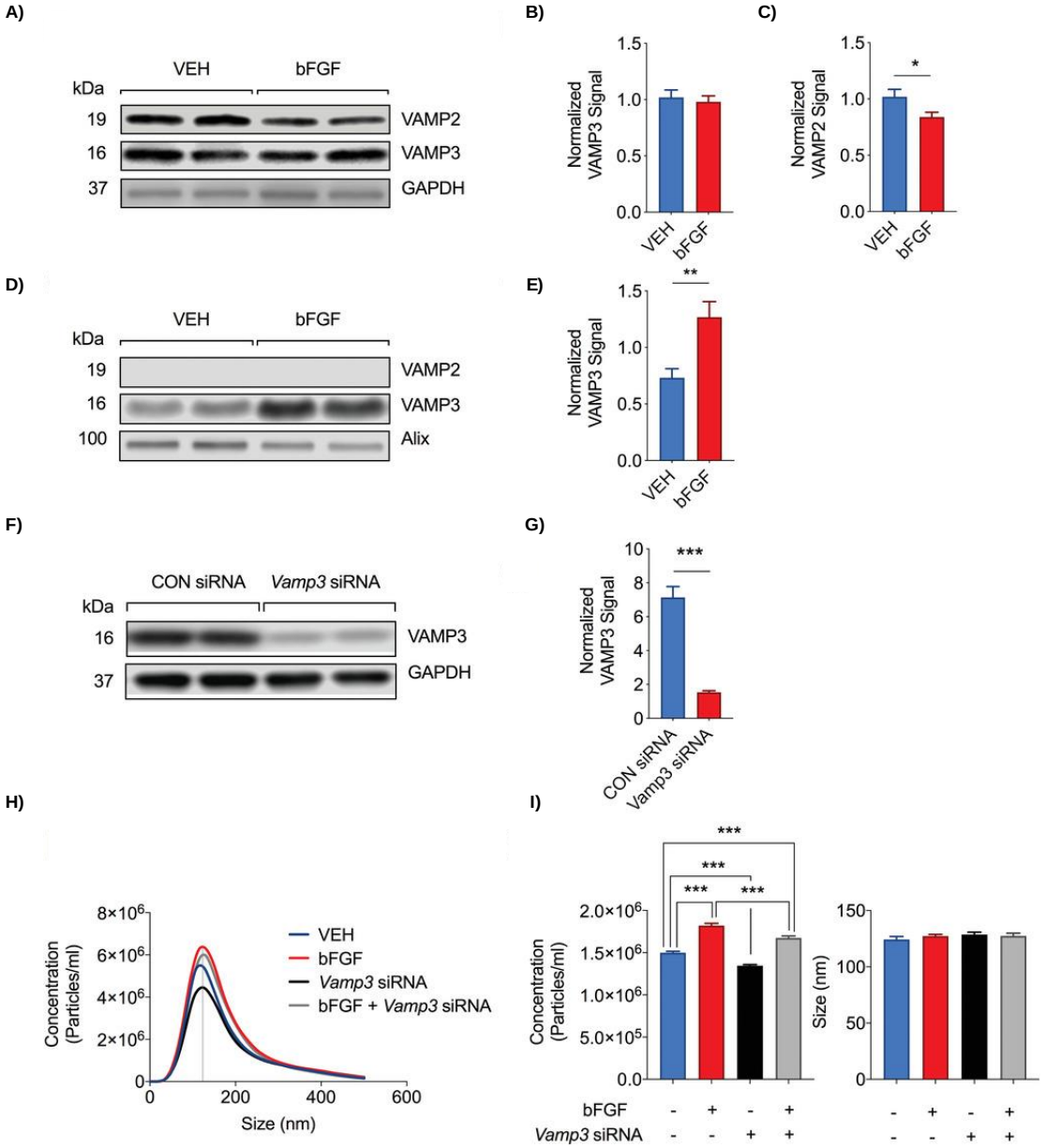

Figure 28. VAMP3 mediates the bFGF-induced increase in EV release. A) The abundance of VAMP2 and VAMP3 in cell lysates is shown via Western blot. B, C) VAMP2 is decreased in neuronal cell lysates in response to bFGF-treatment, whereas the expression level of VAMP3 remains unaffected (n = 26/condition; VAMP3: p = 0.6541; VAMP2: p = 0.0252). D) Western blot confirming the abundance of VAMP2 and VAMP3 in EV-enriched pellets for bFGF- and VEH conditions. E) bFGF increases the VAMP3 level in EVs released from cultured neurons, whereas VAMP2 is undetectable in neuronal EVs (n = 12/condition; p = 0.0027 F, G) Western blot and bar graph illustrating the knock-down of VAMP3 in response to treatment with Vamp3 siRNAs (n = 12/condition; $p < 0.001$). H) Averaged curves from NTA illustrating the number of particles/sizes in the cell culture medium of bFGF or VEH-treated hippocampal neurons with or without co-application of Vamp3 siRNAs. I) Bar graph illustrating a reduced number of EVs in neurons pre-treated with Vamp3 siRNA (10 nm for 48 h). Co-application of Vamp3 siRNAs partially prevents the bFGF-mediated increase in EVs (VEH vs bFGF vs Vamp3 siRNA vs bFGF + Vamp3 siRNA: number of samples/condition n = 24 vs 12 vs 24 vs 12; $p < 0.0001$). bFGF or Vamp3-siRNAs has no effect on the size of EVs as depicted in NTA. Data are shown as mean ± SEM. For comparison, a two-tailed unpaired t-test was used in (C), (E), and (G) and a paired t-test was used (I) ***$p < 0.001$, **$p < 0.01$, *$p < 0.05$. (Published and adapted from [136]).

These proteins were then subjected to a biological pathway enrichment analysis and based upon the up/down-regulated expression of proteins in a module, we identified the most significant LBP-related up/down-regulated biological pathways influenced by bFGF treatment (**Figure 31E**).

3.4.3. High bFGF level triggers a linearized up/down-regulation of protein expression

We compared the proteomic profiles in CL-EV modules to illustrate the bFGF-induced differential signature. It was interesting to note that the bFGF-induced effects-maintained linearity across the proteomic expression, the proteins which were up/downregulated in the CL showed a similar expression pattern in the EV content. In **Figure 32** we showed some of the top proteins among the CL-EV modules. It remains elusive and is beyond the scope of current thesis, why and how such protein-expression patterns are maintained between two datasets and require further investigation.

3.4.4. High bFGF levels can manipulate the neurophysiological milieu in LBP

The **s**ystems level approach allows to connect the dots about the molecular intricacies of LBP across the datasets. Therefore, we developed a composite network (CN) among the modules of DEPs to examine the novel proteomic interactions incited by bFGF (**Figure 33**). We obtained a α-Syn pertinent CN because this protein is found to be central to LB composition [10].There were 20 proteins which we found in our datasets that were direct α-Syn interaction partners. Among those, we choose the candidates having interactions with LBP-related RNA binding proteins (LRBPs), LBP associated channels and receptors, common upregulated proteins among CL-EV modules and common down regulated proteins among CL-EV modules covering a wide spectrum of their involvement from neuronal periphery to its deepest physiological milieu. It is interesting to note that bFGF application exerts a CN which is heterogeneous in its composition considering the up/down-regulation of proteins and together with the fact of fluctuating growth factor levels over the time would therefore help to resolve the molecular basis for various stages of LBP.

In our bFGF guided CN we identified *Nptx2*, *Nedd4* and *Penk* as key up-regulated and *Scn2a*, *Gria2*, *Grin2b* and *Cnr1* as key down-regulated receptors and channels that may act as first line α-Syn interacting responders to a bFGF stimulus. Our data suggest many interactions for *Scn2a* and may be suggestive of a sodium channel-mediated mechanism in LBP at high growth factor levels. To dissect the aftermath of a bFGF trigger at a subcellular level, we identified the α-Syn interacting LRBPs in the CN. Our results included *Hnmph2*, *Eef2*, *Srp14*, *Gspt1*, *Ddx6*, *Lars*, and *Rps14* as key upregulated and *Aco1*, *Hnrnpa2b1*, *Hnrnph3*, *Fus* and *IIf2* as key downregulated LRBPs.

The localization of LRBPs to key subcellular locations is indicative of the reaching effects of bFGF in LBP in different cellular compartments. We found, e.g. *Eef2* localizes to the plasma membrane and cytosol, *Srp14* to nucleoli, *Gspt1* to the cytosol, *Ddx6* to cytoplasmic bodies, *Lars* to nuclear bodies, *Rps14* to the endosomal reticulum and cytosol, *Aco1* found in mitochondria and cytosol, *Eef2* localized to the plasma membrane and cytosol. The further interaction of these candidates with common up/down-regulated proteins across the CL-EV modules in CN provides a description of the interactive molecular scene for LBP accompanied by high growth factor levels. A detailed account of fold change for individual proteins and their interactions can be found in appendix-3 and 4.

3.4.5. bFGF-induced LB pathology associated molecular interactions and possible offshoot in the central nervous system

Exosomes act as freight devices for nervous system (NS) components by transporting bioactive material and LBs appear across the NS in a sequential manner. This led us to develop a theoretical framework of the molecular basis of such a phenomenon during LBP from our datasets, potentially following high growth factor levels. To do so, we back-traced brain region specific proteins to our LBP-modules and studied their interactions from the literature [138]. The key upregulated LBP associated brain region specific proteins were *Slc44a1*, *Adam10*, *Tln1* and *Ephx1* though the proteins *Syn1*, *Myo6*, *Ephb2* and *Eef1d* were downregulated as an effect of bFGF. The overall molecular framework was then calculated by comprising a network of their interactions with α-Syn interacting proteins in our dataset illustrating their direct importance for LBP (**Figure** 34).

We further added the direct interactions of LBP related brain region-specific and α-Syn-interacting proteins to this network, thus extending it to illustrate the possible interactions of proteins transported as EV content and their bilateral association with LBP related proteins in CL. This had enabled us with a molecular framework of consequences of EV transport in LBP encountered at higher growth factor levels which could possibly supplement the LB pathology spread depending upon the severity of PD stages. Detailed information about the fold change of individual proteins determining their up/down-regulated expression and respective interaction partners are charted in appendix-5 and 6.

3.4.6. bFGF affected LBP-proteins/interactions are predominantly associated to the neuronal protein metabolism

We performed biological pathway enrichment analysis to gauge the functional significance of the molecular interactions identified in the networks described above (**Figure** 35).

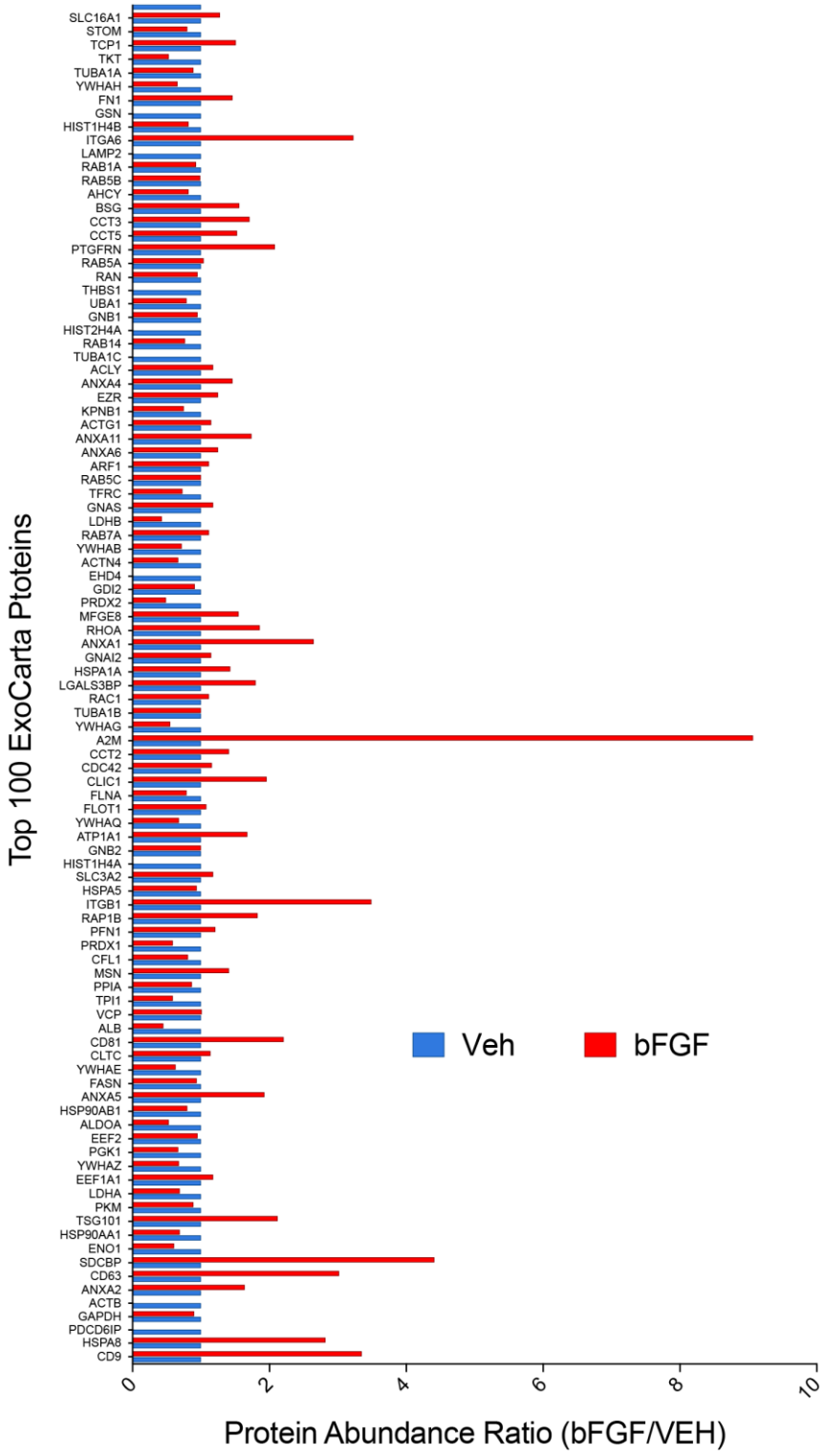

Figure 29. **bFGF-enriched EV-proteins.** The relative abundance of the ExoCarta (http://www.exocarta.org) top 100 EV-proteins from VEH (blue) and bFGF-treated neurons (red) evaluated in mass spectrometry (MS) analysis. The abundance of the listed proteins varies up to ~ 10-fold. Data are shown as mean value relative to the VEH condition (n = 6). (Published and adapted from [136]).

Interestingly the pathways such as protein refolding, protein localization to membrane, translation, lysosomal transport, protein targeting, protein stabilization and intracellular receptor signaling were found to be backed by upregulated LBP-proteins. The downregulated LBP-protein contributions were mainly found to be contributing to the pathways such as spontaneous synaptic transmission, glial cell activation, signal release, pre-synapse organization, neuro-transmitter transport, and glutamatergic synaptic transmission. It can be foreseen from these pathway enrichments that the predominant influence of high growth factor levels is largely restricted to intrinsic protein metabolism and are the most affected pathways during the LBP, therefore it would not be an exaggeration to expect a prominent exosomal involvement in a diseased state rather more effective in comparison to the other vesicular bodies that governs processes like neurotransmission.

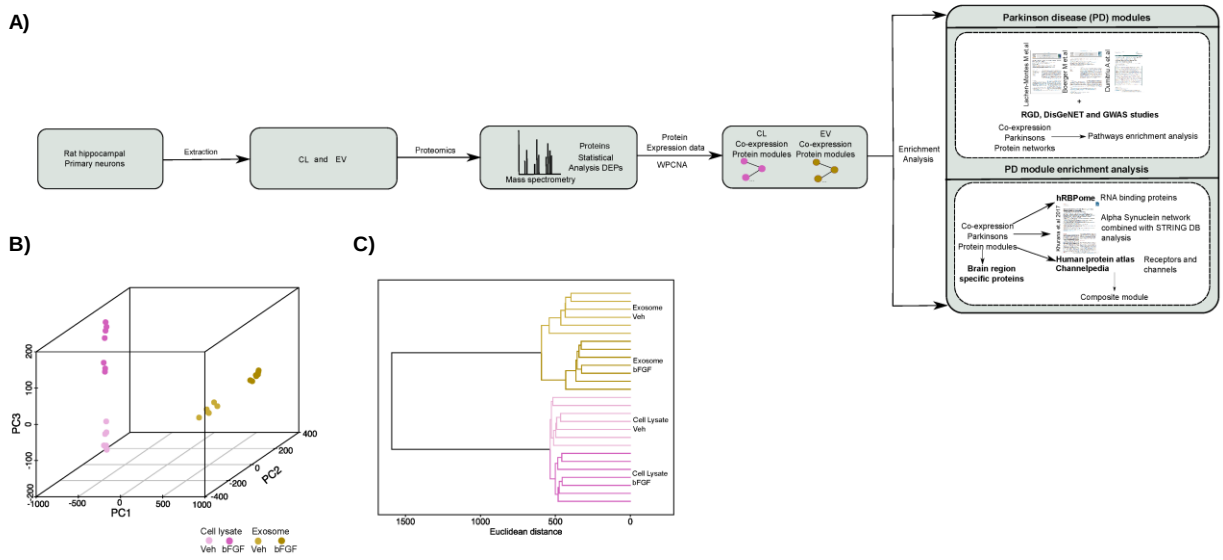

Figure 30.Pipeline used to analyze and validate the relevance of bFGF induced proteomic changes to Lewy body pathology (LBP) A) Work-flow adapted to analyze the mass spectrometer (MS) data from cell lysate (CL) and extracellular vesicle (EV) pellets B) Three dimensional plot of principle component analysis (PCA) showing 86.8% of variance (PC1=82.03%, PC2=3.47%, PC3=1.37%) C) Dendrogram representing hierarchical clustering based on Euclidean distance calculated from log2 LFQ intensities in MS data. (adapted from [137]).

The enrichment of protein metabolism related statistically significant (negative log10 $P \leq 0.05$) biological processes involved in neuronal processes other than neurotransmitter release and uptake by upregulated

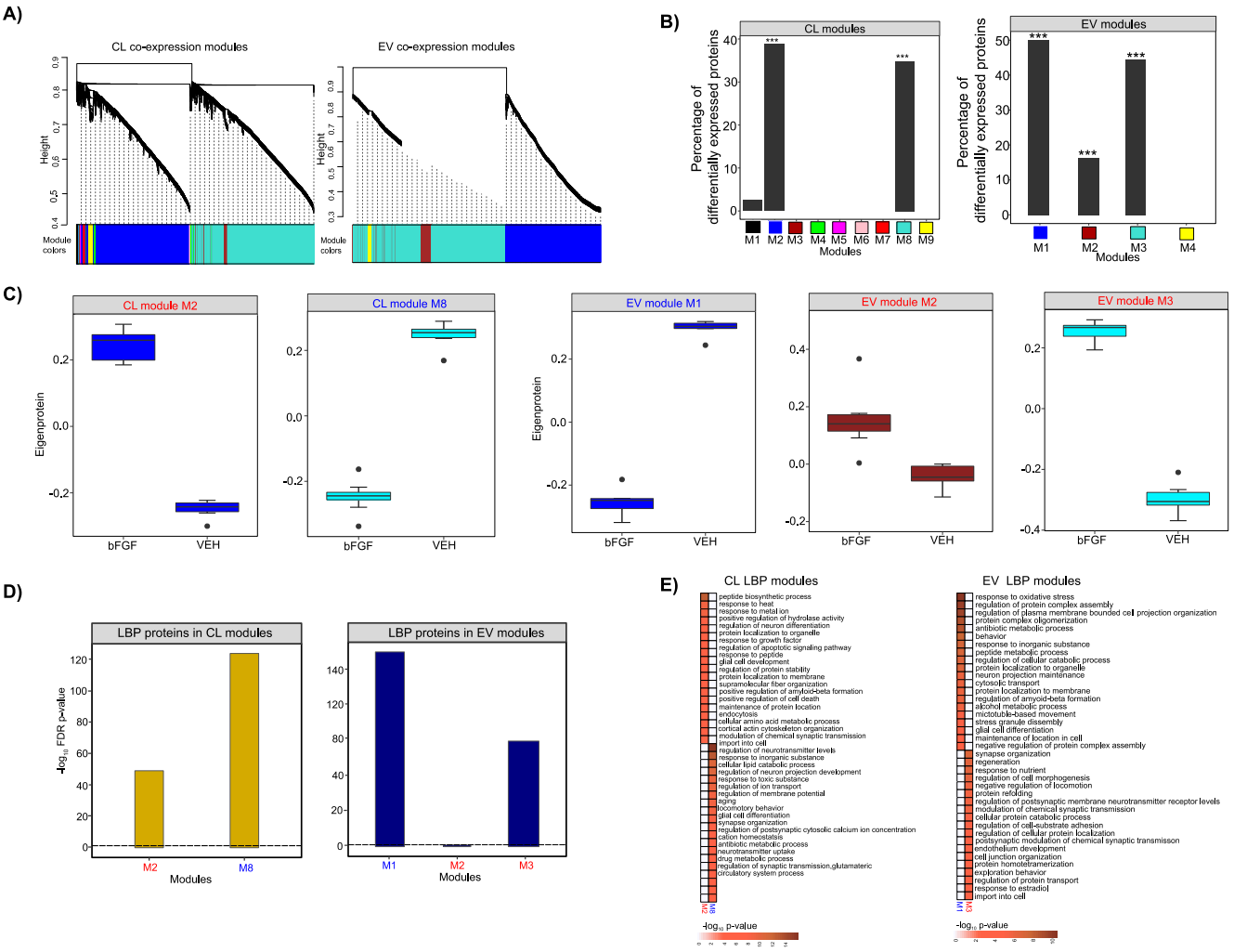

Figure 31. Weighted protein co-expression analysis (WPCNA) of bFGF-induced proteomic signature in cell-lysate (CL) and extracellular vesicles (EVs). A) WPCNA yields nine modules for CL proteins (n=5314) and three co-expression modules for EV proteins (n=2258) as represented in Dendrogram clusters. B) Represents the modules with differentially expressed protein (DEP) signature for both CL and EV modules where x and y axis denote the modules and percentage overlap of the DEP signature (*** $P \leq 0.01$, Negative log10 Benjamini–Hochberg-adjusted P-values; Fisher's exact test). C) Module expression profiles of 2 CL and 3 EV modules (Wilcoxon test P-value: 0.0034, 0.00094) respectively D) Showing modules with maximum proteomic signature relevant for Lewy body pathology (LBP) where y-axis denotes negative log10 Benjamini–Hochberg-adjusted P-values, Fisher's exact test and dotted line represents the statistical significance 1.31 comparable to the P-values ≤ 0.05). E) Showing the biological pathway enrichment of LBP proteins. (adapted from [137]).

α-Syn interacting receptors and channels allow to visualize their consequential significance in protein aggregation and contribution to α-Syn induced toxicity (**Figure** 35A). Thereby, asserts the role of high bFGF levels as a supplementary trigger in LBP that could influence the key protein-metabolism-associated molecular machinery. Furthermore, the statistically significant (negative log10 $P \leq 0.05$) enrichment of

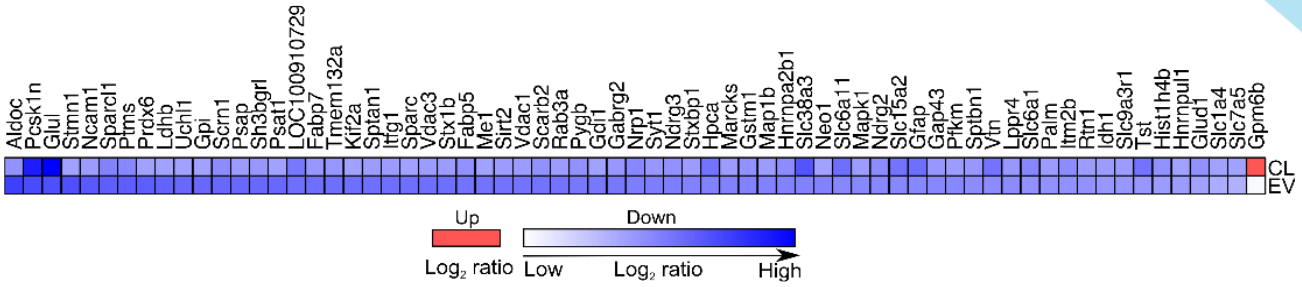

Figure 32. **bFGF results in a linearized protein expression in CL and EVs**. Heat-map exemplifying the candidate proteins following a similar pattern of up/-down-regulated expression in CL and EVs. The proteins down-regulated in CL are also down-regulated in EVs or vice versa hence adapting to a linearized fashion of exodus.

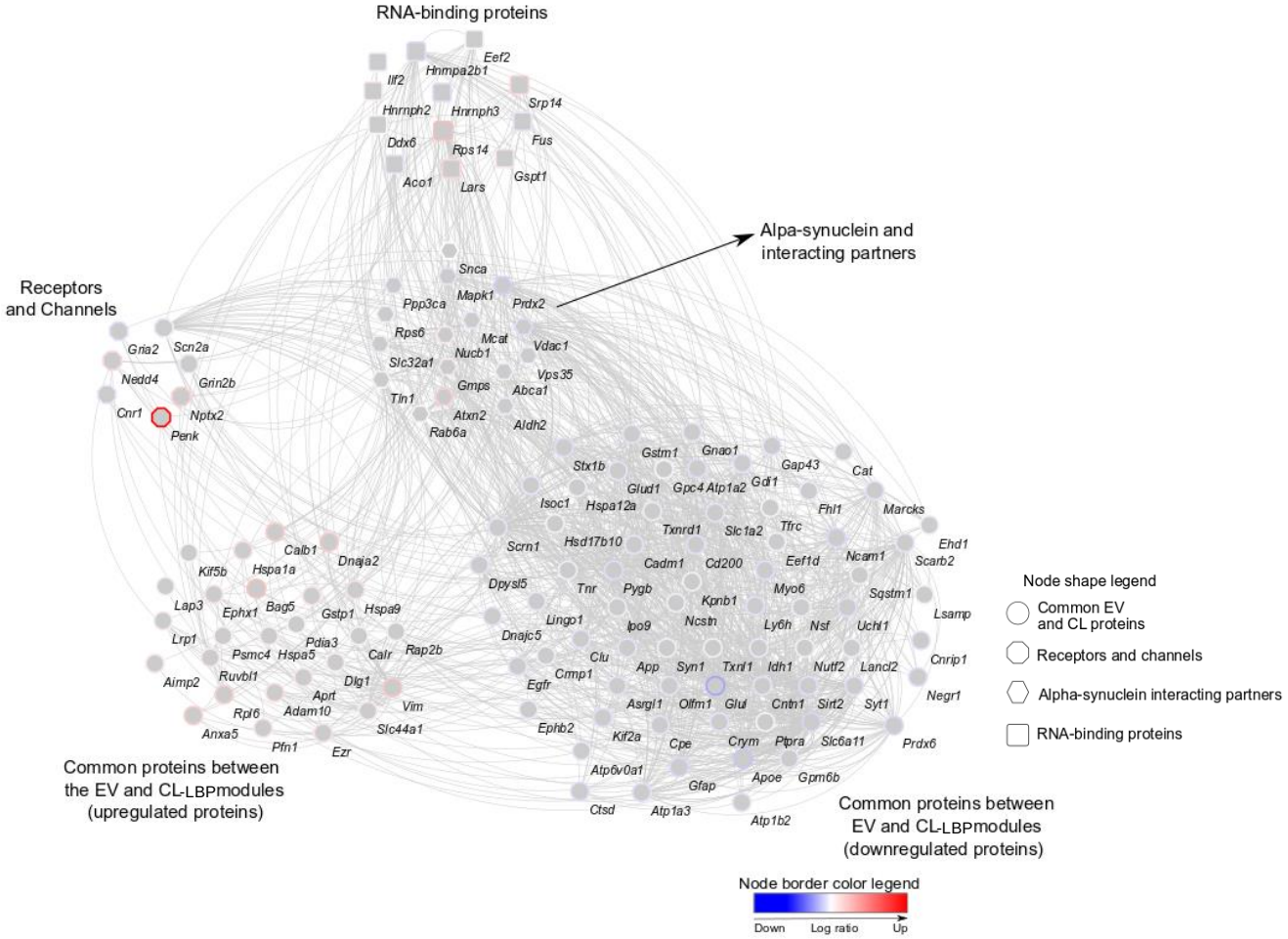

Figure 33. High bFGF levels exert an overwhelming influence on α-Syn-interacting proteins that are central to neuronal physiology. A composite LBP co-expression module (CM) illustrating the interactions between the common LBP proteins from CL, EV, including alpha-synuclein protein interacting partners and receptors, ion channel and RNA binding proteins. Note: Nodes are proteins but labeled with gene symbols. (adapted from [137]).

protein metabolism related pathways by upregulate brain region specific proteins together with α-Syn interacting partners in the CL and EV indicates the possible outreach of high bFGF levels (**Figure** 35B). In summary, these enrichments suggest a prominent involvement of bFGF influenced protein metabolism pathways in LBP.

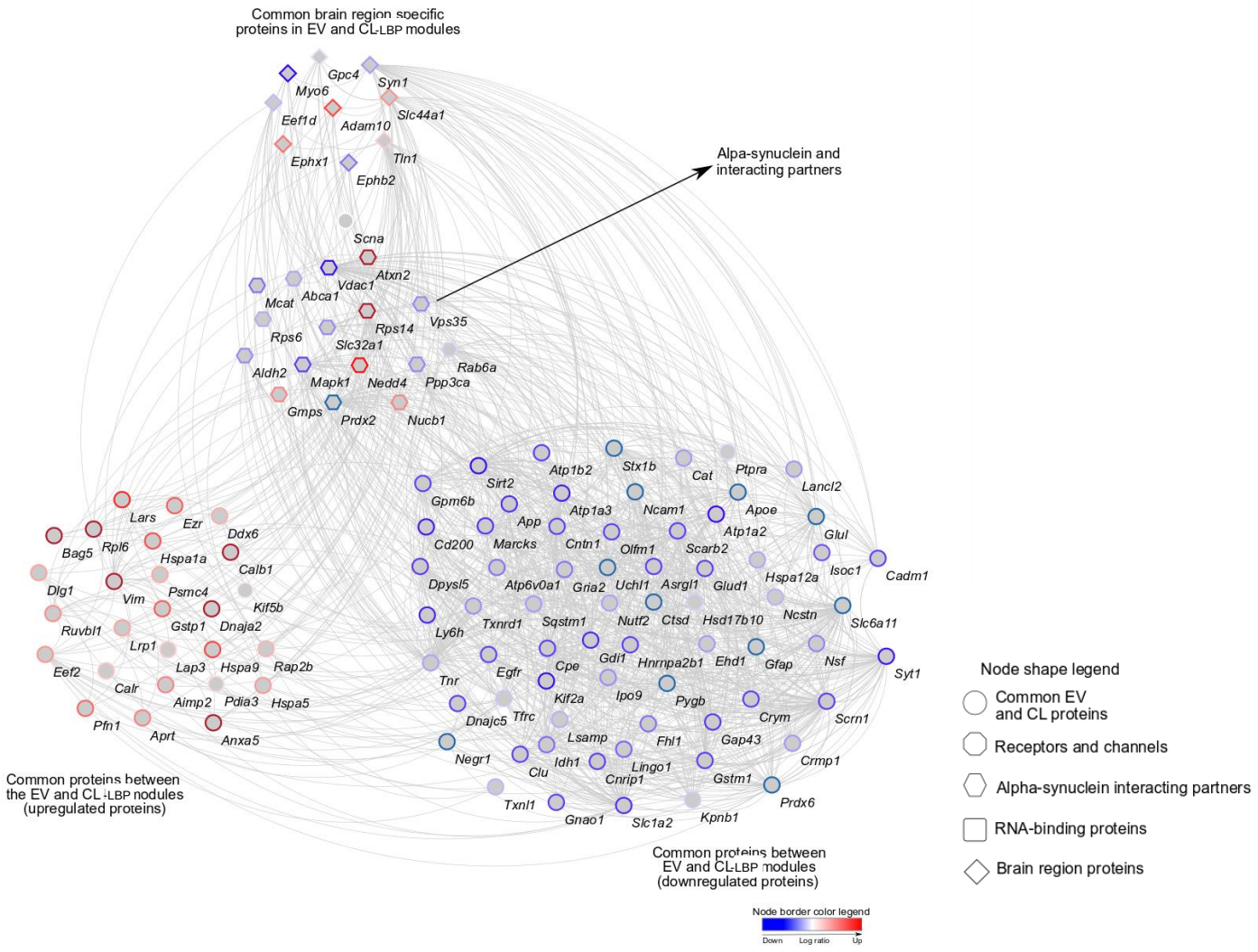

Figure 34. **Brain region specific impact of high bFGF levels.** Combined module of common brain region specific proteins between the CL and EV fraction, common LBP modules α-Syn protein interacting partners and common CL and EV LBP modules. Note: Nodes are proteins but labeled with gene symbols. Overlap analysis revealed that Brain region specific proteins in this network is significantly enriched (P< 0.05; Fisher's exact test). α-Syn PPi protein were extracted from STRING DB(adapted from [137]).

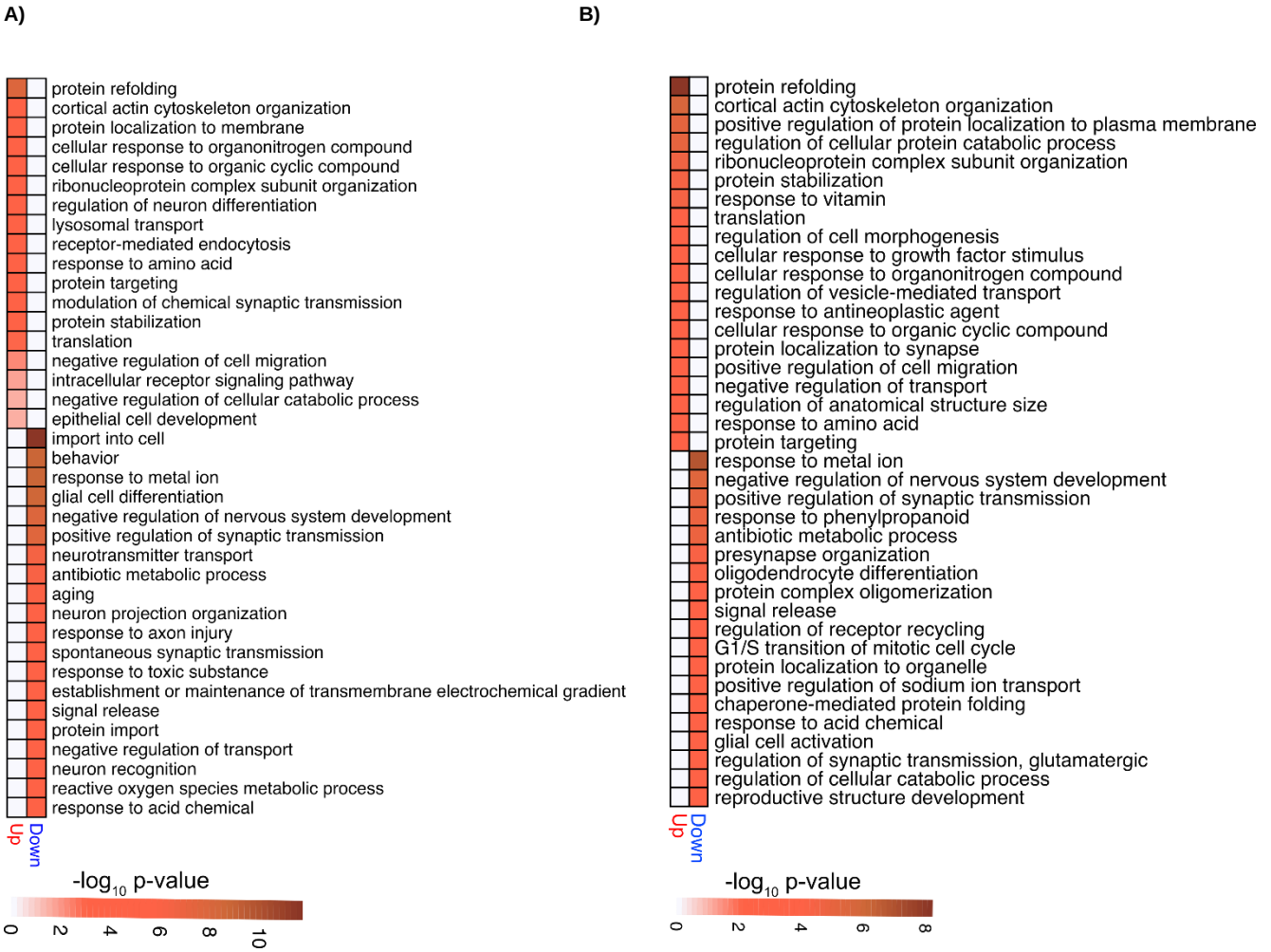

Figure 35. High bFGF influences α-Syn-interacting LBP proteins enriched in key biological pathways. A) Key biological pathways enriched by α-Syn interacting LBP proteins from CL and EV including receptors, ion channel and RNA binding proteins B) Key biological pathways enriched by α-Syn interacting LBP proteins from CL, EV, and the respective brain region specific proteins. The most significant (negative log10 $P \leq 0.05$) biological processes are shown in A) & B).

4. Discussion

The work presented here in general can be seen in two parts where the first half of the thesis is dedicated to understanding the fundamental basis of EV release and the later one to the implications of first half in LBP. Initial observations that overexpression of α-Syn is proportional to the enhanced EV-release in LUHMES cells and hippocampal neurons remained the motivation to understand this phenomenon better (**Figure 16, 17**).

In the current work, we observed a change in the morphology of α-Syn overexpressing LUHMES cells (**Figure 16**) with an increase in surface area that correlated with a higher C*m*, approximately twofold than in WT-LUHMES cells (**Figure 17B**). Electrophysiological studies investigating C*m* allow to study the process of cellular discharge (exocytosis) and uptake (endocytosis) [139-142]. Our LUHMES cell results indicated that the fusion events and ultimately the release of EVs are calcium dependent, which we concluded from the correlation of a rapid C*m* increase in response to a calcium influx (**Figure 17C**). An enhanced abundance of exosomal markers was confirmed in the respective EV-fractions prepared from α-Syn overexpressing LUHMES cells after depolarization with KCl application (**Figure 17D**). Because of the inconsistency we found in LUHMES cell membrane capacitance in response to electrical stimulation in conjunction with the lack of spontaneous activity in these cells, we aimed to investigate our preliminary findings in a more established research model with a broad scope of applicability (**Figure 18,19**). Therefore, we overexpressed α-Syn in primary hippocampal cultured neurons and performed NTA on the media collected from these cultures. The NTA results confirmed the enhanced release of EVs in the samples obtained from α-Syn treated neuronal conditions like LUHMES cells (**Figure 19**). Hence, further experiments were performed in hippocampal neurons and findings from these neurons are of direct importance in LBP with dementia because appearance of LBs is not restrained only to the SNc during the progressive pathophysiology [3].

4.1. Complex calcium-homeostatic mechanisms govern the slower exosome release

The synaptic release from neurotransmitter-carrying vesicles has a temporal resolution of milliseconds and is coupled to an electric stimulus, where a pool of release-ready vesicles at presynaptic sites directly correlates to the magnitude of a postsynaptic response. We found MVB-PM fusion relatively less frequent and therefore allow the subsequent release of exosomes to be seen in a different perspective [143-145]. The key physiological features of MVB-PM fusion that clearly set these events apart from neurotransmitter releasing vesicles is the occurrence of a relatively slow fusion kinetics in the range of seconds-to-minutes in response to a HFS (**Figure 20A-D**). Furthermore, these temporal-irregularities such

as asynchronous release of EVs of heterogeneous sizes associated with stimulus-responsive MVB-PM fusion events argue against a formation of the pool of release-ready MVBs as found in the case of synaptic-transmitter releasing vesicles (**Figure 20E-G**). Future investigations must clarify the existence or non-existence of a release-ready MVB pool such that an adequate estimate of MVB-release probabilities can be determined. Though irrefutably, in comparison to 'fast' synaptic communications the functions mediated by exosomes can be referred to as 'slow' communication between the components of the nervous system.

Fast communication via neurotransmitter filled vesicles at a chemical synapse is dependent on the presynaptic calcium level and shows an approximate linearity to its availability [123]. Moreover, neuronal calcium levels can be modulated and elevated by subjecting neurons to a high-frequency stimulation [146]. We therefore used HFS to study the MVB-PM fusion rates by manipulating the calcium levels (**Figures 14** and **21**). Our results indicated that a 100 Hz stimulus can create a network wide calcium-elevated state (**Figure 15**) that can induce a prolonged chain of burst-like MVB-PM fusion events lasting up to several minutes, which otherwise at basal calcium conditions was found absent (**Figure 21**). However, at basal calcium levels, a few events could be observed during a prolonged recording of several minutes or may be seen in the beginning of a recoding in pre-stimulated neurons. We confirmed such fusion event (data not included) at basal calcium concentrations after blocking the store mediated calcium release highlighting the distinct calcium dependency of exosome-release via MVB-PM fusion. Our experiments confirmed a small population of neurons to exhibit a successful stimulus-responsive release of exosomes at a subsided rate of release. Therefore, a decoupling of bioelectric stimuli and corresponding exosome release can be assumed and may be accompanied by complex calcium dependent mechanisms.

pH fluctuations are associated with calcium levels and alkalization in neurons that raises the basal calcium level [147]. Therefore alternatively, elevation of calcium e.g., via HFS (**Figures 13-15**) must influence the intracellular pH. Taken together, the enhanced, HFS-mediated MVB-PM fusion events and alkali-conditions correlating to high calcium should in principle activate a direct process of enhanced biogenesis of MVBs in linear conceptualization of the entire phenomenon. But on the contrary, an enhanced exosomal yield is observed at a low intracellular pH [148]. This contradicts the linear assertion about calcium-mediated pH changes and corresponding exosome release and proposes a rather more complex role of calcium in exosome release. Alternatively, our findings suggest that immediate influx of calcium during HFS would rather facilitate the MVB-release instead of their immediate biogenesis and the success rate of fusion events is thus limited by the MVB-availability at the release sites.

Besides, a big challenge in exosome physiology relates to their heterogeneity in terms of composition, cargo, and functions etc. [149, 150]. Therefore, our results may help to distinguish the vesicular populations based on their fusion kinetics. The translational aspects of our findings, especially the experimental approach presented here, illustrate the disadvantages of studying exosomal physiology using conventional biochemical assays. In neurodegenerative disorders exosomes transmit pathological proteins [49, 51, 151] therefore resolving EV-physiology may be helpful in order to predetermine the onset and to derive possible co-relations with long-term associative severity of neurodegenerative symptoms e.g. estimation of physiological state, favoring the likely appearance of LBs which otherwise gets overlooked in postmortem studies. Moreover by the logic of disease progression and staging i.e. spanning over several years [152], a slow-vesicular communication between the cellular components with a capability to travel distant ends of the nervous system is more favorable as compared to the fast-vesicular communication to enhance the better understanding of disease progression process.

4.2. Neurotrophic factors are the boosters of MVB-PM fusion

As discussed in earlier sections, the bioelectric stimuli result in subsided rates of MVB-PM fusion and successively the exosome release is affected. Therefore, we looked for other supplements that can boost the fusion events. Our results suggested that neurotrophic factors (bFGF, BDNF and NGF) enhance stimulus-responsive fusion events with a higher probability in bFGF-treated neurons (**Figure 22**). The fact that neurotrophic factors follow common routes of their downstream molecular signaling that are responsible for their pleiotropic functions [103, 153], led us to restrain our initial investigation and focus only to the treatment condition with the highest probability of stimuli-responsive MVB-PM fusion events i.e., bFGF treatment. However, the administration of BDNF and NGF to neurons also led to an increase in the exosomal particle concentration in the culture media collected for these treatment conditions with an offset time of 24-48 hours (**Figure A1.1**). There were no significant direct effects on the immediate membrane associated bioelectric properties induced by these neurotrophic factors, thus illustrating that the overall neuronal membrane's functional integrity remained intact. However, NTF-treatment may influence neuronal activity by triggering the intrinsic mechanisms other than its direct impact and association at the plasma membrane (**Figure 23**). These findings were found in line to the known effects of NTF-treatment on the bioelectric activity of hippocampal neurons as in [135] at a network level and may differ in the case of isolated single neurons e.g. in autaptic cultures. A bFGF-treated, CD63-pHluorin expressing hippocampal neuron exhibits an enhanced fluorescent signal in response to a HFS thus indicating a temporal resolution of minutes for MVB-PM fusion events (**Figure 24 A** and **B**). However,

bFGF treated neurons at a holding potential of -70 mV or untreated neurons with HFS largely depict no fusion events (**Figures 24C** and **D**). Even though we observed significantly larger CD63-pHluorin puncta for bFGF conditions in confocal imaging pictures from these neurons, EM indicated only a non-significant trend leaning towards a higher number of CD63-positive MVBs (**Figure 25**). We attribute these findings to the possibility of bFGF specifically affecting certain MVB/exosomal-populations that may get enriched for other exosome-biomarkers instead for CD63. However, the possibility of small sample size cannot be fully excluded.

4.3. bFGF mediated enhanced EV-release depends on tyrosine kinase activity and is calcium dependent

Bioelectric stimulation of bFGF-treated neurons in real time (**Figure 24**) or bFGF treatment given as a chemical stimulus to neurons; led to an enhanced EV-release (**Figure 26A-C**). This indicates that bFGF somehow facilitates the availability of release ready MVBs which could then be released in response to an HFS or via spontaneous means of MVBs fusion to PM over a longer time span. The down-stream signaling of bFGF is mediated via the tyrosine kinase domain of its receptors [154, 155], therefore blocking tyrosine activity would aid the understanding of the bFGF induced regulatory mechanisms in EV-release. Therefore, neurons were treated with GEN, which inhibits tyrosine kinase activity [156] and EVs were quantified using NTA. The partial reduction of EV-particles; but not complete abolition was observed in GEN-treated neurons with no effect on particle size. We attribute this effect to non-redundant mechanism that accounts for incomplete blocking of EV-release as an effect of GEN and to the pleotropic effects of bFGF (**Figure 26D-F**). Furthermore, we found that the EV-release is calcium dependent as BAPTA treatment of bFGF-treated neurons showed a reduced particle-yield, confirmed by the reduced expression of EV biomarkers in EV-enriched pellets (**Figure 26G-K**). Taken together, we concluded that bFGF mediated EV-release is partially regulated via tyrosine kinase activity and is calcium dependent.

4.4. “e-SNAREs”

If tyrosine kinase activity regulates EV release downstream of bFGF receptor signaling, then what drives MVB-PM fusion? Because of the reverse exosome membrane topology and the entrapped cytosolic material [61], a content analysis on exosomes, likely to carry the clues about the molecular machinery of fusion and a snapshot of the intracellular physiological state. We therefore analyzed the exosomal content by performing MS, revealing a differential expression induced to exosomal proteins by bFGF and these proteins had mainly enriched the pathways related to vesicle secretion and had strong interactional

capabilities (**Figure 27A-F**). The identification of upregulated proteins *Src* and *Grb2* as the top hub-proteins in our centrality analysis on networks of differentially expressed proteins has counter-validated the tyrosine kinase mediated regulation of MVB-PM fusion events because of their key involvement in this signaling pathway [157]. Besides, we found VAMP2 and VAMP3 as hub proteins, where VAMP2 was downregulated and VAMP3 was significantly upregulated after bFGF treatment (**Figure 27G**). These members of the SNARE protein family interact with a variety of other key SNAREs that can facilitate membrane fusion (**Figure 27G**). Therefore up/down-regulation of these proteins will influence and regulate fusion events which is a rather energy-expensive process because of similar membrane polarities. The fact that SNARE members are found as key facilitators of membrane fusion events of vesicles other than MVBs [158-160] illustrates the molecular basis for associated vesicular heterogeneity. The downregulated VAMP2 in EV pellets is mainly associated to synaptic neurotransmitter releasing vesicles [161] and the specific enrichment of VAMP3 in response to bFGF inspired us to refer it and other EV-associated SNAREs as "e-SNARE". The VAMP3 knock-down assay revealed a reduced number of EVs in VAMP3-deficient cells and further established the specificity of the SNAREs and their importance for MVB-PM fusion events (**Figure 28**). Our analyses suggest that bFGF can alter the expression and enrichment of EV-specific proteins up to approximately ten-fold, thus highlighting the overall importance of NTF signaling in the overall EV-secretion and release process (**Figure 29**).

4.5. bFGF has a broad effect on protein expression and their linear exodus as EV-content

The snapshot of intracellular physiology carried by EVs and the independent cargo assortment that may decide their biogenic fates [60, 162] led us to look at the cell lysate (CL) protein expression using MS. By the application of comparative 3D-principal component analysis (PCA) on MS data along with hierarchical clustering, a strong significant differential expression of proteins in the CL along with the EV peptide-content was found (**Figure 30B** and **C**). Using WPCNA and mapping-techniques, the modules of differentially expressed proteins and LBP-associated modules were constructed (**Figure 31A-D**). Interestingly, the pathway enrichment analysis from the upregulated candidates of these modules specifically had functional associations to intrinsic protein metabolism confounded mainly to sub-cellular locations (**Figure 31E**). The comparative looks at the expression levels of proteins in CL and EV content suggested a near linear pattern such that the downregulated proteins in CL are also downregulated in EV content and vice-versa (**Figure 32**). Further investigation is needed to specifically illustrate the biological significance and mechanisms of this side of the bFGF influence however taken together the changes to protein expression levels and enriched functional pathways, we propose that exosome secretion must be

studied jointly with cellular level changes by taking an account of the respective cellular-level physiological states.

4.6. The expression levels of many Lewy body pathology associated proteins are changed by bFGF treatment

A typical LB is an aggregation of misfolded proteins (e.g., α-Syn), lipids and organelle debris formed during dysfunctional traffic mechanisms [163, 164]. In our data we therefore studied the cross-interactions of α-Syn with abundant LB-associated proteins under the influence of bFGF-treatment (**Figure 33**). Patients with LBP are found to show altered NTF levels [89]. Therefore, the information provided by our protein interaction networks specifically highlights the precursor molecules of LBP under a given physiological state of high NTF-levels. We report numerous LBP-related receptors/channels, RNA binding proteins that are influenced by high bFGF levels. The common candidates among the CL and EV based on their expression regulation (up/down) will influence the interaction network accordingly, which allows us to anticipate the possible crosstalk among the neuronal components mediated via EVs. Moreover, the corresponding interactions of α-Syn with CL and EV common proteins allows us to foresee the possible physiological consequences of the secretion of α-Syn in exosomes [50, 51, 165]. Interestingly, it has been found that α-Syn forms that are secreted via exosomes have a higher tendency to aggregate then its cytosolic forms [166] thus highlighting direct significance of this work for LBP initiation.

These interactions provide a founding molecular map for the physiological conditions such as higher concentrations of α-Syn that could facilitate the protein aggregate formation [167], hence the results are also valuable for the general physiological understanding of α-Syn function which is largely undetermined until now. Overall α-Syn interactions with channels and receptors or subcellularly located candidates i.e., RNA binding proteins etc. provide a comprehensive view of LBP and may help to characterize the mechanism of the early disease onset. Furthermore, EV-proteins and their interactions with CL proteins at the subcellular level raise the possibility of physiological manipulations to the host cells once they are carried in exosomal vehicles and gets up-taken at subsequent or distant sites.

Pertaining to the potential consequences of EV-mediated protein transfer [168], we identified possible proteins that are native to the various brain regions and are most likely to act as pathology seeding sites via their interactions with the received pathological discharge (**Figure 34**). Some of the top five percent of the brain region specific proteins were found native to the olfactory bulb region, i.e., one of the centers

of neurogenesis in the adult brain and shown to be associated to the dopaminergic neural circuitry [169, 170]. Together with the role of bFGF in neuronal development and maturation [93, 96, 99] and along with our finding of enhanced EV release [136], these results support the understanding of the molecular associations of early pathology at precursor sites of exposure such as olfactory lobe [171] and further propagation to other regions. Our network analysis interestingly points out how brain-region specific proteins such as *Tln* could indirectly exert physiological controls by directly interacting with α-Syn or its interaction partners which then further has direct physical interactions with the common CL-EV proteins and vice-versa. The information could provide the molecular basis by availing the analysis of intermediate candidates to explain the key LBP symptoms such as cognitive fluctuations [172]. Functional enrichment analysis on bFGF influenced LBP associated proteins suggests, that such physiological conditions mainly exert their effects by influencing the key intrinsic protein metabolism associated pathways (**Figure 35**).

4.7. Stimulus-responsive enhanced EV release has system level implications

EVs can modulate neuronal activity and orchestrate the cross-communication between the neuronal components at various levels [77, 151, 173]. The findings of stimulus-responsive EV release therefore give a new perspective to such communications. The 50-100 Hz stimuli response of neurons along with a NTF stimulus and a network level global rise in calcium availability (**Figures 13-15, 21** and **24**) leads to a corresponding EV secretion, this not only contributes to a cellular level understanding of release process but also evokes multiple parallel possibilities. The stimulus used during our experiments matches fast oscillations in the gamma band frequency (but with a different magnitude without field-stimulation), which is believed to be related to a proper brain function and consecutive cognitive functions [174]. The power of gamma oscillations was noticed to be decreased in elderly patients [175] and the activity of brain regions is regulated at different gamma frequencies [176] with distinct cellular level effects [177]. Currently, therapies such as deep brain stimulation (DBS) are available for patients, but these treatments lack a detailed understanding of impacts of such stimulation at the cellular level although a set of mechanisms have been proposed [178]. It has been shown that DBS in PD patients improves tremor by lessening the power of gamma activity [179]. Our findings therefore could serve as the fundamental basis to resolve the differential actions of DBS and associated subsequent evoked neuronal mechanisms at the cellular level and their respective, overall impact in a state of progressive pathophysiology in the long run.

5. Concluding remarks and future recommendations

The two key general objectives of this work were i) to understand the EV-release process better and ii) to examine its relevance for LBP. The findings presented and discussed in this thesis supports the understanding of stimulus-responsive MVB-PM fusion events and reveals intrinsic physiological factors that control fusion events in hippocampus neurons. We identified key stimuli (electric and chemical) that can trigger such events and ultimately lead to EV-release. Our data suggests that this type of vesicular release has a relatively slow-release kinetics as compared to neurotransmitter carrying vesicles. Our data suggests that VAMP3 is the key SNARE enriched to EVs in an NTF-induced release. We also deduced an interaction network among the members of SNARE family proteins that could contribute to resolve the EV-heterogeneity in the future. We validated that bFGF-induced EV-release is calcium dependent and limited by the availability of release-ready MVBs at the releasing sites which is partially regulated via tyrosine kinase mediated cellular activity. The data included in this thesis do not support the existence of a pool of release ready MVBs close to the PM as, is found in the case of neurotransmitter release at chemical synapses. Furthermore, adapting to a system level analysis of MS data we identified several candidate proteins relevant for LBP. Collectively, the information about LBP associated candidate proteins and their interactional potentials in neuron lysate, with α-Syn along with their cross-interactional partners in EV-content; we generate support and possible understanding of LBP-state under a physiological state of enhanced EV-release that happens either due to electric stimulus or at high NTF levels. The EV-centric perspective of this work therefore aids to understand the molecular basis of LBP seeding and spreading via shuttling of exosomal bioactive-content and points towards the pathological state dependent dual consequences associated to the release process in a clinical setting, which may or may not be protective or severely pathological. The physiological state dependent associations of EVs can therefore support the vision of proper characterization of disease staging and could also contribute to the process of such indexing work in clinics [180]. Future work should characterize the molecular interactions identified in this work and their relevance for LBP *in vivo* in a wet lab setting and accommodate the effects of the specific bioelectric stimuli in appropriate research models. It should be clarified whether the cargo-oriented fate of EV-release is stimulus dependent or not. Moreover, these findings should be used in future to investigate and reverse-engineer the EV-release process such that its therapeutic potentials can be fully realized e.g., to develop an efficient design of EV based drug delivery vehicles with a very specific customized control.

Acknowledgments

Life as a doctoral candidate for the past fifteen years gave me the opportunity to meet many people who knowingly, unknowingly, humane, or inhumane became the part of my journey thus far. At present it is very difficult for me to recall all the names, but I would like to extend my gratitude to everyone for their trust, distrust, negative and positive contributions in all forms that they had bequeathed on me during all these times.

I greatly appreciate the role of my thesis mentor Dr. med Thomas Koeglsperger, primary supervisor Prof. Dr. Günter Höglinger and associated thesis committee member Prof. Dr. Andreas Bausch, for their support and guidance. I really appreciate the role of Prof. Dr. Stefan F. Lichtenthaler for his incessant support and involvement at multiple levels. I am also thankful to Prof. Dr. Gerhard Rammes and Prof. Dr. Kai Bötzel for their involvements. I also appreciate Dr. Sabina Tahirovic, Dr. Alessio-Vittorio Colombo, Dr. Stephan Müller, Dr. Carmelo Sgobio and Dr. Sainitin Donakonda for their continuous encouragement and knowledge-sharing. Equally, I appreciate the generosity received from all other corners of German Center for Neurodegenerative Diseases (DZNE) in Munich and beyond.

Besides these, I acknowledge the role of Prof. Dr. Erwin Neher as a continuous source of inspiration for me to do science and with whom so far, I have shared a relationship like protagonists of *Mahabharata*; 'Guru Dronna and Eklavya' in modern-day settings. Where, based on my association to the field of electrophysiology the *Guru Dakshina* was somewhat different and a scientific equivalent was asked by his close associates and immediate beneficiaries of his scientific brilliance, perhaps without his knowledge and awareness.

I really appreciate the patience of all my friends and family all these years, who are largely naive about my life or the life of a scientist or life outside a Himalayan or rural Indian-emblem, and grateful for allowing me to be absent for the occasions and rituals, which otherwise are must to attend and most certainly might have withstood as the key moments to their respective lives. I am thankful to my parents and their consociates for living in our remote Himalayan lives and villages, cultural essence, and ethics of which might have led them so far to take care of themselves all alone in my absence and deeply value their firm conviction and devotion to do so.

Last but not the least, I appreciate the contribution of German-taxpayers, without which a scientific-ecosystem cannot exist, that could unconventionally allow a student from faraway remote-places like

myself to undertake a research endeavor such as the work presented in this thesis. I am also thankful to the people of India which is the country of my biological-origin and had continuously taught me to embrace the enormity of our universe, to which we all and everything are part of therefore guiding me throughout to keep the scholarly-reductionist approach under check and limited to availing the consequential requirements. As a son of mother-river Sutlej, who shares a deep bond with mother river Isar, I hope this work could serve as a “scientific-offering” to all the humane content existing in our times and hopefully would be a step forward towards the understanding of the neurodegenerative diseases to treat them well.

Literature:

1. Dorsey, E.R., et al., *Global, regional, and national burden of Parkinson's disease, 1990–2016: a systematic analysis for the Global Burden of Disease Study 2016.* The Lancet Neurology, 2018. **17**(11): p. 939-953.
2. Outeiro, T.F., et al., *Dementia with Lewy bodies: an update and outlook.* Molecular neurodegeneration, 2019. **14**(1): p. 5-5.
3. Braak, H. and K. Del Tredici, *Neuropathological Staging of Brain Pathology in Sporadic Parkinson's disease: Separating the Wheat from the Chaff.* J Parkinsons Dis, 2017. **7**(s1): p. S71-S85.
4. Kitada, T., et al., *Mutations in the parkin gene cause autosomal recessive juvenile parkinsonism.* Nature, 1998. **392**(6676): p. 605-608.
5. Takahashi, H., et al., *Familial juvenile parkinsonism: clinical and pathologic study in a family.* Neurology, 1994. **44**(3 Pt 1): p. 437-41.
6. Dauer, W. and S. Przedborski, *Parkinson's Disease: Mechanisms and Models.* Neuron, 2003. **39**(6): p. 889-909.
7. Braak, H. and K. Del Tredici, *Neuroanatomy and pathology of sporadic Parkinson's disease.* Advances in anatomy, embryology, and cell biology, 2009. **201**: p. 1-119.
8. Goedert, M., et al., *100 years of Lewy pathology.* Nature Reviews Neurology, 2013. **9**(1): p. 13-24.
9. Engelhardt, E. and M.d.M. Gomes, *Lewy and his inclusion bodies: Discovery and rejection.* Dementia & neuropsychologia, 2017. **11**(2): p. 198-201.
10. Spillantini, M.G., et al., *α-Synuclein in Lewy bodies.* Nature, 1997. **388**(6645): p. 839-840.
11. Meredith, G.E., G.M. Halliday, and S. Totterdell, *A critical review of the development and importance of proteinaceous aggregates in animal models of Parkinson's disease: new insights into Lewy body formation.* Parkinsonism Relat Disord, 2004. **10**(4): p. 191-202.
12. Liou, H.H., et al., *Environmental risk factors and Parkinson's disease: a case-control study in Taiwan.* Neurology, 1997. **48**(6): p. 1583-8.
13. Vila, M., et al., *Alpha-synuclein up-regulation in substantia nigra dopaminergic neurons following administration of the parkinsonian toxin MPTP.* J Neurochem, 2000. **74**(2): p. 721-9.
14. Petroske, E., et al., *Mouse model of Parkinsonism: a comparison between subacute MPTP and chronic MPTP/probenecid treatment.* Neuroscience, 2001. **106**(3): p. 589-601.
15. Maroteaux, L., J.T. Campanelli, and R.H. Scheller, *Synuclein: a neuron-specific protein localized to the nucleus and presynaptic nerve terminal.* The Journal of Neuroscience, 1988. **8**(8): p. 2804.
16. Clayton, D.F. and J.M. George, *The synucleins: a family of proteins involved in synaptic function, plasticity, neurodegeneration and disease.* Trends in Neurosciences, 1998. **21**(6): p. 249-254.
17. Burré, J., *Properties of native brain alpha synuclein.* Nature, 2013. **498**: p. E4-E7.
18. Burré, J., M. Sharma, and T.C. Südhof, *α-Synuclein assembles into higher-order multimers upon membrane binding to promote SNARE complex formation.* Proceedings of the National Academy of Sciences, 2014. **111**(40): p. E4274.
19. Perrin, R.J., et al., *Exposure to long chain polyunsaturated fatty acids triggers rapid multimerization of synucleins.* J Biol Chem, 2001. **276**(45): p. 41958-62.
20. Sharon, R., et al., *The Formation of Highly Soluble Oligomers of α-Synuclein Is Regulated by Fatty Acids and Enhanced in Parkinson's Disease.* Neuron, 2003. **37**(4): p. 583-595.
21. Winner, B., et al., *In vivo demonstration that α-synuclein oligomers are toxic.* Proceedings of the National Academy of Sciences, 2011. **108**(10): p. 4194.
22. Dettmer, U., et al., *Loss of native alpha-synuclein multimerization by strategically mutating its amphipathic helix causes abnormal vesicle interactions in neuronal cells.* Hum Mol Genet, 2017. **26**(18): p. 3466-3481.
23. Volles, M.J., et al., *Vesicle permeabilization by protofibrillar alpha-synuclein: implications for the pathogenesis and treatment of Parkinson's disease.* Biochemistry, 2001. **40**(26): p. 7812-9.

24. Bird, C.M. and N. Burgess, *The hippocampus and memory: insights from spatial processing.* Nature Reviews Neuroscience, 2008. **9**(3): p. 182-194.
25. Voss, J.L., et al., *A Closer Look at the Hippocampus and Memory.* Trends in cognitive sciences, 2017. **21**(8): p. 577-588.
26. Dickson, D.W., et al., *Hippocampal degeneration differentiates diffuse Lewy body disease (DLBD) from Alzheimer's disease.* Neurology, 1991. **41**(9): p. 1402.
27. Churchyard, A. and A.J. Lees, *The relationship between dementia and direct involvement of the hippocampus and amygdala in Parkinson's disease.* Neurology, 1997. **49**(6): p. 1570.
28. Kim, H.B.A., M. Gearing, and S.S. Mirra, *Ubiquitin-positive CA2/3 neurites in hippocampus coexist with cortical Lewy bodies.* Neurology, 1995. **45**(9): p. 1768.
29. Hall, H., et al., *Hippocampal Lewy pathology and cholinergic dysfunction are associated with dementia in Parkinson's disease.* Brain, 2014. **137**(9): p. 2493-2508.
30. Galvin, J.E., et al., *Axon pathology in Parkinson's disease and Lewy body dementia hippocampus contains α-, β-, and γ-synuclein.* Proceedings of the National Academy of Sciences, 1999. **96**(23): p. 13450.
31. Liu, A.K.L., et al., *Hippocampal CA2 Lewy pathology is associated with cholinergic degeneration in Parkinson's disease with cognitive decline.* Acta Neuropathologica Communications, 2019. **7**(1): p. 61.
32. Adamowicz, D.H., et al., *Hippocampal α-Synuclein in Dementia with Lewy Bodies Contributes to Memory Impairment and Is Consistent with Spread of Pathology.* The Journal of neuroscience : the official journal of the Society for Neuroscience, 2017. **37**(7): p. 1675-1684.
33. Beach, T.G., et al., *Unified staging system for Lewy body disorders: correlation with nigrostriatal degeneration, cognitive impairment and motor dysfunction.* Acta Neuropathologica, 2009. **117**(6): p. 613-634.
34. Braak, H., et al., *Staging of brain pathology related to sporadic Parkinson's disease.* Neurobiology of Aging, 2003. **24**(2): p. 197-211.
35. Jellinger, K.A., *A critical reappraisal of current staging of Lewy-related pathology in human brain.* Acta Neuropathologica, 2008. **116**(1): p. 1.
36. Kordower, J.H., et al., *Lewy body–like pathology in long-term embryonic nigral transplants in Parkinson's disease.* Nature Medicine, 2008. **14**(5): p. 504-506.
37. Li, J.Y., et al., *Lewy bodies in grafted neurons in subjects with Parkinson's disease suggest host-to-graft disease propagation.* Nat Med, 2008. **14**(5): p. 501-3.
38. Rey, N.L., et al., *Widespread transneuronal propagation of α-synucleinopathy triggered in olfactory bulb mimics prodromal Parkinson's disease.* The Journal of Experimental Medicine, 2016. **213**(9): p. 1759.
39. Sacino, A.N., et al., *Intramuscular injection of α-synuclein induces CNS α-synuclein pathology and a rapid-onset motor phenotype in transgenic mice.* Proc Natl Acad Sci U S A, 2014. **111**(29): p. 10732-7.
40. Holmqvist, S., et al., *Direct evidence of Parkinson pathology spread from the gastrointestinal tract to the brain in rats.* Acta Neuropathol, 2014. **128**(6): p. 805-20.
41. Recasens, A., et al., *Lewy body extracts from Parkinson disease brains trigger α-synuclein pathology and neurodegeneration in mice and monkeys.* Annals of Neurology, 2014. **75**(3): p. 351-362.
42. Luk, K.C., et al., *Pathological α-Synuclein Transmission Initiates Parkinson-like Neurodegeneration in Nontransgenic Mice.* Science, 2012. **338**(6109): p. 949.
43. Luk, K.C., et al., *Intracerebral inoculation of pathological α-synuclein initiates a rapidly progressive neurodegenerative α-synucleinopathy in mice.* The Journal of Experimental Medicine, 2012. **209**(5): p. 975.
44. Angot, E., et al., *Alpha-synuclein cell-to-cell transfer and seeding in grafted dopaminergic neurons in vivo.* PLoS One, 2012. **7**(6): p. e39465.
45. Peelaerts, W., et al., *alpha-Synuclein strains cause distinct synucleinopathies after local and systemic administration.* Nature, 2015. **522**(7556): p. 340-4.
46. Men, Y., et al., *Exosome reporter mice reveal the involvement of exosomes in mediating neuron to astroglia communication in the CNS.* Nature Communications, 2019. **10**(1): p. 4136.

47. Ngolab, J., et al., *Brain-derived exosomes from dementia with Lewy bodies propagate alpha-synuclein pathology.* Acta Neuropathol Commun, 2017. **5**(1): p. 46.
48. Surmeier, D.J., J.A. Obeso, and G.M. Halliday, *Parkinson's Disease Is Not Simply a Prion Disorder.* The Journal of Neuroscience, 2017. **37**(41): p. 9799.
49. Tomlinson, P.R., et al., *Identification of distinct circulating exosomes in Parkinson's disease.* Ann Clin Transl Neurol, 2015. **2**(4): p. 353-61.
50. Grey, M., et al., *Acceleration of alpha-synuclein aggregation by exosomes.* J Biol Chem, 2015. **290**(5): p. 2969-82.
51. Kunadt, M., et al., *Extracellular vesicle sorting of alpha-Synuclein is regulated by sumoylation.* Acta Neuropathol, 2015. **129**(5): p. 695-713.
52. Chang, C., et al., *Exosomes of BV-2 cells induced by alpha-synuclein: important mediator of neurodegeneration in PD.* Neurosci Lett, 2013. **548**: p. 190-5.
53. Spencer, B., et al., *alpha-Synuclein interferes with the ESCRT-III complex contributing to the pathogenesis of Lewy body disease.* Hum Mol Genet, 2016. **25**(6): p. 1100-15.
54. Trams, E.G., et al., *Exfoliation of membrane ecto-enzymes in the form of micro-vesicles.* Biochimica et Biophysica Acta (BBA) - Biomembranes, 1981. **645**(1): p. 63-70.
55. Harding, C., J. Heuser, and P. Stahl, *Receptor-mediated endocytosis of transferrin and recycling of the transferrin receptor in rat reticulocytes.* The Journal of Cell Biology, 1983. **97**(2): p. 329-339.
56. Colombo, M., G. Raposo, and C. Thery, *Biogenesis, secretion, and intercellular interactions of exosomes and other extracellular vesicles.* Annu Rev Cell Dev Biol, 2014. **30**: p. 255-89.
57. Escola, J.M., et al., *Selective enrichment of tetraspan proteins on the internal vesicles of multivesicular endosomes and on exosomes secreted by human B-lymphocytes.* J Biol Chem, 1998. **273**(32): p. 20121-7.
58. Hemler, M.E., *Tetraspanin proteins mediate cellular penetration, invasion, and fusion events and define a novel type of membrane microdomain.* Annu Rev Cell Dev Biol, 2003. **19**: p. 397-422.
59. Larios, J., et al., *ALIX- and ESCRT-III-dependent sorting of tetraspanins to exosomes.* J Cell Biol, 2020. **219**(3).
60. van Niel, G., et al., *The tetraspanin CD63 regulates ESCRT-independent and -dependent endosomal sorting during melanogenesis.* Dev Cell, 2011. **21**(4): p. 708-21.
61. Schöneberg, J., et al., *Reverse-topology membrane scission by the ESCRT proteins.* Nat Rev Mol Cell Biol, 2017. **18**(1): p. 5-17.
62. Kostelansky, M.S., et al., *Structural and functional organization of the ESCRT-I trafficking complex.* Cell, 2006. **125**(1): p. 113-26.
63. Hierro, A., et al., *Structure of the ESCRT-II endosomal trafficking complex.* Nature, 2004. **431**(7005): p. 221-5.
64. Teis, D., S. Saksena, and S.D. Emr, *Ordered assembly of the ESCRT-III complex on endosomes is required to sequester cargo during MVB formation.* Dev Cell, 2008. **15**(4): p. 578-89.
65. Adell, M.A. and D. Teis, *Assembly and disassembly of the ESCRT-III membrane scission complex.* FEBS Lett, 2011. **585**(20): p. 3191-6.
66. Chassefeyre, R., et al., *Regulation of Postsynaptic Function by the Dementia-Related ESCRT-III Subunit CHMP2B.* The Journal of Neuroscience, 2015. **35**(7): p. 3155.
67. Firkowska, M., M. Macias, and J. Jaworski, *ESCRT Proteins Control the Dendritic Morphology of Developing and Mature Hippocampal Neurons.* Mol Neurobiol, 2019. **56**(7): p. 4866-4879.
68. Loncle, N., et al., *An ESCRT module is required for neuron pruning.* Scientific Reports, 2015. **5**(1): p. 8461.
69. van Niel, G., G. D'Angelo, and G. Raposo, *Shedding light on the cell biology of extracellular vesicles.* Nature Reviews Molecular Cell Biology, 2018. **19**(4): p. 213-228.
70. Lee, J.-A., et al., *ESCRT-III Dysfunction Causes Autophagosome Accumulation and Neurodegeneration.* Current Biology, 2007. **17**(18): p. 1561-1567.
71. Mathieu, M., et al., *Specificities of secretion and uptake of exosomes and other extracellular vesicles for cell-to-cell communication.* Nature Cell Biology, 2019. **21**(1): p. 9-17.

72. Doherty, G.J. and H.T. McMahon, *Mechanisms of Endocytosis.* Annual Review of Biochemistry, 2009. **78**(1): p. 857-902.
73. Mayor, S. and R.E. Pagano, *Pathways of clathrin-independent endocytosis.* Nature Reviews Molecular Cell Biology, 2007. **8**(8): p. 603-612.
74. Costa Verdera, H., et al., *Cellular uptake of extracellular vesicles is mediated by clathrin-independent endocytosis and macropinocytosis.* Journal of Controlled Release, 2017. **266**: p. 100-108.
75. Svensson, K.J., et al., *Exosome uptake depends on ERK1/2-heat shock protein 27 signaling and lipid Raft-mediated endocytosis negatively regulated by caveolin-1.* J Biol Chem, 2013. **288**(24): p. 17713-24.
76. Fitzner, D., et al., *Selective transfer of exosomes from oligodendrocytes to microglia by macropinocytosis.* J Cell Sci, 2011. **124**(Pt 3): p. 447-58.
77. Chivet, M., et al., *Exosomes secreted by cortical neurons upon glutamatergic synapse activation specifically interact with neurons.* J Extracell Vesicles, 2014. **3**: p. 24722.
78. Parolini, I., et al., *Microenvironmental pH is a key factor for exosome traffic in tumor cells.* J Biol Chem, 2009. **284**(49): p. 34211-22.
79. Alvarez-Erviti, L., et al., *Delivery of siRNA to the mouse brain by systemic injection of targeted exosomes.* Nature Biotechnology, 2011. **29**(4): p. 341-345.
80. Jang, S.C., et al., *In vivo kinetic biodistribution of nano-sized outer membrane vesicles derived from bacteria.* Small, 2015. **11**(4): p. 456-61.
81. Srinivasan, S., et al., *TLR-exosomes exhibit distinct kinetics and effector function.* Sci Rep, 2017. **7**: p. 41623.
82. Haney, M.J., et al., *Exosomes as drug delivery vehicles for Parkinson's disease therapy.* J Control Release, 2015. **207**: p. 18-30.
83. Bieri, G., A.D. Gitler, and M. Brahic, *Internalization, axonal transport and release of fibrillar forms of alpha-synuclein.* Neurobiol Dis, 2018. **109**(Pt B): p. 219-225.
84. Palasz, E., et al., *BDNF as a Promising Therapeutic Agent in Parkinson's Disease.* Int J Mol Sci, 2020. **21**(3).
85. Morel, L., et al., *Revisiting the Role of Neurotrophic Factors in Inflammation.* Cells, 2020. **9**(4).
86. Lin, L.F., et al., *GDNF: a glial cell line-derived neurotrophic factor for midbrain dopaminergic neurons.* Science, 1993. **260**(5111): p. 1130.
87. Imamura, K., et al., *Cytokine production of activated microglia and decrease in neurotrophic factors of neurons in the hippocampus of Lewy body disease brains.* Acta Neuropathol, 2005. **109**(2): p. 141-50.
88. Zhao, Y., et al., *GDNF-transfected macrophages produce potent neuroprotective effects in Parkinson's disease mouse model.* PLoS One, 2014. **9**(9): p. e106867.
89. Ventriglia, M., et al., *Serum brain-derived neurotrophic factor levels in different neurological diseases.* Biomed Res Int, 2013. **2013**: p. 901082.
90. Scalzo, P., et al., *Serum levels of brain-derived neurotrophic factor correlate with motor impairment in Parkinson's disease.* Journal of Neurology, 2010. **257**(4): p. 540-545.
91. Hegarty, S.V., et al., *Effects of intracerebral neurotrophic factor application on motor symptoms in Parkinson's disease: A systematic review and meta-analysis.* Parkinsonism & Related Disorders, 2017. **38**: p. 19-25.
92. Eswarakumar, V.P., I. Lax, and J. Schlessinger, *Cellular signaling by fibroblast growth factor receptors.* Cytokine & Growth Factor Reviews, 2005. **16**(2): p. 139-149.
93. Dono, R., et al., *Impaired cerebral cortex development and blood pressure regulation in FGF-2-deficient mice.* The EMBO Journal, 1998. **17**(15): p. 4213-4225.
94. Sluzalska, K.D., et al., *Intracellular partners of fibroblast growth factors 1 and 2 - implications for functions.* Cytokine Growth Factor Rev, 2020.
95. Bean, A.J., et al., *Expression of acidic and basic fibroblast growth factors in the substantia nigra of rat, monkey, and human.* Proc Natl Acad Sci U S A, 1991. **88**(22): p. 10237-41.
96. Araujo, D.M. and C.W. Cotman, *Basic FGF in astroglial, microglial, and neuronal cultures: characterization of binding sites and modulation of release by lymphokines and trophic factors.* J Neurosci, 1992. **12**(5): p. 1668-78.

97. Claus, P., et al., *Expression of the fibroblast growth factor-2 isoforms and the FGF receptor 1–4 transcripts in the rat model system of Parkinson's disease.* Neuroscience Letters, 2004. **360**(3): p. 117-120.
98. Korada, S., et al., *Fibroblast Growth Factor 2 Is Necessary for the Growth of Glutamate Projection Neurons in the Anterior Neocortex.* The Journal of Neuroscience, 2002. **22**(3): p. 863.
99. Fadda, P., et al., *Reduction of Corticostriatal Glutamatergic Fibers in Basic Fibroblast Growth Factor Deficient Mice is Associated with Hyperactivity and Enhanced Dopaminergic Transmission.* Biological Psychiatry, 2007. **62**(3): p. 235-242.
100. Ratzka, A., et al., *Fibroblast growth factor 2 regulates dopaminergic neuron development in vivo.* Journal of Neurochemistry, 2012. **122**(1): p. 94-105.
101. Tooyama, I., et al., *Retention of basic fibroblast growth factor immunoreactivity in dopaminergic neurons of the substantia nigra during normal aging in humans contrast with loss in Parkinson's disease.* Brain Research, 1994. **656**(1): p. 165-168.
102. Tooyama, I., et al., *Loss of basic fibroblast growth factor in substantia nigra neurons in Parkinson's disease.* Neurology, 1993. **43**(2): p. 372-6.
103. Wang, D., et al., *Investigational fibroblast growth factor receptor 2 antagonists in early phase clinical trials to treat solid tumors.* Expert Opin Investig Drugs, 2019. **28**(10): p. 903-916.
104. Guimond, S.E. and J.E. Turnbull, *Fibroblast growth factor receptor signalling is dictated by specific heparan sulphate saccharides.* Current Biology, 1999. **9**(22): p. 1343-1346.
105. Grothe, C. and M. Timmer, *The physiological and pharmacological role of basic fibroblast growth factor in the dopaminergic nigrostriatal system.* Brain Research Reviews, 2007. **54**(1): p. 80-91.
106. Li, A., et al., *Apomorphine-induced activation of dopamine receptors modulates FGF-2 expression in astrocytic cultures and promotes survival of dopaminergic neurons.* The FASEB Journal, 2006. **20**(8): p. 1263-1265.
107. Suzuki, K., et al., *Transient upregulation of the glial glutamate transporter GLAST in response to fibroblast growth factor, insulin-like growth factor and epidermal growth factor in cultured astrocytes.* Journal of Cell Science, 2001. **114**(20): p. 3717.
108. Romanos, J., et al., *Differences in glutamate uptake between cortical regions impact neuronal NMDA receptor activation.* Communications Biology, 2019. **2**(1): p. 127.
109. Kinoshita, Y., et al., *Basic fibroblast growth factor promotes adhesive interactions of neuroepithelial cells from chick neural tube with extracellular matrix proteins in culture.* Development, 1993. **119**(3): p. 943-56.
110. Upadhya, R., et al., *Astrocyte-derived extracellular vesicles: Neuroreparative properties and role in the pathogenesis of neurodegenerative disorders.* J Control Release, 2020. **323**: p. 225-239.
111. Erwin Neher and B. Sakmann, *Noise Analysis of Drug Induced Voltage Clamp Currents in Denervated Frog Muscle Fibres.* Journal of Physiology, 1976. **258**: p. 705-729.
112. Hamill, O.P., et al., *Improved patch-clamp techniques for high-resolution current recording from cells and cell-free membrane patches.* Pflügers Archiv, 1981. **391**(2): p. 85-100.
113. Neher, E., *Asymteric membranes resulting from the fusion of two black lipid bilayers.* Biochimiea et Biophysica Acta, 1974. **373**(1): p. 327-326.
114. Neher, E., *The Influence of Intracellular Calcium Concentration On Deregulation Of Dialysed Mast Cells From Rat Peritoneum.* Journal of Physiology, 1988. **395**: p. 193-214.
115. Neher, E., *Control on calcium influx.* Nature, 1992. **355**: p. 298-299.
116. Neher, E., *Ion channels for communication between and within Cells.* The EMBO Journal, 1992. **11**(5): p. 1673-1679.
117. Depboylu, C., et al., *Neuregulin-1 receptor tyrosine kinase ErbB4 is upregulated in midbrain dopaminergic neurons in Parkinson disease.* Neurosci Lett, 2012. **531**(2): p. 209-14.
118. Kumar, R., et al., *FGF2-mediated regulation of exosome release depends on VAMPs/cellubrevin in cultured hippocampal neurons.* Advanced science (Weinheim, Baden-Wurttemberg, Germany) 20.

119. Escudero, C.A., et al., *The p75 neurotrophin receptor evades the endolysosomal route in neuronal cells, favouring multivesicular bodies specialised for exosomal release.* Journal of Cell Science, 2014. **127**(9): p. 1966.
120. Paroutis, P., N. Touret, and S. Grinstein, *The pH of the Secretory Pathway: Measurement, Determinants, and Regulation.* Physiology, 2004. **19**(4): p. 207-215.
121. Nelson, N., *Structure and function of V-ATPases in endocytic and secretory organelles.* The Journal of Experimental Biology, 1992. **172**(1): p. 149.
122. Miesenböck, G., D.A. De Angelis, and J.E. Rothman, *Visualizing secretion and synaptic transmission with pH-sensitive green fluorescent proteins.* Nature, 1998. **394**(6689): p. 192-195.
123. Ralf Schneggenburger and E. Neher, *Intracellular calcium dependence of transmitter release rates at a fast central synapse.* Nature, 2000. **406**: p. 889-893.
124. Gardiner, C., et al., *Extracellular vesicle sizing and enumeration by nanoparticle tracking analysis.* Journal of Extracellular Vesicles, 2013. **2**(1): p. 19671.
125. Saveyn, H., et al., *Accurate particle size distribution determination by nanoparticle tracking analysis based on 2-D Brownian dynamics simulation.* Journal of Colloid and Interface Science, 2010. **352**(2): p. 593-600.
126. Dragovic, R.A., et al., *Sizing and phenotyping of cellular vesicles using Nanoparticle Tracking Analysis.* Nanomedicine: Nanotechnology, Biology and Medicine, 2011. **7**(6): p. 780-788.
127. Langfelder, P. and S. Horvath, *WGCNA: an R package for weighted correlation network analysis.* BMC Bioinformatics, 2008. **9**(1): p. 559-559.
128. Christian von Mering, M.H., Daniel Jaeggi, Steffen Schmidt, Peer Bork, Berend Snel, *STRING: a database of predicted functional associations between proteins.* Nucleic Acids Research, 2003. **31**(1): p. 258-261.
129. Höllerhage, M., et al., *Trifluoperazine rescues human dopaminergic cells from wild-type α-synuclein-induced toxicity.* Neurobiology of Aging, 2014. **35**(7): p. 1700-1711.
130. J.M.Fernandez, E.Neher, and D.G. B, *Capacitance Measurment reveals stepwise fusion events in degranulating mast cells.* Nature 1984. **312**.
131. Kumar, R., G.U. Höglinger, and T. Koeglsperger, *Decoding Parkinson Disorder (PD) Pathophysiology: α-Synuclein over-expression enhances inward calcium influx and exosome release in LUHMES cells.* ScienceOpen Posters.
132. Scholz, D., et al., *Rapid, complete and large-scale generation of post-mitotic neurons from the human LUHMES cell line.* J Neurochem, 2011. **119**(5): p. 957-71.
133. Erwin Neher and T. Sakaba, *Combining Deconvolution and Noise Analysis for the Estimation of Transmitter Release Rates at the calyx of Held.* The Journal of Neuroscience, 2001. **21**(2): p. 444-461.
134. Erwin Neher and T. Sakaba, *Estimating transmitter release rates from Presynaptic current fluctuations.* The Journal of Neuroscience, 2001. **21**(24): p. 9638-9654.
135. Mistry, S.K., et al., *Cultured rat hippocampal neural progenitors generate spontaneously active neural networks.* Proceedings of the National Academy of Sciences, 2002. **99**(3): p. 1621.
136. Kumar, R., et al., *Fibroblast Growth Factor 2-Mediated Regulation of Neuronal Exosome Release Depends on VAMP3/Cellubrevin in Hippocampal Neurons.* Advanced Science, 2020: p. 1902372.
137. Kumar, R., et al., *Basic Fibroblast Growth Factor 2-induced Proteome Changes Endorse Lewy Body Pathology in Hippocampal Neurons.* iScience, 2020: p. 101349.
138. Sharma, K., et al., *Cell type- and brain region-resolved mouse brain proteome.* Nat Neurosci, 2015. **18**(12): p. 1819-31.
139. Corey Smith and E. Neher, *Multiple Forms of Endocytosis In Bovine Adrenal Chromaffin Cells.* The Journal of Cell Biology, 1997. **139**(4): p. 885-894.
140. Dirk Beutner, et al., *Calcium Dependence of Exocytosis and Endocytosis at the Cochlear inner Hair Cell Afferent Synapse.* Neuron, 2001. **29**(1): p. 681-690.
141. E.Neher and A.Marty, *Discrete Changes of Cell Membrane Capacitance observed under conditions of enhanced secretion in bovine adrenal chromaffin cells.* Proc Natl Acad Sci U S A, 1982. **79**: p. 6712-6716.

142. Reinhold Penner and E. Neher, *The patch-clamp technique in the study of secretion.* Trends in Neuroscience, 1989. **12**(4): p. 159-163.
143. Alexander C Meyer, Erwin NEher, and R. Schneggenburger, *Estimation of Quantal Size and Number of Functional Active Zones at Calyx of Held Synapse by Nonstationary EPSC Variance Analysis.* The Journal of Neuroscience, 2001. **21**(20): p. 7889-7900.
144. Haucke, V., E. Neher, and S.J. Sigrist, *Protein scaffolds in the coupling of synaptic exocytosis and endocytosis.* Nat Rev Neurosci, 2011. **12**(3): p. 127-38.
145. Katz, B., *Quantal Mechanism of Neural Transmitter Release.* Science, 1971. **173**(3992): p. 123.
146. Bonsi, P., et al., *Coordinate high-frequency pattern of stimulation and calcium levels control the induction of LTP in striatal cholinergic interneurons.* Learn Mem, 2004. **11**(6): p. 755-60.
147. Willoughby, D., R. Thomas, and C. Schwiening, *The effects of intracellular pH changes on resting cytosolic calcium in voltage-clamped snail neurones.* The Journal of physiology, 2001. **530**(Pt 3): p. 405-416.
148. Ban, J.J., et al., *Low pH increases the yield of exosome isolation.* Biochem Biophys Res Commun, 2015. **461**(1): p. 76-9.
149. Willms, E., et al., *Cells release subpopulations of exosomes with distinct molecular and biological properties.* Sci Rep, 2016. **6**: p. 22519.
150. Kowal, J., et al., *Proteomic comparison defines novel markers to characterize heterogeneous populations of extracellular vesicle subtypes.* Proc Natl Acad Sci U S A, 2016. **113**(8): p. E968-77.
151. Fruhbeis, C., et al., *Neurotransmitter-triggered transfer of exosomes mediates oligodendrocyte-neuron communication.* PLoS Biol, 2013. **11**(7): p. e1001604.
152. Seeley, W.W., *Mapping Neurodegenerative Disease Onset and Progression.* Cold Spring Harb Perspect Biol, 2017. **9**(8).
153. Reichardt, L.F., *Neurotrophin-regulated signalling pathways.* Philos Trans R Soc Lond B Biol Sci, 2006. **361**(1473): p. 1545-64.
154. Mohammadi, M., J. Schlessinger, and S.R. Hubbard, *Structure of the FGF receptor tyrosine kinase domain reveals a novel autoinhibitory mechanism.* Cell, 1996. **86**(4): p. 577-87.
155. Dai, S., et al., *Fibroblast Growth Factor Receptors (FGFRs): Structures and Small Molecule Inhibitors.* Cells, 2019. **8**(6): p. 614.
156. Liu, L., S.A. Yang T Fau - Simon, and S.A. Simon, *The protein tyrosine kinase inhibitor, genistein, decreases excitability of nociceptive neurons.* (0304-3959 (Print)).
157. Sayeski, P.P. and M.S. Ali, *The critical role of c-Src and the Shc/Grb2/ERK2 signaling pathway in angiotensin II-dependent VSMC proliferation.* Exp Cell Res, 2003. **287**(2): p. 339-49.
158. Lakomek, N.A., et al., *Structural dynamics and transient lipid binding of synaptobrevin-2 tune SNARE assembly and membrane fusion.* Proc Natl Acad Sci U S A, 2019. **116**(18): p. 8699-8708.
159. Oelkers, M., et al., *SNARE-mediated membrane fusion trajectories derived from force-clamp experiments.* Proc Natl Acad Sci U S A, 2016. **113**(46): p. 13051-13056.
160. Das, D., et al., *Resolving kinetic intermediates during the regulated assembly and disassembly of fusion pores.* Nat Commun, 2020. **11**(1): p. 231.
161. Sun, J., et al., *Functional cooperation of α-synuclein and VAMP2 in synaptic vesicle recycling.* Proc Natl Acad Sci U S A, 2019. **116**(23): p. 11113-11115.
162. Gruenberg, J., G. Griffiths, and K.E. Howell, *Characterization of the early endosome and putative endocytic carrier vesicles in vivo and with an assay of vesicle fusion in vitro.* The Journal of Cell Biology, 1989. **108**(4): p. 1301-1316.
163. Bartels, T., *A traffic jam leads to Lewy bodies.* Nat Neurosci, 2019. **22**(7): p. 1043-1045.
164. Shahmoradian, S.H., et al., *Lewy pathology in Parkinson's disease consists of crowded organelles and lipid membranes.* Nature Neuroscience, 2019. **22**(7): p. 1099-1109.
165. Gustafsson, G., et al., *Secretion and Uptake of α-Synuclein Via Extracellular Vesicles in Cultured Cells.* Cell Mol Neurobiol, 2018. **38**(8): p. 1539-1550.

166. Lee, H.J., S. Patel, and S.J. Lee, *Intravesicular localization and exocytosis of alpha-synuclein and its aggregates.* J Neurosci, 2005. **25**(25): p. 6016-24.
167. Kim, C. and S.J. Lee, *Controlling the mass action of alpha-synuclein in Parkinson's disease.* (1471-4159 (Electronic)).
168. Fevrier, B., et al., *Cells release prions in association with exosomes.* Proc Natl Acad Sci U S A, 2004. **101**(26): p. 9683-8.
169. Hoglinger, G.U., et al., *Origin of the dopaminergic innervation of adult neurogenic areas.* J Comp Neurol, 2014. **522**(10): p. 2336-48.
170. Hoglinger, G.U., et al., *Dopamine depletion impairs precursor cell proliferation in Parkinson disease.* Nat Neurosci, 2004. **7**(7): p. 726-35.
171. Saito, Y., et al., *Lewy body pathology involves the olfactory cells in Parkinson's disease and related disorders.* Mov Disord, 2016. **31**(1): p. 135-8.
172. O'Dowd, S., et al., *Fluctuating cognition in the Lewy body dementias.* Brain, 2019. **142**(11): p. 3338-3350.
173. Korkut, C., et al., *Regulation of postsynaptic retrograde signaling by presynaptic exosome release.* Neuron, 2013. **77**(6): p. 1039-46.
174. Mably, A.J. and L.L. Colgin, *Gamma oscillations in cognitive disorders.* Curr Opin Neurobiol, 2018. **52**: p. 182-187.
175. Murty, D., et al., *Gamma oscillations weaken with age in healthy elderly in human EEG.* Neuroimage, 2020. **215**: p. 116826.
176. Lasztóczi, B. and T. Klausberger, *Distinct gamma oscillations in the distal dendritic fields of the dentate gyrus and the CA1 area of mouse hippocampus.* Brain Struct Funct, 2017. **222**(7): p. 3355-3365.
177. Tamura, H., S. Shiosaka, and S. Morikawa, *Trophic modulation of gamma oscillations: The key role of processing protease for Neuregulin-1 and BDNF precursors.* Neurochem Int, 2018. **119**: p. 2-10.
178. Buzsáki, G. and X.J. Wang, *Mechanisms of gamma oscillations.* Annu Rev Neurosci, 2012. **35**: p. 203-25.
179. Beudel, M., et al., *Tremor Reduction by Deep Brain Stimulation Is Associated With Gamma Power Suppression in Parkinson's Disease.* Neuromodulation, 2015. **18**(5): p. 349-54.
180. McCann, H., H. Cartwright, and G.M. Halliday, *Neuropathology of α-synuclein propagation and braak hypothesis.* Mov Disord, 2016. **31**(2): p. 152-60.

Appendix-1

A.1. EV-release is also boosted by BDNF and NGF:

The NTF other than bFGF i.e., BDNF and NGF have resulted higher number of particles in the culture media collected from cultured primary hippocampal neurons after their respective treatments. A significantly higher particle concentration was observed only in NTA though were reported with abate electrical stimuli responsive MVB-PM fusion events (**Figure A1.1A, B**). NTA results show no change in extracellular particle size (**Figure A1.1C**).

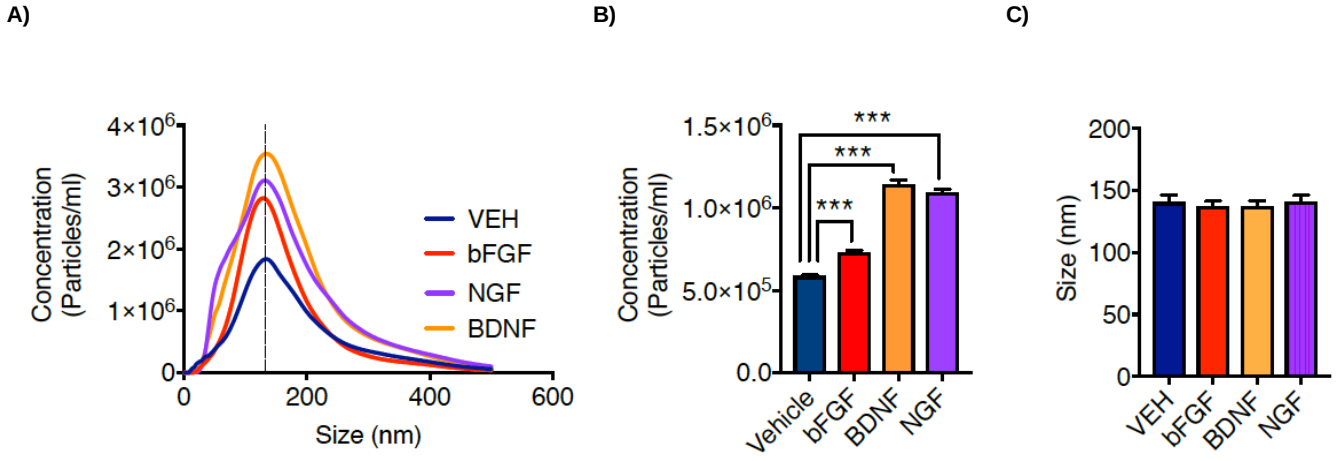

Figure A1.1. Other than bFGF, brain-derived neurotrophic factor (BDNF) and nerve growth factor (NGF) also increase neuronal EV release. A) NTA illustrating the particle number/size in cultured neurons treated with bFGF (50 ng/ml), BDNF (25 ng/ml) or NGF (50 ng/ml) for 24 hrs. B, C) bFGF, BDNF and NGF increase the number of particles in the cell culture medium from cultured neurons without affecting particle size. (n = 8/condition). Data are shown in mean ± SEM. For comparison, a two-tailed, paired t-test was used. ***$p < 0.001$. (Adapted from [136]).

Appendix-2

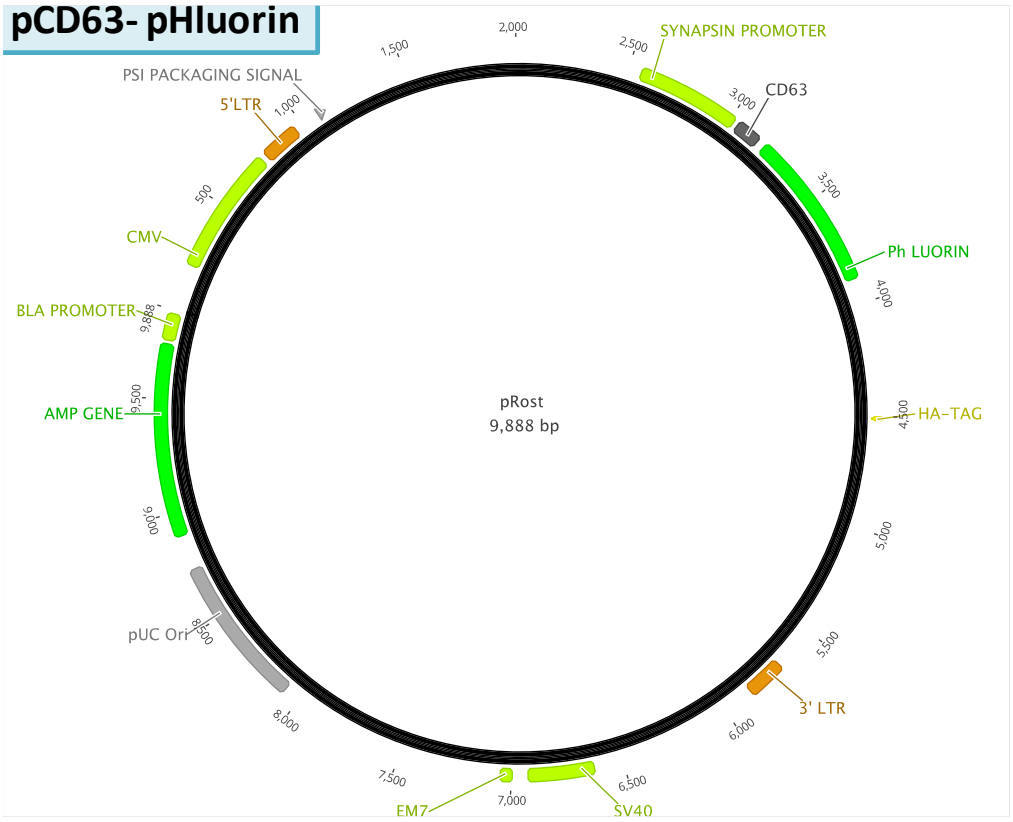

Figure A1.2. Molecular architecture of CD63-pHluorin construct used to label MVBs/exosomes in Veh and growth-factor treated neuronal hippocampal cultures.

Appendix-3

Fold changes of composite Network proteins	
Proteins	**Log2FC**
Kif5b	0.037361875
Fhl1	-0.359470018
Syt1	-0.605456935
Ctsd	-0.641905863
Hspa1a	0.443511786
Fus	-0.41592125
Aprt	0.300968452
Hspa9	0.458044768
Hspa5	0.236668155
Uchl1	-0.660274881
Vdac1	-0.628701339
Rps6	-0.1999395
Lsamp	-0.189775565
Nsf	-0.308227619
Eef1d	-0.165125161
Gstp1	0.399396815
Dlg1	0.206693214
Myo6	-0.643863482
Lrp1	0.210946696
Lars	0.608743333
Grin2b	-0.296774286

Aco1	-0.436535714
Txnl1	-0.17297
Ezr	0.403093631
Ipo9	-0.284785833
Slc6a11	-0.854160298
Hnrnph3	-0.570725357
Slc1a2	-0.535539107
Lap3	0.110207887
Cadm1	-0.489637917
Hsd17b10	-0.10325747
Hspa12a	-0.214776905
Ilf2	-0.2176125
Isoc1	-0.424375982
Tnr	-0.223805565
Crmp1	-0.251080119
Psmc4	0.193720208
Sirt2	-0.634705804
Marcks	-0.520000327
Ehd1	-0.243993452
Lancl2	-0.256357054
Calr	0.12625628
Apoe	-1.289632857
App	-0.535791548
Atp1a2	-0.631370893
Ly6h	-0.565237589

Pfn1	0.364466964
Prdx6	-0.744218155
Atp1a3	-0.587409048
Pygb	-0.669492589
Pdia3	0.064618869
Mcat	-0.36622125
Tfrc	-0.127207679
Hnrnph2	0.23251875
Cd200	-0.588231756
Clu	-0.489637917
Ncstn	-0.183850036
Cntn1	-0.489637917
Gmps	0.2903075
Nptx2	0.78537
Cpe	-0.489637917
Negr1	-0.641787232
Crym	-0.489637917
Rpl6	0.750924286
Dpysl5	-0.502732202
Nucb1	0.296125982
Olfm1	-0.489637917
Eef2	-0.070501667
Egfr	-0.481502589
Gap43	-0.508305893
Gdi1	-0.556943631

Gfap	-0.800368542
Glud1	-0.489637917
Glul	-2.185684911
Gpm6b	-0.489637917
Gstm1	-0.489637917
Ruvbl1	0.267276101
Sqstm1	-0.242422679
Hnrnpa2b1	-0.722175
Ppp3ca	-0.3000025
Idh1	-0.366698958
Aldh2	-0.290851012
Txnrd1	-0.27713997
Kif2a	-0.624128274
Kpnb1	-0.11759378
Mapk1	-0.490248125
Asrgl1	-0.489637917
Ncam1	-0.797035208
Atp1b2	-0.489637917
Gria2	-0.506568857
Nutf2	-0.229851696
Atp6v0a1	-0.354079643
Syn1	-0.24695631
Aimp2	0.297189048
Cat	-0.251706429
Cnr1	-0.35676375

Anxa5	0.777323274
Cnrip1	-0.489637917
Prdx2	-1.039205238
Scn2a	-0.27
Vim	0.964364018
Rap2b	0.165301399
Abca1	-0.217331369
Lingo1	-0.382743244
Adam10	0.453489494
Srp14	0.63451125
Slc44a1	0.269878393
Ephx1	0.347479792
Gnao1	-0.489637917
Rab6a	-0.086914911
Nedd4	0.611500643
Bag5	1.158340161
Dnajc5	-0.489637917
Penk	5.085214643
Calb1	0.808010446
Scarb2	-0.489637917
Gpc4	-0.051612679
Scrn1	-0.489637917
Rps14	1.187525238
Ephb2	-0.358113333
Tln1	0.111913125

Vps35	-0.3
Atxn2	0.786815
Dnaja2	0.889432292
Ddx6	0.044408857
Ptpra	-0.078511071
Slc32a1	-0.29806125
Stx1b	-0.653677232
Gspt1	0.2814525
Snca	

Appendix-4

Interaction data: Composite Network proteins		
Protein1	**Protein2**	**Weights (WPCNA)**
Syt1	*Stx1b*	0.042850308
Syt1	*Slc6a11*	0.036454311
Syt1	*Scrn1*	0.041639382
Syt1	*Scarb2*	0.039815124
Syt1	*Pygb*	0.116921349
Syt1	*Prdx6*	0.222447557
Syt1	*Prdx2*	0.048603485
Syt1	*Ncam1*	0.081072425
Syt1	*Marcks*	0.086065485
Syt1	*Mapk1*	0.022470491

Syt1	*Lingo1*	0.02508038
Syt1	*Kpnb1*	0.021627366
Syt1	*Idh1*	0.073651634
Syt1	*Hnrnpa2b1*	0.04355053
Syt1	*Gstm1*	0.088524788
Syt1	*Gpm6b*	0.266692754
Syt1	*Glul*	0.202636424
Syt1	*Glud1*	0.072210347
Syt1	*Gdi1*	0.161552634
Syt1	*Egfr*	0.073251388
Syt1	*Dpysl5*	0.081867058
Syt1	*Crym*	0.022697125
Syt1	*Cpe*	0.102724297
Syt1	*Cntn1*	0.084055723
Syt1	*Clu*	0.031024022
Syt1	*Cd200*	0.11319222
Syt1	*Cadm1*	0.056557981
Syt1	*Atp1a3*	0.118317854
Syt1	*Atp1a2*	0.033782189
Syt1	*App*	0.06282504
Syt1	*Apoe*	0.150418417
Syt1	*Aco1*	0.058228419
Syt1	*Slc6a11*	0.114849645
Syt1	*Slc1a2*	0.115480401
Syt1	*Scrn1*	0.032716701

Syt1	*Rap2b*	0.027090399
Syt1	*Pygb*	0.068243039
Syt1	*Ptpra*	0.026290973
Syt1	*Myo6*	0.077240391
Syt1	*Lsamp*	0.052377907
Syt1	*Hspa12a*	0.020221621
Syt1	*Gstm1*	0.053455915
Syt1	*Gpc4*	0.026336954
Syt1	*Glul*	0.180936138
Syt1	*Glud1*	0.04304082
Syt1	*Gfap*	0.088110344
Syt1	*Ephb2*	0.050962
Syt1	*Ctsd*	0.041020517
Syt1	*Crym*	0.070383776
Syt1	*Cpe*	0.07274275
Syt1	*Cntn1*	0.047204711
Syt1	*Cat*	0.023618517
Syt1	*Cadm1*	0.094793548
Syt1	*Atp1a3*	0.060210997
Syt1	*Atp1a2*	0.127545674
Syt1	*Asrgl1*	0.049376451
Syt1	*Apoe*	0.09272955
Syt1	*Aldh2*	0.044821408
Syt1	*Adam10*	0.02287919
Syt1	*Abca1*	0.059796403

Uchl1	*Syt1*	0.082110351
Uchl1	*Stx1b*	0.14144408
Uchl1	*Sqstm1*	0.039265942
Uchl1	*Slc6a11*	0.052674126
Uchl1	*Sirt2*	0.076916172
Uchl1	*Scrn1*	0.072345121
Uchl1	*Scarb2*	0.103184782
Uchl1	*Rab6a*	0.054872012
Uchl1	*Pygb*	0.120799379
Uchl1	*Prdx6*	0.167789016
Uchl1	*Prdx2*	0.087408578
Uchl1	*Ncam1*	0.097797852
Uchl1	*Marcks*	0.164773825
Uchl1	*Mapk1*	0.115786179
Uchl1	*Kpnb1*	0.055940784
Uchl1	*Kif2a*	0.080532037
Uchl1	*Idh1*	0.08366495
Uchl1	*Hnrnpa2b1*	0.123798695
Uchl1	*Gstm1*	0.160144935
Uchl1	*Gpm6b*	0.37124573
Uchl1	*Glul*	0.184916081
Uchl1	*Glud1*	0.066829917
Uchl1	*Gfap*	0.091212615
Uchl1	*Gdi1*	0.131331723
Uchl1	*Gap43*	0.109524467

Uchl1	*Egfr*	0.082140136
Uchl1	*Eef2*	0.0471493
Uchl1	*Eef1d*	0.035094114
Uchl1	*Dpysl5*	0.143428281
Uchl1	*Crym*	0.107462599
Uchl1	*Crmp1*	0.030610271
Uchl1	*Cpe*	0.116018827
Uchl1	*Cntn1*	0.155518611
Uchl1	*Clu*	0.143333952
Uchl1	*Cd200*	0.066061389
Uchl1	*Cadm1*	0.048841495
Uchl1	*Atp1a3*	0.194307905
Uchl1	*Atp1a2*	0.131238404
Uchl1	*App*	0.129558366
Uchl1	*Apoe*	0.252961851
Vdac1	*Uchl1*	0.050952153
Vdac1	*Txnrd1*	0.028985364
Vdac1	*Stx1b*	0.035716769
Vdac1	*Scrn1*	0.031765703
Vdac1	*Scarb2*	0.025125045
Vdac1	*Pygb*	0.10195008
Vdac1	*Prdx6*	0.090240996
Vdac1	*Prdx2*	0.106779108
Vdac1	*Ncam1*	0.020896823
Vdac1	*Marcks*	0.090620561

Vdac1	*Kpnb1*	0.03366518
Vdac1	*Hnrnpa2b1*	0.05432051
Vdac1	*Gstm1*	0.068959372
Vdac1	*Gpm6b*	0.122662366
Vdac1	*Glul*	0.046274853
Vdac1	*Gdi1*	0.089690612
Vdac1	*Dpysl5*	0.02911306
Vdac1	*Cpe*	0.080053836
Vdac1	*Cntn1*	0.030350088
Vdac1	*Clu*	0.021164566
Vdac1	*Atp1a3*	0.071978725
Vdac1	*Atp1a2*	0.035069597
Vdac1	*App*	0.068622212
Vdac1	*Apoe*	0.094824174
Vdac1	*Tnr*	0.033411964
Vdac1	*Slc6a11*	0.035510587
Vdac1	*Slc1a2*	0.046941779
Vdac1	*Scrn1*	0.020669885
Vdac1	*Pygb*	0.029212308
Vdac1	*Negr1*	0.023758038
Vdac1	*Myo6*	0.041880943
Vdac1	*Lsamp*	0.023473115
Vdac1	*Isoc1*	0.026061451
Vdac1	*Gstm1*	0.024208934
Vdac1	*Gpc4*	0.032291373

Vdac1	*Glul*	0.050491239
Vdac1	*Gfap*	0.050257537
Vdac1	*Ephx1*	0.044418517
Vdac1	*Ephb2*	0.020821162
Vdac1	*Egfr*	0.026685929
Vdac1	*Dpysl5*	0.038283317
Vdac1	*Crym*	0.052597621
Vdac1	*Cpe*	0.028973299
Vdac1	*Cntn1*	0.033894308
Vdac1	*Cadm1*	0.045024237
Vdac1	*Atp1a3*	0.031513196
Vdac1	*Atp1a2*	0.076686766
Vdac1	*Asrgl1*	0.030261387
Vdac1	*Apoe*	0.070462709
Vdac1	*Aldh2*	0.026319361
Vdac1	*Abca1*	0.035792004
Rps6	*Atxn2*	0.056188423
Rps6	*Rpl6*	0.056188423
Rps6	*Rps14*	0.056188423
Txnl1	*Eef2*	0.056188423
Txnl1	*Hspa5*	0.056188423
Txnl1	*Lars*	0.056188423
Slc6a11	*Slc44a1*	0.026329786
Slc6a11	*Slc32a1*	0.0311017
Slc6a11	*Slc1a2*	0.19990023

Slc6a11	*Sirt2*	0.068540912
Slc6a11	*Scrn1*	0.125427562
Slc6a11	*Scn2a*	0.073993336
Slc6a11	*Scarb2*	0.071808898
Slc6a11	*Rap2b*	0.108349513
Slc6a11	*Pygb*	0.114491751
Slc6a11	*Pygb*	0.03257175
Slc6a11	*Ptpra*	0.098205642
Slc6a11	*Prdx6*	0.080848243
Slc6a11	*Prdx6*	0.031511275
Slc6a11	*Ncam1*	0.03240243
Slc6a11	*Ppp3ca*	0.020825599
Slc6a11	*Marcks*	0.07960533
Slc6a11	*Idh1*	0.029210651
Slc6a11	*Gstm1*	0.036681744
Slc6a11	*Gpm6b*	0.113848135
Slc6a11	*Glul*	0.093232971
Slc6a11	*Gdi1*	0.061841622
Slc6a11	*Egfr*	0.037303211
Slc6a11	*Olfm1*	0.102752726
Slc6a11	*Dpysl5*	0.033935656
Slc6a11	*Cntn1*	0.081159347
Slc6a11	*Clu*	0.036605767
Slc6a11	*Negr1*	0.10266138
Slc6a11	*Atp1a3*	0.088227336

Slc6a11	*Atp1a2*	0.022089086
Slc6a11	*App*	0.02387224
Slc6a11	*Apoe*	0.094605662
Slc6a11	*Ncstn*	0.03343399
Slc6a11	*Myo6*	0.148154294
Slc6a11	*Mcat*	0.03769739
Slc6a11	*Mapk1*	0.060053254
Slc6a11	*Ly6h*	0.089011965
Slc6a11	*Lsamp*	0.159183051
Slc6a11	*Lrp1*	0.022976313
Slc6a11	*Lingo1*	0.075144517
Slc6a11	*Lancl2*	0.061043876
Slc6a11	*Kif2a*	0.042821621
Slc6a11	*Isoc1*	0.145220841
Slc6a11	*Ilf2*	0.021753741
Slc6a11	*Idh1*	0.086124644
Slc6a11	*Hspa12a*	0.094913841
Slc6a11	*Hnrnph3*	0.0410167
Slc6a11	*Hnrnpa2b1*	0.059190014
Slc6a11	*Gstm1*	0.10726307
Slc6a11	*Grin2b*	0.063036108
Slc6a11	*Gria2*	0.052714838
Slc6a11	*Gpm6b*	0.038797242
Slc6a11	*Gpc4*	0.11091263
Slc6a11	*Gnao1*	0.059455903

Slc6a11	*Glul*	0.262420354
Slc6a11	*Glud1*	0.169104112
Slc6a11	*Gfap*	0.163031078
Slc6a11	*Gdi1*	0.038620557
Slc6a11	*Fus*	0.100763972
Slc6a11	*Fhl1*	0.138772566
Slc6a11	*Ephx1*	0.027580281
Slc6a11	*Ephb2*	0.185478442
Slc6a11	*Ehd1*	0.080216506
Slc6a11	*Egfr*	0.129573888
Slc6a11	*Dpysl5*	0.087674493
Slc6a11	*Dnajc5*	0.069900401
Slc6a11	*Dlg1*	0.047590439
Slc6a11	*Ctsd*	0.12385862
Slc6a11	*Crym*	0.165794701
Slc6a11	*Cpe*	0.175791133
Slc6a11	*Cntn1*	0.131285877
Slc6a11	*Cnrip1*	0.119483468
Slc6a11	*Cnr1*	0.036140314
Slc6a11	*Clu*	0.057502173
Slc6a11	*Cat*	0.144496409
Slc6a11	*Cadm1*	0.153848295
Slc6a11	*Atp6v0a1*	0.033107861
Slc6a11	*Atp1b2*	0.105392327
Slc6a11	*Atp1a3*	0.163813523

Slc6a11	*Atp1a2*	0.229442413
Slc6a11	*Asrgl1*	0.119020952
Slc6a11	*Apoe*	0.162932002
Slc6a11	*Aldh2*	0.098843319
Slc6a11	*Adam10*	0.112615338
Slc6a11	*Abca1*	0.145005543
Slc1a2	*Sirt2*	0.119220179
Slc1a2	*Scrn1*	0.134809029
Slc1a2	*Scn2a*	0.122981051
Slc1a2	*Scarb2*	0.093941779
Slc1a2	*Rap2b*	0.184576455
Slc1a2	*Pygb*	0.182546526
Slc1a2	*Ptpra*	0.089825094
Slc1a2	*Prdx6*	0.03490757
Slc1a2	*Olfm1*	0.134361718
Slc1a2	*Nsf*	0.028866299
Slc1a2	*Negr1*	0.117225218
Slc1a2	*Ncstn*	0.064732402
Slc1a2	*Myo6*	0.192462489
Slc1a2	*Mcat*	0.030261862
Slc1a2	*Mapk1*	0.114023865
Slc1a2	*Ly6h*	0.076611607
Slc1a2	*Lsamp*	0.131788601
Slc1a2	*Lrp1*	0.056951215
Slc1a2	*Lingo1*	0.112799117

Slc1a2	*Lancl2*	0.112107863
Slc1a2	*Kif2a*	0.072358671
Slc1a2	*Isoc1*	0.174098238
Slc1a2	*Ilf2*	0.039512941
Slc1a2	*Idh1*	0.135893776
Slc1a2	*Hspa12a*	0.162422906
Slc1a2	*Hsd17b10*	0.032730333
Slc1a2	*Hnrnph3*	0.109217768
Slc1a2	*Hnrnpa2b1*	0.077983639
Slc1a2	*Gstm1*	0.138943264
Slc1a2	*Grin2b*	0.081762727
Slc1a2	*Gria2*	0.049295504
Slc1a2	*Gpm6b*	0.062592809
Slc1a2	*Gpc4*	0.125270476
Slc1a2	*Gnao1*	0.096054715
Slc1a2	*Glul*	0.261419538
Slc1a2	*Glud1*	0.159171899
Slc1a2	*Gfap*	0.19857622
Slc1a2	*Gdi1*	0.041435955
Slc1a2	*Fus*	0.155964759
Slc1a2	*Fhl1*	0.116840172
Slc1a2	*Ephx1*	0.033317559
Slc1a2	*Ephb2*	0.17084636
Slc1a2	*Ehd1*	0.117144462
Slc1a2	*Egfr*	0.189078637

Slc1a2	*Dpysl5*	0.122378322
Slc1a2	*Dnajc5*	0.079748196
Slc1a2	*Dlg1*	0.083173325
Slc1a2	*Ctsd*	0.126779079
Slc1a2	*Crym*	0.211950487
Slc1a2	*Cpe*	0.192711378
Slc1a2	*Cntn1*	0.18884765
Slc1a2	*Cnrip1*	0.140163158
Slc1a2	*Cnr1*	0.06054685
Slc1a2	*Clu*	0.06481365
Slc1a2	*Cat*	0.174679255
Slc1a2	*Cadm1*	0.169598609
Slc1a2	*Atp6v0a1*	0.061101122
Slc1a2	*Atp1b2*	0.126771661
Slc1a2	*Atp1a3*	0.19595181
Slc1a2	*Atp1a2*	0.280262426
Slc1a2	*Asrgl1*	0.162210529
Slc1a2	*Apoe*	0.195937244
Slc1a2	*Aldh2*	0.171548903
Slc1a2	*Adam10*	0.141804606
Slc1a2	*Abca1*	0.188548877
Tnr	*Syt1*	0.081100851
Tnr	*Syn1*	0.094610439
Tnr	*Slc6a11*	0.148563461
Tnr	*Slc44a1*	0.02564276

Tnr	*Slc32a1*	0.021884392
Tnr	*Slc1a2*	0.206135672
Tnr	*Sirt2*	0.066658251
Tnr	*Scrn1*	0.08271873
Tnr	*Scn2a*	0.116507922
Tnr	*Scarb2*	0.070542581
Tnr	*Rap2b*	0.128419978
Tnr	*Pygb*	0.130720039
Tnr	*Ptpra*	0.082884024
Tnr	*Olfm1*	0.092129687
Tnr	*Nsf*	0.026033693
Tnr	*Negr1*	0.090365337
Tnr	*Ncstn*	0.050160234
Tnr	*Myo6*	0.116607187
Tnr	*Mapk1*	0.102394167
Tnr	*Ly6h*	0.038221453
Tnr	*Lsamp*	0.083779859
Tnr	*Lrp1*	0.034449129
Tnr	*Lingo1*	0.113080087
Tnr	*Lancl2*	0.086355565
Tnr	*Kif2a*	0.069785359
Tnr	*Isoc1*	0.123611528
Tnr	*Ilf2*	0.020447382
Tnr	*Idh1*	0.090117058
Tnr	*Hspa12a*	0.14689686

Tnr	*Hsd17b10*	0.039609926
Tnr	*Hnrnph3*	0.053988805
Tnr	*Hnrnpa2b1*	0.034922732
Tnr	*Gstm1*	0.098625518
Tnr	*Grin2b*	0.062338107
Tnr	*Gria2*	0.033097739
Tnr	*Gpm6b*	0.040530031
Tnr	*Gpc4*	0.092117179
Tnr	*Gnao1*	0.043582946
Tnr	*Glul*	0.22762677
Tnr	*Glud1*	0.09065647
Tnr	*Gfap*	0.174894298
Tnr	*Gdi1*	0.026873416
Tnr	*Fus*	0.091667203
Tnr	*Fhl1*	0.056472524
Tnr	*Ephx1*	0.020034841
Tnr	*Ephb2*	0.100503007
Tnr	*Ehd1*	0.100866594
Tnr	*Egfr*	0.126583965
Tnr	*Dpysl5*	0.083464081
Tnr	*Dnajc5*	0.044693739
Tnr	*Dlg1*	0.031007152
Tnr	*Ctsd*	0.091500133
Tnr	*Crym*	0.129250787
Tnr	*Cpe*	0.141279268

Tnr	*Cntn1*	0.134846863
Tnr	*Cnrip1*	0.070302957
Tnr	*Cnr1*	0.041463699
Tnr	*Clu*	0.037190472
Tnr	*Cat*	0.097562981
Tnr	*Cadm1*	0.123447106
Tnr	*Atp6v0a1*	0.054344267
Tnr	*Atp1b2*	0.097089445
Tnr	*Atp1a3*	0.141458258
Tnr	*Atp1a2*	0.258291507
Tnr	*Asrgl1*	0.118578731
Tnr	*Apoe*	0.191843073
Tnr	*Aldh2*	0.117489035
Tnr	*Adam10*	0.091387708
Tnr	*Abca1*	0.104699219
Sirt2	*Hnrnpa2b1*	0.023379289
Sirt2	*Gstm1*	0.056366994
Sirt2	*Gpm6b*	0.128628391
Sirt2	*Glul*	0.105049614
Sirt2	*Gdi1*	0.041695909
Sirt2	*Dpysl5*	0.027257069
Sirt2	*Cpe*	0.033881068
Sirt2	*Cntn1*	0.026670444
Sirt2	*Clu*	0.02981546
Sirt2	*Atp1a3*	0.053038879

Sirt2	*App*	0.033354098
Sirt2	*Apoe*	0.071326986
Sirt2	*Scrn1*	0.07049247
Sirt2	*Scarb2*	0.042449369
Sirt2	*Rap2b*	0.035387856
Sirt2	*Pygb*	0.091494992
Sirt2	*Olfm1*	0.031100624
Sirt2	*Negr1*	0.025169413
Sirt2	*Myo6*	0.07744051
Sirt2	*Mapk1*	0.031004239
Sirt2	*Ly6h*	0.020273389
Sirt2	*Lsamp*	0.05252087
Sirt2	*Lrp1*	0.021694551
Sirt2	*Lancl2*	0.035382348
Sirt2	*Isoc1*	0.021117885
Sirt2	*Idh1*	0.02992285
Sirt2	*Hspa12a*	0.021291821
Sirt2	*Hnrnph3*	0.024675167
Sirt2	*Gstm1*	0.105826079
Sirt2	*Gpm6b*	0.059228611
Sirt2	*Gpc4*	0.036592577
Sirt2	*Gnao1*	0.047173606
Sirt2	*Glul*	0.126205581
Sirt2	*Gfap*	0.120638174
Sirt2	*Fus*	0.042537017

Sirt2	*Ephb2*	0.043698188
Sirt2	*Ehd1*	0.024734472
Sirt2	*Egfr*	0.026588383
Sirt2	*Dnajc5*	0.04112233
Sirt2	*Dlg1*	0.046814068
Sirt2	*Ctsd*	0.042682522
Sirt2	*Crym*	0.072069639
Sirt2	*Cpe*	0.060734668
Sirt2	*Cntn1*	0.062212052
Sirt2	*Cnrip1*	0.022466628
Sirt2	*Cadm1*	0.070208608
Sirt2	*Pygb*	0.027840419
Sirt2	*Atp6v0a1*	0.020063612
Sirt2	*Atp1a3*	0.099562181
Sirt2	*Atp1a2*	0.184963293
Sirt2	*Prdx6*	0.066429458
Sirt2	*Asrgl1*	0.099584887
Sirt2	*Apoe*	0.171531241
Sirt2	*Aldh2*	0.086171388
Sirt2	*Adam10*	0.041126854
Sirt2	*Abca1*	0.103559505
Sirt2	*Marcks*	0.041601899
Marcks	*Mapk1*	0.098102164
Marcks	*Kpnb1*	0.078572036
Marcks	*Kif2a*	0.104742025

Marcks	*Idh1*	0.108340974
Marcks	*Hnrnpa2b1*	0.117123095
Marcks	*Gstm1*	0.151015031
Marcks	*Gpm6b*	0.350131653
Marcks	*Glul*	0.16168305
Marcks	*Glud1*	0.068723023
Marcks	*Gfap*	0.092908674
Marcks	*Gdi1*	0.16766803
Marcks	*Gap43*	0.119806319
Marcks	*Egfr*	0.140083231
Marcks	*Eef2*	0.052779619
Marcks	*Eef1d*	0.043225199
Marcks	*Dpysl5*	0.133726993
Marcks	*Ctsd*	0.020543977
Marcks	*Crym*	0.078680696
Marcks	*Crmp1*	0.059272977
Marcks	*Cpe*	0.100858116
Marcks	*Cntn1*	0.143935727
Marcks	*Clu*	0.144209279
Marcks	*Cd200*	0.059188311
Marcks	*Cadm1*	0.028313701
Marcks	*Atp1a3*	0.160370815
Marcks	*Atp1a2*	0.184151194
Marcks	*App*	0.154248916
Marcks	*Apoe*	0.290594721

Prdx6	*Prdx2*	0.166899521
Prdx6	*Ncam1*	0.161319023
Prdx6	*Marcks*	0.179666947
Prdx6	*Mapk1*	0.135194991
Prdx6	*Kpnb1*	0.118587346
Prdx6	*Kif2a*	0.051404178
Prdx6	*Idh1*	0.205400241
Prdx6	*Hnrnpa2b1*	0.158798212
Prdx6	*Gstm1*	0.195103596
Prdx6	*Gpm6b*	0.415190599
Prdx6	*Glul*	0.245956695
Prdx6	*Glud1*	0.160870032
Prdx6	*Gfap*	0.105058481
Prdx6	*Gdi1*	0.226674833
Prdx6	*Gap43*	0.060831379
Prdx6	*Ehd1*	0.022346498
Prdx6	*Egfr*	0.187258516
Prdx6	*Eef2*	0.030141915
Prdx6	*Dpysl5*	0.198157569
Prdx6	*Crym*	0.104676473
Prdx6	*Crmp1*	0.044887816
Prdx6	*Cpe*	0.220458814
Prdx6	*Cntn1*	0.215516196
Prdx6	*Clu*	0.147216255
Prdx6	*Cd200*	0.184457431

Prdx6	*Cadm1*	0.06529251
Prdx6	*Atp1a3*	0.212003809
Prdx6	*Atp1a2*	0.143904647
Prdx6	*App*	0.1570516
Prdx6	*Apoe*	0.254551448
Prdx6	*Aco1*	0.079195693
Pygb	*Prdx6*	0.2207281
Pygb	*Prdx2*	0.172348919
Pygb	*Ncam1*	0.094556928
Pygb	*Marcks*	0.137875048
Pygb	*Mapk1*	0.113913765
Pygb	*Kpnb1*	0.145816386
Pygb	*Kif2a*	0.050545498
Pygb	*Idh1*	0.141646453
Pygb	*Hnrnpa2b1*	0.144810059
Pygb	*Gstm1*	0.157542054
Pygb	*Gpm6b*	0.361217901
Pygb	*Glul*	0.181007669
Pygb	*Glud1*	0.086292823
Pygb	*Gfap*	0.101415894
Pygb	*Gdi1*	0.197067207
Pygb	*Gap43*	0.040531381
Pygb	*Ehd1*	0.024707928
Pygb	*Egfr*	0.107680029
Pygb	*Eef2*	0.044100506

Pygb	*Dpysl5*	0.137837681
Pygb	*Crym*	0.072341788
Pygb	*Crmp1*	0.033512153
Pygb	*Cpe*	0.162767732
Pygb	*Cntn1*	0.108675091
Pygb	*Clu*	0.120003231
Pygb	*Cd200*	0.074755574
Pygb	*Cadm1*	0.023648666
Pygb	*Atp1a3*	0.123489951
Pygb	*Atp1a2*	0.117080003
Pygb	*App*	0.172192611
Pygb	*Apoe*	0.24759205
Pygb	*Aco1*	0.048219939
Tfrc	*Syt1*	0.030508073
Tfrc	*Scrn1*	0.02210287
Tfrc	*Pygb*	0.023634544
Tfrc	*Prdx6*	0.046952193
Tfrc	*Gpm6b*	0.045191824
Tfrc	*Glul*	0.047261
Tfrc	*Gdi1*	0.031681738
Tfrc	*Cpe*	0.040721079
Tfrc	*Apoe*	0.022441656
Tfrc	*Calb1*	0.056188423
Tfrc	*Calr*	0.056188423
Tfrc	*Ddx6*	0.056188423

Tfrc	*Eef1d*	0.056188423
Tfrc	*Eef2*	0.056188423
Tfrc	*Gstp1*	0.056188423
Tfrc	*Hspa5*	0.056188423
Tfrc	*Lars*	0.056188423
Tfrc	*Nedd4*	0.056188423
Tfrc	*Pdia3*	0.056188423
Tfrc	*Rab6a*	0.056188423
Tfrc	*Aprt*	0.056188423
Tfrc	*Atxn2*	0.056188423
Rpl6	*Atxn2*	0.056188423
Rpl6	*Ddx6*	0.056188423
Rpl6	*Eef2*	0.056188423
Rpl6	*Hspa5*	0.056188423
Rpl6	*Lars*	0.056188423
Rpl6	*Nucb1*	0.042649189
Gap43	*Dpysl5*	0.039715512
Gap43	*Cpe*	0.022046754
Gap43	*Cntn1*	0.043860495
Gap43	*Clu*	0.029291834
Gap43	*Atp1a3*	0.108348856
Gap43	*Atp1a2*	0.067164326
Gap43	*App*	0.040763891
Gap43	*Apoe*	0.117799173
Gdi1	*Gap43*	0.064063624

Gdi1	*Egfr*	0.147774058
Gdi1	*Eef2*	0.045292924
Gdi1	*Dpysl5*	0.169773213
Gdi1	*Crym*	0.101726017
Gdi1	*Crmp1*	0.060339755
Gdi1	*Cpe*	0.170500144
Gdi1	*Cntn1*	0.143957024
Gdi1	*Clu*	0.137339343
Gdi1	*Cd200*	0.107789479
Gdi1	*Cadm1*	0.035749854
Gdi1	*Atp1a3*	0.152106539
Gdi1	*Atp1a2*	0.155981225
Gdi1	*App*	0.160231486
Gdi1	*Apoe*	0.263272135
Gdi1	*Aco1*	0.059438234
Gfap	*Gdi1*	0.113249683
Gfap	*Dpysl5*	0.04883831
Gfap	*Cpe*	0.072388554
Gfap	*Cntn1*	0.023905193
Gfap	*Clu*	0.113334203
Gfap	*Atp1a3*	0.055903849
Gfap	*App*	0.196433175
Gfap	*Apoe*	0.186124753
Glud1	*Gdi1*	0.127132538
Glud1	*Dpysl5*	0.047434333

Glud1	*Cpe*	0.081903636
Glud1	*Cntn1*	0.042177311
Glud1	*Clu*	0.04645202
Glud1	*Cd200*	0.043812209
Glud1	*Atp1a3*	0.078438672
Glud1	*Atp1a2*	0.02022562
Glud1	*App*	0.074198137
Glud1	*Apoe*	0.127260676
Glud1	*Aco1*	0.022834298
Glul	*Glud1*	0.172740042
Glul	*Gfap*	0.105962502
Glul	*Gdi1*	0.202900267
Glul	*Gap43*	0.046741089
Glul	*Egfr*	0.145829248
Glul	*Eef2*	0.026759345
Glul	*Dpysl5*	0.191105039
Glul	*Crym*	0.119891441
Glul	*Crmp1*	0.040077013
Glul	*Cpe*	0.202220152
Glul	*Cntn1*	0.204410301
Glul	*Clu*	0.151606581
Glul	*Cd200*	0.174144014
Glul	*Cadm1*	0.066359796
Glul	*Atp1a3*	0.199003789
Glul	*Atp1a2*	0.113134427

Glul	*App*	0.15005839
Glul	*Apoe*	0.25679514
Glul	*Aco1*	0.067940391
Gpm6b	*Glul*	0.43369134
Gpm6b	*Glud1*	0.245243482
Gpm6b	*Gfap*	0.207308464
Gpm6b	*Gdi1*	0.376092891
Gpm6b	*Gap43*	0.116996792
Gpm6b	*Ehd1*	0.021903082
Gpm6b	*Egfr*	0.228433635
Gpm6b	*Eef2*	0.092684135
Gpm6b	*Eef1d*	0.040351485
Gpm6b	*Dpysl5*	0.368912966
Gpm6b	*Crym*	0.215350666
Gpm6b	*Crmp1*	0.073273828
Gpm6b	*Cpe*	0.369820573
Gpm6b	*Cntn1*	0.337744374
Gpm6b	*Clu*	0.342121322
Gpm6b	*Cd200*	0.20605245
Gpm6b	*Cadm1*	0.076677009
Gpm6b	*Atp1a3*	0.389427076
Gpm6b	*Atp1a2*	0.266898946
Gpm6b	*App*	0.338152383
Gpm6b	*Apoe*	0.398958619
Gpm6b	*Aco1*	0.07420905

Gstm1	*Gpm6b*	0.408964589
Gstm1	*Glul*	0.203096626
Gstm1	*Glud1*	0.129544021
Gstm1	*Gfap*	0.135171842
Gstm1	*Gdi1*	0.160897377
Gstm1	*Gap43*	0.042283539
Gstm1	*Egfr*	0.077665522
Gstm1	*Eef2*	0.053541636
Gstm1	*Eef1d*	0.028682998
Gstm1	*Dpysl5*	0.126724727
Gstm1	*Crym*	0.071210811
Gstm1	*Cpe*	0.168296607
Gstm1	*Cntn1*	0.113868994
Gstm1	*Clu*	0.167798031
Gstm1	*Cd200*	0.080246938
Gstm1	*Cadm1*	0.026760267
Gstm1	*Atp1a3*	0.149926724
Gstm1	*Atp1a2*	0.1064691
Gstm1	*App*	0.182269802
Gstm1	*Apoe*	0.25171345
Ruvbl1	*Anxa5*	0.056188423
Ruvbl1	*Aprt*	0.056188423
Ruvbl1	*Eef2*	0.056188423
Ruvbl1	*Ezr*	0.056188423
Ruvbl1	*Hspa1a*	0.056188423

Ruvbl1	*Hspa5*	0.056188423
Ruvbl1	*Hspa9*	0.056188423
Ruvbl1	*Kpnb1*	0.056188423
Ruvbl1	*Lars*	0.056188423
Ruvbl1	*Nedd4*	0.056188423
Ruvbl1	*Pfn1*	0.056188423
Sqstm1	*Atxn2*	0.056188423
Sqstm1	*Calb1*	0.056188423
Sqstm1	*Ddx6*	0.056188423
Sqstm1	*Eef1d*	0.056188423
Sqstm1	*Eef2*	0.056188423
Sqstm1	*Gmps*	0.056188423
Sqstm1	*Gstp1*	0.056188423
Sqstm1	*Hspa5*	0.056188423
Sqstm1	*Lars*	0.056188423
Sqstm1	*Nedd4*	0.056188423
Sqstm1	*Pdia3*	0.056188423
Sqstm1	*Rpl6*	0.056188423
Sqstm1	*Rps14*	0.056188423
Sqstm1	*Marcks*	0.031420514
Sqstm1	*Gstm1*	0.022223413
Sqstm1	*Gpm6b*	0.053632184
Sqstm1	*Clu*	0.029096645
Sqstm1	*Atp1a3*	0.027144732
Sqstm1	*App*	0.026264225

Sqstm1	*Apoe*	0.051674771
Hnrnpa2b1	*Gstm1*	0.166703663
Hnrnpa2b1	*Gpm6b*	0.303210072
Hnrnpa2b1	*Glul*	0.14559511
Hnrnpa2b1	*Glud1*	0.040651449
Hnrnpa2b1	*Gfap*	0.136740774
Hnrnpa2b1	*Gdi1*	0.15644209
Hnrnpa2b1	*Gap43*	0.024192584
Hnrnpa2b1	*Egfr*	0.037579433
Hnrnpa2b1	*Eef2*	0.054654018
Hnrnpa2b1	*Dpysl5*	0.074417821
Hnrnpa2b1	*Crym*	0.049297643
Hnrnpa2b1	*Cpe*	0.133011871
Hnrnpa2b1	*Cntn1*	0.049977491
Hnrnpa2b1	*Clu*	0.08716797
Hnrnpa2b1	*Cd200*	0.027995338
Hnrnpa2b1	*Atp1a3*	0.089987641
Hnrnpa2b1	*Atp1a2*	0.061268882
Hnrnpa2b1	*App*	0.211632031
Hnrnpa2b1	*Apoe*	0.222672282
Idh1	*Hnrnpa2b1*	0.055528837
Idh1	*Gstm1*	0.134979957
Idh1	*Gpm6b*	0.316230216
Idh1	*Glul*	0.185314073
Idh1	*Glud1*	0.094948896

Idh1	*Gdi1*	0.173827907
Idh1	*Egfr*	0.04711472
Idh1	*Dpysl5*	0.080826818
Idh1	*Crym*	0.021032179
Idh1	*Cpe*	0.108040274
Idh1	*Cntn1*	0.055891396
Idh1	*Clu*	0.06977202
Idh1	*Cd200*	0.051922157
Idh1	*Atp1a3*	0.107127139
Idh1	*Atp1a2*	0.034854659
Idh1	*App*	0.112223747
Idh1	*Apoe*	0.192527365
Idh1	*Aco1*	0.067677586
Txnrd1	*Pygb*	0.029808395
Txnrd1	*Prdx6*	0.028736447
Txnrd1	*Prdx2*	0.033127862
Txnrd1	*Gpm6b*	0.02342132
Txnrd1	*Gdi1*	0.025030429
Txnrd1	*Cpe*	0.033680792
Txnrd1	*Anxa5*	0.056188423
Txnrd1	*Aprt*	0.056188423
Txnrd1	*Calr*	0.056188423
Txnrd1	*Ddx6*	0.056188423
Txnrd1	*Eef2*	0.056188423
Txnrd1	*Ezr*	0.056188423

Txnrd1	*Hspa5*	0.056188423
Txnrd1	*Hspa9*	0.056188423
Txnrd1	*Kif5b*	0.056188423
Txnrd1	*Kpnb1*	0.056188423
Txnrd1	*Lars*	0.056188423
Txnrd1	*Nedd4*	0.056188423
Txnrd1	*Pfn1*	0.056188423
Txnrd1	*Rab6a*	0.056188423
Txnrd1	*Tln1*	0.056188423
Kif2a	*Hnrnpa2b1*	0.033651093
Kif2a	*Gstm1*	0.036977282
Kif2a	*Gpm6b*	0.108216084
Kif2a	*Glul*	0.039287582
Kif2a	*Gdi1*	0.057445933
Kif2a	*Dpysl5*	0.048397161
Kif2a	*Cpe*	0.021682397
Kif2a	*Cntn1*	0.032787543
Kif2a	*Clu*	0.054543276
Kif2a	*Atp1a3*	0.062678775
Kif2a	*Atp1a2*	0.036721449
Kif2a	*App*	0.068966817
Kif2a	*Apoe*	0.147765025
Kpnb1	*Idh1*	0.022435118
Kpnb1	*Hnrnpa2b1*	0.122980984
Kpnb1	*Gstm1*	0.100161403

Kpnb1	*Gpm6b*	0.164891426
Kpnb1	*Glul*	0.076545994
Kpnb1	*Gfap*	0.023605239
Kpnb1	*Gdi1*	0.130216766
Kpnb1	*Dpysl5*	0.044453798
Kpnb1	*Cpe*	0.12729824
Kpnb1	*Clu*	0.042550775
Kpnb1	*Atp1a3*	0.05299185
Kpnb1	*Atp1a2*	0.023233054
Kpnb1	*App*	0.141689643
Kpnb1	*Apoe*	0.122006401
Mapk1	*Idh1*	0.02392482
Mapk1	*Hnrnpa2b1*	0.075816993
Mapk1	*Gstm1*	0.097172087
Mapk1	*Gpm6b*	0.225592848
Mapk1	*Glul*	0.105455595
Mapk1	*Gfap*	0.028094973
Mapk1	*Gdi1*	0.113537128
Mapk1	*Dpysl5*	0.059531361
Mapk1	*Cpe*	0.068998337
Mapk1	*Cntn1*	0.041898992
Mapk1	*Clu*	0.078073437
Mapk1	*Atp1a3*	0.098730636
Mapk1	*Atp1a2*	0.026303368
Mapk1	*App*	0.113745577

Mapk1	*Apoe*	0.167624973
Ncam1	*Marcks*	0.113164413
Ncam1	*Idh1*	0.048295233
Ncam1	*Hnrnpa2b1*	0.035274502
Ncam1	*Gstm1*	0.079016741
Ncam1	*Gpm6b*	0.235513309
Ncam1	*Glul*	0.137357781
Ncam1	*Glud1*	0.028921658
Ncam1	*Gdi1*	0.120321285
Ncam1	*Gap43*	0.033673172
Ncam1	*Egfr*	0.044041462
Ncam1	*Dpysl5*	0.068592038
Ncam1	*Cpe*	0.071280189
Ncam1	*Cntn1*	0.080845392
Ncam1	*Clu*	0.034811534
Ncam1	*Cd200*	0.041323076
Ncam1	*Cadm1*	0.035290688
Ncam1	*Atp1a3*	0.146709857
Ncam1	*Atp1a2*	0.038352077
Ncam1	*App*	0.059475701
Ncam1	*Apoe*	0.148513049
Gria2	*Cd200*	0.022078495
Syn1	*Slc6a11*	0.052313585
Syn1	*Slc1a2*	0.096887179
Syn1	*Sirt2*	0.025574278

Syn1	*Scrn1*	0.028710512
Syn1	*Scn2a*	0.030530252
Syn1	*Scarb2*	0.027906613
Syn1	*Rap2b*	0.055315322
Syn1	*Pygb*	0.10436978
Syn1	*Olfm1*	0.022368497
Syn1	*Myo6*	0.049369509
Syn1	*Mapk1*	0.03080609
Syn1	*Lsamp*	0.022637775
Syn1	*Lrp1*	0.020555949
Syn1	*Lancl2*	0.030862259
Syn1	*Isoc1*	0.021527819
Syn1	*Idh1*	0.023093047
Syn1	*Hspa12a*	0.033900946
Syn1	*Gstm1*	0.05078256
Syn1	*Gpc4*	0.024140634
Syn1	*Glul*	0.088854573
Syn1	*Gfap*	0.111176727
Syn1	*Ephb2*	0.025975519
Syn1	*Ctsd*	0.021145716
Syn1	*Crym*	0.072118093
Syn1	*Cpe*	0.070511819
Syn1	*Cntn1*	0.065135362
Syn1	*Cadm1*	0.053023014
Syn1	*Atp1a3*	0.070128253

Syn1	*Atp1a2*	0.147717072
Syn1	*Asrgl1*	0.082596726
Syn1	*Apoe*	0.134077828
Syn1	*Aldh2*	0.06790548
Syn1	*Abca1*	0.052852234
Prdx2	*Ncam1*	0.043742812
Prdx2	*Marcks*	0.110597383
Prdx2	*Mapk1*	0.055432444
Prdx2	*Kpnb1*	0.135348135
Prdx2	*Kif2a*	0.027644996
Prdx2	*Idh1*	0.063992957
Prdx2	*Hnrnpa2b1*	0.104640514
Prdx2	*Gstm1*	0.124798743
Prdx2	*Gpm6b*	0.271604274
Prdx2	*Glul*	0.118098589
Prdx2	*Glud1*	0.033279116
Prdx2	*Gfap*	0.053924669
Prdx2	*Gdi1*	0.163401888
Prdx2	*Gap43*	0.024837159
Prdx2	*Ehd1*	0.025661407
Prdx2	*Egfr*	0.048277101
Prdx2	*Eef2*	0.040659656
Prdx2	*Dpysl5*	0.084060709
Prdx2	*Crym*	0.029978906
Prdx2	*Cpe*	0.156635723

Prdx2	*Cntn1*	0.045681696
Prdx2	*Clu*	0.063039327
Prdx2	*Cd200*	0.02848101
Prdx2	*Atp1a3*	0.090469192
Prdx2	*Atp1a2*	0.069273054
Prdx2	*App*	0.166348662
Prdx2	*Apoe*	0.194110673
Prdx2	*Aco1*	0.020469565
Scn2a	*Rap2b*	0.030889151
Scn2a	*Pygb*	0.076935174
Scn2a	*Olfm1*	0.037018129
Scn2a	*Myo6*	0.057909562
Scn2a	*Lsamp*	0.035328214
Scn2a	*Lancl2*	0.025733943
Scn2a	*Isoc1*	0.023957626
Scn2a	*Hspa12a*	0.047700393
Scn2a	*Hsd17b10*	0.039417859
Scn2a	*Gstm1*	0.056966566
Scn2a	*Gpc4*	0.04064143
Scn2a	*Glul*	0.120292136
Scn2a	*Glud1*	0.024862079
Scn2a	*Gfap*	0.09275094
Scn2a	*Fus*	0.023098674
Scn2a	*Ephb2*	0.027348011
Scn2a	*Ehd1*	0.023078494

Scn2a	*Egfr*	0.021489735
Scn2a	*Dpysl5*	0.020090723
Scn2a	*Ctsd*	0.028629667
Scn2a	*Crym*	0.056620543
Scn2a	*Cpe*	0.062433425
Scn2a	*Cntn1*	0.089178492
Scn2a	*Cat*	0.030149619
Scn2a	*Cadm1*	0.094656622
Scn2a	*Atp6v0a1*	0.035665396
Scn2a	*Atp1b2*	0.020271186
Scn2a	*Atp1a3*	0.076797302
Scn2a	*Atp1a2*	0.180691746
Scn2a	*Asrgl1*	0.077223777
Scn2a	*Apoe*	0.117124922
Scn2a	*Aldh2*	0.074063156
Scn2a	*Abca1*	0.058671086
Vim	*Nedd4*	0.056188423
Vim	*Nptx2*	0.056188423
Vim	*Nucb1*	0.056188423
Vim	*Pdia3*	0.056188423
Vim	*Pfn1*	0.056188423
Vim	*Psmc4*	0.056188423
Vim	*Rab6a*	0.056188423
Vim	*Rps14*	0.056188423
Vim	*Ruvbl1*	0.056188423

Vim	*Srp14*	0.056188423
Vim	*Tln1*	0.056188423
Vim	*Txnrd1*	0.056188423
Vim	*Anxa5*	0.056188423
Vim	*App*	0.056188423
Vim	*Aprt*	0.056188423
Vim	*Atxn2*	0.056188423
Vim	*Calb1*	0.056188423
Vim	*Calr*	0.056188423
Vim	*Ddx6*	0.056188423
Vim	*Eef1d*	0.056188423
Vim	*Eef2*	0.056188423
Vim	*Ezr*	0.056188423
Vim	*Gmps*	0.056188423
Vim	*Gstp1*	0.056188423
Vim	*Hnrnph2*	0.056188423
Vim	*Hspa1a*	0.056188423
Vim	*Hspa5*	0.056188423
Vim	*Hspa9*	0.056188423
Vim	*Ipo9*	0.056188423
Vim	*Kif5b*	0.056188423
Vim	*Kpnb1*	0.056188423
Vim	*Lap3*	0.056188423
Vim	*Lars*	0.056188423
Rap2b	*Dnaja2*	0.119567657

Rap2b	*Adam10*	0.172492624
Rap2b	*Abca1*	0.11062137
Rap2b	*Penk*	0.092177617
Rap2b	*Lrp1*	0.100118369
Rap2b	*Ephx1*	0.026787514
Lingo1	*Aldh2*	0.020282976
Srp14	*Atxn2*	0.056188423
Srp14	*Ddx6*	0.056188423
Srp14	*Eef1d*	0.056188423
Srp14	*Eef2*	0.056188423
Srp14	*Gmps*	0.056188423
Srp14	*Hspa5*	0.056188423
Srp14	*Lars*	0.056188423
Srp14	*Nedd4*	0.056188423
Srp14	*Nptx2*	0.056188423
Srp14	*Pdia3*	0.056188423
Srp14	*Rps14*	0.056188423
Slc44a1	*Hspa9*	0.031384298
Slc44a1	*Hspa1a*	0.062665965
Slc44a1	*Gpc4*	0.075468753
Slc44a1	*Ephx1*	0.102793676
Slc44a1	*Slc1a2*	0.033385406
Slc44a1	*Pygb*	0.020586965
Slc44a1	*Myo6*	0.030684001
Slc44a1	*Lsamp*	0.022242188

Slc44a1	*Gpc4*	0.021356606
Slc44a1	*Glul*	0.037934837
Slc44a1	*Gfap*	0.03030827
Slc44a1	*Cpe*	0.022225432
Slc44a1	*Cntn1*	0.039989947
Slc44a1	*Cadm1*	0.03470466
Slc44a1	*Atp1a3*	0.025575716
Slc44a1	*Atp1a2*	0.048436406
Slc44a1	*Asrgl1*	0.032959235
Slc44a1	*Apoe*	0.029840419
Slc44a1	*Dlg1*	0.088739831
Slc44a1	*Calb1*	0.033283568
Slc44a1	*Bag5*	0.092918141
Slc44a1	*Anxa5*	0.045301182
Slc44a1	*Aimp2*	0.054131909
Slc44a1	*Adam10*	0.065668225
Slc44a1	*Rps14*	0.166871476
Slc44a1	*Rap2b*	0.033678093
Slc44a1	*Penk*	0.225804766
Slc44a1	*Nedd4*	0.071142424
Slc44a1	*Lrp1*	0.048859023
Rab6a	*Pygb*	0.094347742
Rab6a	*Prdx6*	0.082443633
Rab6a	*Prdx2*	0.056061297
Rab6a	*Ncam1*	0.021516615

Rab6a	*Marcks*	0.129031993
Rab6a	*Idh1*	0.028968126
Rab6a	*Hnrnpa2b1*	0.041805445
Rab6a	*Gstm1*	0.057947101
Rab6a	*Gpm6b*	0.13291691
Rab6a	*Glul*	0.048240167
Rab6a	*Gdi1*	0.104045476
Rab6a	*Egfr*	0.021232299
Rab6a	*Dpysl5*	0.042073916
Rab6a	*Ctsd*	0.061379425
Rab6a	*Cpe*	0.03308719
Rab6a	*Cntn1*	0.030449435
Rab6a	*Clu*	0.065770406
Rab6a	*Atp1a3*	0.071610006
Rab6a	*Atp1a2*	0.056775283
Rab6a	*App*	0.085788096
Rab6a	*Apoe*	0.141487413
Scarb2	*Rap2b*	0.024586297
Scarb2	*Pygb*	0.082136685
Scarb2	*Olfm1*	0.040360669
Scarb2	*Negr1*	0.030056284
Scarb2	*Myo6*	0.066914158
Scarb2	*Mapk1*	0.033794828
Scarb2	*Lsamp*	0.054656422
Scarb2	*Lancl2*	0.0299789

Scarb2	*Isoc1*	0.034140553
Scarb2	*Idh1*	0.023402594
Scarb2	*Hspa12a*	0.023895876
Scarb2	*Gstm1*	0.087992786
Scarb2	*Gpm6b*	0.040469224
Scarb2	*Gpc4*	0.049346946
Scarb2	*Gnao1*	0.030396916
Scarb2	*Glul*	0.106833197
Scarb2	*Gfap*	0.126990996
Scarb2	*Fus*	0.027702017
Scarb2	*Ephx1*	0.021004564
Scarb2	*Ephb2*	0.048262919
Scarb2	*Dnajc5*	0.028952563
Scarb2	*Dlg1*	0.022570048
Scarb2	*Ctsd*	0.044332053
Scarb2	*Crym*	0.073007257
Scarb2	*Cpe*	0.067138542
Scarb2	*Cntn1*	0.073848357
Scarb2	*Cadm1*	0.073353435
Scarb2	*Atp1a3*	0.099795353
Scarb2	*Atp1a2*	0.166358526
Scarb2	*Asrgl1*	0.117335281
Scarb2	*Apoe*	0.179937626
Scarb2	*Aldh2*	0.074839577
Scarb2	*Adam10*	0.02706026

Scarb2	*Abca1*	0.084828454
Scarb2	*Pygb*	0.126508067
Scarb2	*Prdx6*	0.183446543
Scarb2	*Prdx2*	0.068375383
Scarb2	*Ncam1*	0.020487269
Scarb2	*Marcks*	0.108702345
Scarb2	*Kpnb1*	0.034366374
Scarb2	*Idh1*	0.029277
Scarb2	*Hnrnpa2b1*	0.080135362
Scarb2	*Gstm1*	0.126546724
Scarb2	*Gpm6b*	0.241307797
Scarb2	*Glul*	0.150165406
Scarb2	*Gfap*	0.023957088
Scarb2	*Gdi1*	0.145412103
Scarb2	*Egfr*	0.026477527
Scarb2	*Dpysl5*	0.050814892
Scarb2	*Cpe*	0.104916867
Scarb2	*Cntn1*	0.055529265
Scarb2	*Clu*	0.049160836
Scarb2	*Cd200*	0.025736676
Scarb2	*Atp1a3*	0.10622825
Scarb2	*Atp1a2*	0.027979548
Scarb2	*App*	0.100277548
Scarb2	*Apoe*	0.162417965
Scrn1	*Scarb2*	0.037631627

Scrn1	*Pygb*	0.152486767
Scrn1	*Prdx6*	0.174435039
Scrn1	*Prdx2*	0.117919142
Scrn1	*Ncam1*	0.020226391
Scrn1	*Marcks*	0.063487157
Scrn1	*Mapk1*	0.023470139
Scrn1	*Kpnb1*	0.071539687
Scrn1	*Idh1*	0.029821659
Scrn1	*Hnrnpa2b1*	0.111376491
Scrn1	*Gstm1*	0.116747516
Scrn1	*Gpm6b*	0.249363173
Scrn1	*Glul*	0.143631862
Scrn1	*Glud1*	0.022007559
Scrn1	*Gfap*	0.025634962
Scrn1	*Gdi1*	0.146333016
Scrn1	*Ehd1*	0.048984705
Scrn1	*Dpysl5*	0.06946602
Scrn1	*Cpe*	0.201804636
Scrn1	*Cntn1*	0.031692889
Scrn1	*Clu*	0.03304698
Scrn1	*Cd200*	0.021866148
Scrn1	*Atp1a3*	0.067961775
Scrn1	*App*	0.125252203
Scrn1	*Apoe*	0.137904118
Scrn1	*Scn2a*	0.023255091

Scrn1	*Scarb2*	0.075188137
Scrn1	*Rap2b*	0.046907063
Scrn1	*Pygb*	0.071967791
Scrn1	*Ptpra*	0.040982366
Scrn1	*Prdx6*	0.033476376
Scrn1	*Olfm1*	0.057946303
Scrn1	*Nutf2*	0.057116433
Scrn1	*Negr1*	0.072091188
Scrn1	*Ncstn*	0.026193173
Scrn1	*Myo6*	0.076505564
Scrn1	*Mcat*	0.024835659
Scrn1	*Mapk1*	0.056353716
Scrn1	*Ly6h*	0.048998547
Scrn1	*Lsamp*	0.095933837
Scrn1	*Lingo1*	0.043338196
Scrn1	*Lancl2*	0.048082731
Scrn1	*Isoc1*	0.068859726
Scrn1	*Idh1*	0.054851898
Scrn1	*Hspa12a*	0.031959159
Scrn1	*Hnrnph3*	0.024262072
Scrn1	*Hnrnpa2b1*	0.02303874
Scrn1	*Gstm1*	0.103123187
Scrn1	*Grin2b*	0.023438806
Scrn1	*Gpm6b*	0.051377459
Scrn1	*Gpc4*	0.062837675

Scrn1	*Gnao1*	0.033779122
Scrn1	*Glul*	0.17423403
Scrn1	*Glud1*	0.034954985
Scrn1	*Gfap*	0.16211515
Scrn1	*Fus*	0.060268672
Scrn1	*Fhl1*	0.036855819
Scrn1	*Ephx1*	0.029661753
Scrn1	*Ephb2*	0.09524663
Scrn1	*Ehd1*	0.045154885
Scrn1	*Egfr*	0.047598802
Scrn1	*Dpysl5*	0.029356211
Scrn1	*Dnajc5*	0.04510338
Scrn1	*Dlg1*	0.036081081
Scrn1	*Ctsd*	0.077164302
Scrn1	*Crym*	0.093348519
Scrn1	*Cpe*	0.074924938
Scrn1	*Cntn1*	0.060546011
Scrn1	*Cnrip1*	0.045337319
Scrn1	*Clu*	0.03840103
Scrn1	*Cat*	0.035002149
Scrn1	*Cadm1*	0.099955681
Scrn1	*Atp1b2*	0.042780968
Scrn1	*Atp1a3*	0.144203345
Scrn1	*Atp1a2*	0.200996322
Scrn1	*Asrgl1*	0.115441169

Scrn1	*Apoe*	0.206752288
Scrn1	*Aldh2*	0.068245508
Scrn1	*Adam10*	0.057995271
Scrn1	*Abca1*	0.117888048
Rps14	*Aimp2*	0.112815147
Rps14	*Adam10*	0.105876956
Rps14	*Atxn2*	0.056188423
Rps14	*Calb1*	0.056188423
Rps14	*Ddx6*	0.056188423
Rps14	*Eef1d*	0.056188423
Rps14	*Eef2*	0.056188423
Rps14	*Ezr*	0.056188423
Rps14	*Gmps*	0.056188423
Rps14	*Gspt1*	0.056188423
Rps14	*Gstp1*	0.056188423
Rps14	*Hspa5*	0.056188423
Rps14	*Lars*	0.056188423
Rps14	*Nedd4*	0.056188423
Rps14	*Nptx2*	0.056188423
Rps14	*Pdia3*	0.056188423
Rps14	*Rpl6*	0.056188423
Rps14	*Rap2b*	0.058453375
Rps14	*Penk*	0.245892321
Rps14	*Nedd4*	0.094389926
Rps14	*Lrp1*	0.082896561

Rps14	*Hspa9*	0.037044771
Rps14	*Hspa1a*	0.06930457
Rps14	*Gpc4*	0.128902334
Rps14	*Ephx1*	0.124134324
Rps14	*Dnaja2*	0.150278545
Rps14	*Dlg1*	0.142226045
Rps14	*Calb1*	0.048237529
Rps14	*Bag5*	0.138632394
Rps14	*Anxa5*	0.061223531
Tln1	*Nedd4*	0.056188423
Tln1	*Nptx2*	0.056188423
Tln1	*Nucb1*	0.056188423
Tln1	*Pdia3*	0.056188423
Tln1	*Pfn1*	0.056188423
Tln1	*Psmc4*	0.056188423
Tln1	*Rab6a*	0.056188423
Tln1	*Rps14*	0.056188423
Tln1	*Ruvbl1*	0.056188423
Tln1	*Sqstm1*	0.056188423
Tln1	*Srp14*	0.056188423
Tln1	*Tfrc*	0.056188423
Tln1	*Anxa5*	0.056188423
Tln1	*App*	0.056188423
Tln1	*Aprt*	0.056188423
Tln1	*Atxn2*	0.056188423

Tln1	*Bag5*	0.056188423
Tln1	*Calb1*	0.056188423
Tln1	*Calr*	0.056188423
Tln1	*Ddx6*	0.056188423
Tln1	*Eef1d*	0.056188423
Tln1	*Eef2*	0.056188423
Tln1	*Ezr*	0.056188423
Tln1	*Gmps*	0.056188423
Tln1	*Gstp1*	0.056188423
Tln1	*Hspa1a*	0.056188423
Tln1	*Hspa5*	0.056188423
Tln1	*Hspa9*	0.056188423
Tln1	*Ipo9*	0.056188423
Tln1	*Kif5b*	0.056188423
Tln1	*Kpnb1*	0.056188423
Tln1	*Lars*	0.056188423
Vps35	*Gpm6b*	0.025702461
Vps35	*Apoe*	0.0253596
Slc32a1	*Atp1a3*	0.048189251
Slc32a1	*Atp1a2*	0.044075976
Slc32a1	*Asrgl1*	0.027853115
Slc32a1	*Apoe*	0.039215727
Slc32a1	*Abca1*	0.028225007
Slc32a1	*Slc1a2*	0.028451402
Slc32a1	*Scrn1*	0.020672343

Slc32a1	*Lsamp*	0.031121783
Slc32a1	*Gstm1*	0.034566824
Slc32a1	*Glul*	0.041946532
Slc32a1	*Gfap*	0.037108146
Slc32a1	*Ctsd*	0.025445587
Slc32a1	*Cadm1*	0.024532016
Stx1b	*Slc6a11*	0.032574815
Stx1b	*Scrn1*	0.026616939
Stx1b	*Scarb2*	0.042986482
Stx1b	*Rab6a*	0.035216175
Stx1b	*Pygb*	0.111357006
Stx1b	*Prdx6*	0.171874917
Stx1b	*Prdx2*	0.067456351
Stx1b	*Ncam1*	0.044656946
Stx1b	*Marcks*	0.167563986
Stx1b	*Mapk1*	0.027956413
Stx1b	*Kpnb1*	0.031264486
Stx1b	*Kif2a*	0.024538782
Stx1b	*Idh1*	0.029697891
Stx1b	*Hnrnpa2b1*	0.070160551
Stx1b	*Gstm1*	0.106896155
Stx1b	*Gpm6b*	0.285878598
Stx1b	*Glul*	0.147585072
Stx1b	*Glud1*	0.020916575
Stx1b	*Gfap*	0.022930623

Stx1b	*Gdi1*	0.156769084
Stx1b	*Gap43*	0.076883004
Stx1b	*Egfr*	0.059624878
Stx1b	*Dpysl5*	0.091639146
Stx1b	*Crym*	0.025402247
Stx1b	*Crmp1*	0.03049496
Stx1b	*Cpe*	0.088804506
Stx1b	*Cntn1*	0.077005196
Stx1b	*Clu*	0.056211028
Stx1b	*Cd200*	0.028895479
Stx1b	*Atp1a3*	0.150855362
Stx1b	*Atp1a2*	0.062998328
Stx1b	*App*	0.104947365
Stx1b	*Apoe*	0.234166687

Appendix-5

Brain region Specific Composite Network proteins	
Proteins	**Log2FC**
Hspa5	0.236668155
Aprt	0.300968452
Kif5b	0.037361875
Ddx6	0.185046929
Atxn2	0.786815
Tln1	0.11

Vim	0.964364018
Ruvbl1	0.267276101
Nucb1	0.296125982
Rpl6	0.750924286
Lrp1	0.210946696
Dlg1	0.206693214
Hspa9	0.458044768
Hspa1a	0.443511786
Ptpra	-0.078511071
Dnaja2	0.889432292
Rps14	0.843319494
Gpc4	-0.05
Calb1	0.808010446
Bag5	1.158340161
Nedd4	0.611500643
Ephx1	0.34
Slc44a1	0.26
Adam10	0.453489494
Abca1	-0.217331369
Rap2b	0.165301399
Anxa5	0.777323274
Aimp2	0.297189048
Vps35	-0.3
Txnrd1	-0.27713997
Tfrc	-0.127207679

Ctsd	-0.641905863
Slc6a11	-0.854160298
Eef1d	-0.16
Syn1	-0.24
Gnao1	-0.489637917
Lingo1	-0.382743244
Gria2	-0.345508179
Aldh2	-0.290851012
Ehd1	-0.243993452
Nutf2	-0.229851696
Crmp1	-0.251080119
Cadm1	-0.489637917
Slc32a1	-0.29806125
Vdac1	-0.628701339
Nsf	-0.308227619
Uchl1	-0.660274881
Syt1	-0.605456935
Stx1b	-0.653677232
Scrn1	-0.489637917
Scarb2	-0.489637917
Rab6a	-0.086914911
Prdx2	-1.039205238
Ppp3ca	-0.3000025
Ncam1	-0.797035208
Olfm1	-0.489637917

Mapk1	-0.490248125
Kpnb1	-0.11759378
Kif2a	-0.624128274
Negr1	-0.641787232
Idh1	-0.366698958
Ncstn	-0.183850036
Hnrnpa2b1	-0.489637917
Sqstm1	-0.242422679
Gstm1	-0.489637917
Mcat	-0.36622125
Gpm6b	-0.489637917
Ly6h	-0.565237589
Glul	-2.185684911
Lancl2	-0.256357054
Glud1	-0.489637917
Gfap	-0.800368542
Gdi1	-0.556943631
Tnr	-0.223805565
Gap43	-0.508305893
Egfr	-0.481502589
Isoc1	-0.424375982
Eef2	0.248511667
Dpysl5	-0.502732202
Hspa12a	-0.214776905
Hsd17b10	-0.10325747

Slc1a2	-0.535539107
Crym	-0.489637917
Cpe	-0.489637917
Cntn1	-0.489637917
Clu	-0.489637917
Cd200	-0.588231756
Pygb	-0.669492589
Atp1a3	-0.587409048
Myo6	-0.64
Prdx6	-0.744218155
Atp1a2	-0.631370893
Lsamp	-0.189775565
App	-0.535791548
Apoe	-1.289632857
Fhl1	-0.359470018
Marcks	-0.520000327
Sirt2	-0.634705804
Ephb2	-0.35
Dnajc5	-0.489637917
Cnrip1	-0.489637917
Cat	-0.251706429
Atp6v0a1	-0.354079643
Atp1b2	-0.489637917
Asrgl1	-0.489637917
Txnl1	-0.17297

Rps6	-0.1999395
Gmps	0.2903075
Pdia3	0.064618869
Pfn1	0.364466964
Calr	0.12625628
Psmc4	0.193720208
Lap3	0.110207887
Ipo9	-0.284785833
Ezr	0.403093631
Lars	0.540072292
Gstp1	0.399396815
Scna	

Appendix-6

Interaction data: Brain region specific composite network proteins		
Protein1	**Protein2**	**Weights (WPCNA)**
Tln1	*Lars*	0.056188423
Tln1	*Kpnb1*	0.056188423
Tln1	*Kif5b*	0.056188423
Tln1	*Ipo9*	0.056188423
Tln1	*Hspa9*	0.056188423

Tln1	*Hspa5*	0.056188423
Tln1	*Hspa1a*	0.056188423
Tln1	*Gstp1*	0.056188423
Tln1	*Gmps*	0.056188423
Tln1	*Ezr*	0.056188423
Tln1	*Eef2*	0.056188423
Tln1	*Eef1d*	0.056188423
Tln1	*Ddx6*	0.056188423
Tln1	*Calr*	0.056188423
Tln1	*Calb1*	0.056188423
Tln1	*Bag5*	0.056188423
Tln1	*Atxn2*	0.056188423
Tln1	*Aprt*	0.056188423
Tln1	*App*	0.056188423
Tln1	*Anxa5*	0.056188423
Tln1	*Tfrc*	0.056188423
Tln1	*Sqstm1*	0.056188423
Tln1	*Ruvbl1*	0.056188423
Tln1	*Rps14*	0.056188423
Tln1	*Rab6a*	0.056188423
Tln1	*Psmc4*	0.056188423
Tln1	*Pfn1*	0.056188423
Tln1	*Pdia3*	0.056188423
Tln1	*Nucb1*	0.056188423
Tln1	*Nedd4*	0.056188423

Vim	*Lars*	0.056188423
Vim	*Lap3*	0.056188423
Vim	*Kpnb1*	0.056188423
Vim	*Kif5b*	0.056188423
Vim	*Ipo9*	0.056188423
Vim	*Hspa9*	0.056188423
Vim	*Hspa5*	0.056188423
Vim	*Hspa1a*	0.056188423
Vim	*Gstp1*	0.056188423
Vim	*Gmps*	0.056188423
Vim	*Ezr*	0.056188423
Vim	*Eef2*	0.056188423
Vim	*Eef1d*	0.056188423
Vim	*Ddx6*	0.056188423
Vim	*Calr*	0.056188423
Vim	*Calb1*	0.056188423
Vim	*Atxn2*	0.056188423
Vim	*Aprt*	0.056188423
Vim	*App*	0.056188423
Vim	*Anxa5*	0.056188423
Vim	*Txnrd1*	0.056188423
Vim	*Tln1*	0.056188423
Vim	*Ruvbl1*	0.056188423
Vim	*Rps14*	0.056188423
Vim	*Rab6a*	0.056188423

Vim	*Psmc4*	0.056188423
Vim	*Pfn1*	0.056188423
Vim	*Pdia3*	0.056188423
Vim	*Nucb1*	0.056188423
Vim	*Nedd4*	0.056188423
Ruvbl1	*Pfn1*	0.056188423
Ruvbl1	*Nedd4*	0.056188423
Ruvbl1	*Lars*	0.056188423
Ruvbl1	*Kpnb1*	0.056188423
Ruvbl1	*Hspa9*	0.056188423
Ruvbl1	*Hspa5*	0.056188423
Ruvbl1	*Hspa1a*	0.056188423
Ruvbl1	*Ezr*	0.056188423
Ruvbl1	*Eef2*	0.056188423
Ruvbl1	*Aprt*	0.056188423
Ruvbl1	*Anxa5*	0.056188423
Rpl6	*Nucb1*	0.042649189
Rpl6	*Lars*	0.056188423
Rpl6	*Hspa5*	0.056188423
Rpl6	*Eef2*	0.056188423
Rpl6	*Ddx6*	0.056188423
Rpl6	*Atxn2*	0.056188423
Rps14	*Adam10*	0.105876956
Rps14	*Aimp2*	0.112815147
Rps14	*Anxa5*	0.061223531

Rps14	*Bag5*	0.138632394
Rps14	*Calb1*	0.048237529
Rps14	*Dlg1*	0.142226045
Rps14	*Dnaja2*	0.150278545
Rps14	*Ephx1*	0.124134324
Rps14	*Gpc4*	0.128902334
Rps14	*Hspa1a*	0.06930457
Rps14	*Hspa9*	0.037044771
Rps14	*Lrp1*	0.082896561
Rps14	*Nedd4*	0.094389926
Rps14	*Rap2b*	0.058453375
Rps14	*Rpl6*	0.056188423
Rps14	*Pdia3*	0.056188423
Rps14	*Nedd4*	0.056188423
Rps14	*Lars*	0.056188423
Rps14	*Hspa5*	0.056188423
Rps14	*Gstp1*	0.056188423
Rps14	*Gmps*	0.056188423
Rps14	*Ezr*	0.056188423
Rps14	*Eef2*	0.056188423
Rps14	*Eef1d*	0.056188423
Rps14	*Ddx6*	0.056188423
Rps14	*Calb1*	0.056188423
Rps14	*Atxn2*	0.056188423
Slc44a1	*Ephx1*	0.102793676

Slc44a1	*Gpc4*	0.075468753
Slc44a1	*Hspa1a*	0.062665965
Slc44a1	*Hspa9*	0.031384298
Slc44a1	*Lrp1*	0.048859023
Slc44a1	*Nedd4*	0.071142424
Slc44a1	*Rap2b*	0.033678093
Slc44a1	*Rps14*	0.166871476
Slc44a1	*Adam10*	0.065668225
Slc44a1	*Aimp2*	0.054131909
Slc44a1	*Anxa5*	0.045301182
Slc44a1	*Bag5*	0.092918141
Slc44a1	*Calb1*	0.033283568
Slc44a1	*Dlg1*	0.088739831
Slc44a1	*Apoe*	0.029840419
Slc44a1	*Asrgl1*	0.032959235
Slc44a1	*Atp1a2*	0.048436406
Slc44a1	*Atp1a3*	0.025575716
Slc44a1	*Cadm1*	0.03470466
Slc44a1	*Cntn1*	0.039989947
Slc44a1	*Cpe*	0.022225432
Slc44a1	*Gfap*	0.03030827
Slc44a1	*Glul*	0.037934837
Slc44a1	*Gpc4*	0.021356606
Slc44a1	*Lsamp*	0.022242188
Slc44a1	*Myo6*	0.030684001

Slc44a1	*Pygb*	0.020586965
Slc44a1	*Slc1a2*	0.033385406
Rap2b	*Abca1*	0.11062137
Rap2b	*Adam10*	0.172492624
Rap2b	*Dnaja2*	0.119567657
Rap2b	*Ephx1*	0.026787514
Rap2b	*Lrp1*	0.100118369
Vps35	*Apoe*	0.0253596
Vps35	*Gpm6b*	0.025702461
Txnrd1	*Cpe*	0.033680792
Txnrd1	*Gdi1*	0.025030429
Txnrd1	*Gpm6b*	0.02342132
Txnrd1	*Prdx2*	0.033127862
Txnrd1	*Prdx6*	0.028736447
Txnrd1	*Pygb*	0.029808395
Txnrd1	*Tln1*	0.056188423
Txnrd1	*Rab6a*	0.056188423
Txnrd1	*Pfn1*	0.056188423
Txnrd1	*Nedd4*	0.056188423
Txnrd1	*Lars*	0.056188423
Txnrd1	*Kpnb1*	0.056188423
Txnrd1	*Kif5b*	0.056188423
Txnrd1	*Hspa9*	0.056188423
Txnrd1	*Hspa5*	0.056188423
Txnrd1	*Ezr*	0.056188423

Txnrd1	*Eef2*	0.056188423
Txnrd1	*Ddx6*	0.056188423
Txnrd1	*Calr*	0.056188423
Txnrd1	*Aprt*	0.056188423
Txnrd1	*Anxa5*	0.056188423
Tfrc	*Apoe*	0.022441656
Tfrc	*Cpe*	0.040721079
Tfrc	*Gdi1*	0.031681738
Tfrc	*Glul*	0.047261
Tfrc	*Gpm6b*	0.045191824
Tfrc	*Prdx6*	0.046952193
Tfrc	*Pygb*	0.023634544
Tfrc	*Scrn1*	0.02210287
Tfrc	*Syt1*	0.030508073
Tfrc	*Atxn2*	0.056188423
Tfrc	*Aprt*	0.056188423
Tfrc	*Rab6a*	0.056188423
Tfrc	*Pdia3*	0.056188423
Tfrc	*Nedd4*	0.056188423
Tfrc	*Lars*	0.056188423
Tfrc	*Hspa5*	0.056188423
Tfrc	*Gstp1*	0.056188423
Tfrc	*Eef2*	0.056188423
Tfrc	*Eef1d*	0.056188423
Tfrc	*Ddx6*	0.056188423

Tfrc	*Calr*	0.056188423
Tfrc	*Calb1*	0.056188423
Slc6a11	*Apoe*	0.094605662
Slc6a11	*App*	0.02387224
Slc6a11	*Atp1a2*	0.022089086
Slc6a11	*Atp1a3*	0.088227336
Slc6a11	*Clu*	0.036605767
Slc6a11	*Cntn1*	0.081159347
Slc6a11	*Dpysl5*	0.033935656
Slc6a11	*Egfr*	0.037303211
Slc6a11	*Gdi1*	0.061841622
Slc6a11	*Glul*	0.093232971
Slc6a11	*Gpm6b*	0.113848135
Slc6a11	*Gstm1*	0.036681744
Slc6a11	*Idh1*	0.029210651
Slc6a11	*Marcks*	0.07960533
Slc6a11	*Ncam1*	0.03240243
Slc6a11	*Prdx6*	0.080848243
Slc6a11	*Pygb*	0.03257175
Slc6a11	*Abca1*	0.145005543
Slc6a11	*Adam10*	0.112615338
Slc6a11	*Aldh2*	0.098843319
Slc6a11	*Apoe*	0.162932002
Slc6a11	*Asrgl1*	0.119020952
Slc6a11	*Atp1a2*	0.229442413

Slc6a11	*Atp1a3*	0.163813523
Slc6a11	*Atp1b2*	0.105392327
Slc6a11	*Atp6v0a1*	0.033107861
Slc6a11	*Cadm1*	0.153848295
Slc6a11	*Cat*	0.144496409
Slc6a11	*Clu*	0.057502173
Slc6a11	*Cnrip1*	0.119483468
Slc6a11	*Cntn1*	0.131285877
Slc6a11	*Cpe*	0.175791133
Slc6a11	*Crym*	0.165794701
Slc6a11	*Ctsd*	0.12385862
Slc6a11	*Dlg1*	0.047590439
Slc6a11	*Dnajc5*	0.069900401
Slc6a11	*Dpysl5*	0.087674493
Slc6a11	*Egfr*	0.129573888
Slc6a11	*Ehd1*	0.080216506
Slc6a11	*Ephb2*	0.185478442
Slc6a11	*Ephx1*	0.027580281
Slc6a11	*Fhl1*	0.138772566
Slc6a11	*Gdi1*	0.038620557
Slc6a11	*Gfap*	0.163031078
Slc6a11	*Glud1*	0.169104112
Slc6a11	*Glul*	0.262420354
Slc6a11	*Gnao1*	0.059455903
Slc6a11	*Gpc4*	0.11091263

Slc6a11	*Gpm6b*	0.038797242
Slc6a11	*Gria2*	0.052714838
Slc6a11	*Gstm1*	0.10726307
Slc6a11	*Hnrnpa2b1*	0.059190014
Slc6a11	*Hspa12a*	0.094913841
Slc6a11	*Idh1*	0.086124644
Slc6a11	*Isoc1*	0.145220841
Slc6a11	*Kif2a*	0.042821621
Slc6a11	*Lancl2*	0.061043876
Slc6a11	*Lingo1*	0.075144517
Slc6a11	*Lrp1*	0.022976313
Slc6a11	*Lsamp*	0.159183051
Slc6a11	*Ly6h*	0.089011965
Slc6a11	*Mapk1*	0.060053254
Slc6a11	*Mcat*	0.03769739
Slc6a11	*Myo6*	0.148154294
Slc6a11	*Ncstn*	0.03343399
Slc6a11	*Negr1*	0.10266138
Slc6a11	*Olfm1*	0.102752726
Slc6a11	*Ppp3ca*	0.020825599
Slc6a11	*Prdx6*	0.031511275
Slc6a11	*Ptpra*	0.098205642
Slc6a11	*Pygb*	0.114491751
Slc6a11	*Rap2b*	0.108349513
Slc6a11	*Scarb2*	0.071808898

Slc6a11	*Scrn1*	0.125427562
Slc6a11	*Sirt2*	0.068540912
Slc6a11	*Slc1a2*	0.19990023
Slc6a11	*Slc32a1*	0.0311017
Slc6a11	*Slc44a1*	0.026329786
Syn1	*Abca1*	0.052852234
Syn1	*Aldh2*	0.06790548
Syn1	*Apoe*	0.134077828
Syn1	*Asrgl1*	0.082596726
Syn1	*Atp1a2*	0.147717072
Syn1	*Atp1a3*	0.070128253
Syn1	*Cadm1*	0.053023014
Syn1	*Cntn1*	0.065135362
Syn1	*Cpe*	0.070511819
Syn1	*Crym*	0.072118093
Syn1	*Ctsd*	0.021145716
Syn1	*Ephb2*	0.025975519
Syn1	*Gfap*	0.111176727
Syn1	*Glul*	0.088854573
Syn1	*Gpc4*	0.024140634
Syn1	*Gstm1*	0.05078256
Syn1	*Hspa12a*	0.033900946
Syn1	*Idh1*	0.023093047
Syn1	*Isoc1*	0.021527819
Syn1	*Lancl2*	0.030862259

Syn1	*Lrp1*	0.020555949
Syn1	*Lsamp*	0.022637775
Syn1	*Mapk1*	0.03080609
Syn1	*Myo6*	0.049369509
Syn1	*Olfm1*	0.022368497
Syn1	*Pygb*	0.10436978
Syn1	*Rap2b*	0.055315322
Syn1	*Scarb2*	0.027906613
Syn1	*Scrn1*	0.028710512
Syn1	*Sirt2*	0.025574278
Syn1	*Slc1a2*	0.096887179
Syn1	*Slc6a11*	0.052313585
Lingo1	*Aldh2*	0.020282976
Gria2	*Cd200*	0.022078495
Slc32a1	*Abca1*	0.028225007
Slc32a1	*Apoe*	0.039215727
Slc32a1	*Asrgl1*	0.027853115
Slc32a1	*Atp1a2*	0.044075976
Slc32a1	*Atp1a3*	0.048189251
Slc32a1	*Cadm1*	0.024532016
Slc32a1	*Ctsd*	0.025445587
Slc32a1	*Gfap*	0.037108146
Slc32a1	*Glul*	0.041946532
Slc32a1	*Gstm1*	0.034566824
Slc32a1	*Lsamp*	0.031121783

Slc32a1	*Scrn1*	0.020672343
Slc32a1	*Slc1a2*	0.028451402
Vdac1	*Apoe*	0.094824174
Vdac1	*App*	0.068622212
Vdac1	*Atp1a2*	0.035069597
Vdac1	*Atp1a3*	0.071978725
Vdac1	*Clu*	0.021164566
Vdac1	*Cntn1*	0.030350088
Vdac1	*Cpe*	0.080053836
Vdac1	*Dpysl5*	0.02911306
Vdac1	*Gdi1*	0.089690612
Vdac1	*Glul*	0.046274853
Vdac1	*Gpm6b*	0.122662366
Vdac1	*Gstm1*	0.068959372
Vdac1	*Hnrnpa2b1*	0.05432051
Vdac1	*Kpnb1*	0.03366518
Vdac1	*Marcks*	0.090620561
Vdac1	*Ncam1*	0.020896823
Vdac1	*Prdx2*	0.106779108
Vdac1	*Prdx6*	0.090240996
Vdac1	*Pygb*	0.10195008
Vdac1	*Scarb2*	0.025125045
Vdac1	*Scrn1*	0.031765703
Vdac1	*Stx1b*	0.035716769
Vdac1	*Txnrd1*	0.028985364

Vdac1	*Uchl1*	0.050952153
Vdac1	*Abca1*	0.035792004
Vdac1	*Aldh2*	0.026319361
Vdac1	*Apoe*	0.070462709
Vdac1	*Asrgl1*	0.030261387
Vdac1	*Atp1a2*	0.076686766
Vdac1	*Atp1a3*	0.031513196
Vdac1	*Cadm1*	0.045024237
Vdac1	*Cntn1*	0.033894308
Vdac1	*Cpe*	0.028973299
Vdac1	*Crym*	0.052597621
Vdac1	*Dpysl5*	0.038283317
Vdac1	*Egfr*	0.026685929
Vdac1	*Ephb2*	0.020821162
Vdac1	*Ephx1*	0.044418517
Vdac1	*Gfap*	0.050257537
Vdac1	*Glul*	0.050491239
Vdac1	*Gpc4*	0.032291373
Vdac1	*Gstm1*	0.024208934
Vdac1	*Isoc1*	0.026061451
Vdac1	*Lsamp*	0.023473115
Vdac1	*Myo6*	0.041880943
Vdac1	*Negr1*	0.023758038
Vdac1	*Pygb*	0.029212308
Vdac1	*Scrn1*	0.020669885

Vdac1	*Slc1a2*	0.046941779
Vdac1	*Slc6a11*	0.035510587
Vdac1	*Tnr*	0.033411964
Uchl1	*Apoe*	0.252961851
Uchl1	*App*	0.129558366
Uchl1	*Atp1a2*	0.131238404
Uchl1	*Atp1a3*	0.194307905
Uchl1	*Cadm1*	0.048841495
Uchl1	*Cd200*	0.066061389
Uchl1	*Clu*	0.143333952
Uchl1	*Cntn1*	0.155518611
Uchl1	*Cpe*	0.116018827
Uchl1	*Crmp1*	0.030610271
Uchl1	*Crym*	0.107462599
Uchl1	*Dpysl5*	0.143428281
Uchl1	*Eef1d*	0.035094114
Uchl1	*Eef2*	0.0471493
Uchl1	*Egfr*	0.082140136
Uchl1	*Gap43*	0.109524467
Uchl1	*Gdi1*	0.131331723
Uchl1	*Gfap*	0.091212615
Uchl1	*Glud1*	0.066829917
Uchl1	*Glul*	0.184916081
Uchl1	*Gpm6b*	0.37124573
Uchl1	*Gstm1*	0.160144935

Uchl1	*Hnrnpa2b1*	0.123798695
Uchl1	*Idh1*	0.08366495
Uchl1	*Kif2a*	0.080532037
Uchl1	*Kpnb1*	0.055940784
Uchl1	*Mapk1*	0.115786179
Uchl1	*Marcks*	0.164773825
Uchl1	*Ncam1*	0.097797852
Uchl1	*Prdx2*	0.087408578
Uchl1	*Prdx6*	0.167789016
Uchl1	*Pygb*	0.120799379
Uchl1	*Rab6a*	0.054872012
Uchl1	*Scarb2*	0.103184782
Uchl1	*Scrn1*	0.072345121
Uchl1	*Sirt2*	0.076916172
Uchl1	*Slc6a11*	0.052674126
Uchl1	*Sqstm1*	0.039265942
Uchl1	*Stx1b*	0.14144408
Uchl1	*Syt1*	0.082110351
Syt1	*Apoe*	0.150418417
Syt1	*App*	0.06282504
Syt1	*Atp1a2*	0.033782189
Syt1	*Atp1a3*	0.118317854
Syt1	*Cadm1*	0.056557981
Syt1	*Cd200*	0.11319222
Syt1	*Clu*	0.031024022

Syt1	*Cntn1*	0.084055723
Syt1	*Cpe*	0.102724297
Syt1	*Crym*	0.022697125
Syt1	*Dpysl5*	0.081867058
Syt1	*Egfr*	0.073251388
Syt1	*Gdi1*	0.161552634
Syt1	*Glud1*	0.072210347
Syt1	*Glul*	0.202636424
Syt1	*Gpm6b*	0.266692754
Syt1	*Gstm1*	0.088524788
Syt1	*Hnrnpa2b1*	0.04355053
Syt1	*Idh1*	0.073651634
Syt1	*Kpnb1*	0.021627366
Syt1	*Lingo1*	0.02508038
Syt1	*Mapk1*	0.022470491
Syt1	*Marcks*	0.086065485
Syt1	*Ncam1*	0.081072425
Syt1	*Prdx2*	0.048603485
Syt1	*Prdx6*	0.222447557
Syt1	*Pygb*	0.116921349
Syt1	*Scarb2*	0.039815124
Syt1	*Scrn1*	0.041639382
Syt1	*Slc6a11*	0.036454311
Syt1	*Stx1b*	0.042850308
Syt1	*Abca1*	0.059796403

Syt1	*Adam10*	0.02287919
Syt1	*Aldh2*	0.044821408
Syt1	*Apoe*	0.09272955
Syt1	*Asrgl1*	0.049376451
Syt1	*Atp1a2*	0.127545674
Syt1	*Atp1a3*	0.060210997
Syt1	*Cadm1*	0.094793548
Syt1	*Cat*	0.023618517
Syt1	*Cntn1*	0.047204711
Syt1	*Cpe*	0.07274275
Syt1	*Crym*	0.070383776
Syt1	*Ctsd*	0.041020517
Syt1	*Ephb2*	0.050962
Syt1	*Gfap*	0.088110344
Syt1	*Glud1*	0.04304082
Syt1	*Glul*	0.180936138
Syt1	*Gpc4*	0.026336954
Syt1	*Gstm1*	0.053455915
Syt1	*Hspa12a*	0.020221621
Syt1	*Lsamp*	0.052377907
Syt1	*Myo6*	0.077240391
Syt1	*Ptpra*	0.026290973
Syt1	*Pygb*	0.068243039
Syt1	*Rap2b*	0.027090399
Syt1	*Scrn1*	0.032716701

Syt1	*Slc1a2*	0.115480401
Syt1	*Slc6a11*	0.114849645
Stx1b	*Apoe*	0.234166687
Stx1b	*App*	0.104947365
Stx1b	*Atp1a2*	0.062998328
Stx1b	*Atp1a3*	0.150855362
Stx1b	*Cd200*	0.028895479
Stx1b	*Clu*	0.056211028
Stx1b	*Cntn1*	0.077005196
Stx1b	*Cpe*	0.088804506
Stx1b	*Crmp1*	0.03049496
Stx1b	*Crym*	0.025402247
Stx1b	*Dpysl5*	0.091639146
Stx1b	*Egfr*	0.059624878
Stx1b	*Gap43*	0.076883004
Stx1b	*Gdi1*	0.156769084
Stx1b	*Gfap*	0.022930623
Stx1b	*Glud1*	0.020916575
Stx1b	*Glul*	0.147585072
Stx1b	*Gpm6b*	0.285878598
Stx1b	*Gstm1*	0.106896155
Stx1b	*Hnrnpa2b1*	0.070160551
Stx1b	*Idh1*	0.029697891
Stx1b	*Kif2a*	0.024538782
Stx1b	*Kpnb1*	0.031264486

Stx1b	*Mapk1*	0.027956413
Stx1b	*Marcks*	0.167563986
Stx1b	*Ncam1*	0.044656946
Stx1b	*Prdx2*	0.067456351
Stx1b	*Prdx6*	0.171874917
Stx1b	*Pygb*	0.111357006
Stx1b	*Rab6a*	0.035216175
Stx1b	*Scarb2*	0.042986482
Stx1b	*Scrn1*	0.026616939
Stx1b	*Slc6a11*	0.032574815
Scrn1	*Olfm1*	0.057946303
Scrn1	*Prdx6*	0.033476376
Scrn1	*Ptpra*	0.040982366
Scrn1	*Pygb*	0.071967791
Scrn1	*Rap2b*	0.046907063
Scrn1	*Scarb2*	0.075188137
Scrn1	*Apoe*	0.137904118
Scrn1	*App*	0.125252203
Scrn1	*Atp1a3*	0.067961775
Scrn1	*Cd200*	0.021866148
Scrn1	*Clu*	0.03304698
Scrn1	*Cntn1*	0.031692889
Scrn1	*Cpe*	0.201804636
Scrn1	*Dpysl5*	0.06946602
Scrn1	*Ehd1*	0.048984705

Scrn1	*Gdi1*	0.146333016
Scrn1	*Gfap*	0.025634962
Scrn1	*Glud1*	0.022007559
Scrn1	*Glul*	0.143631862
Scrn1	*Gpm6b*	0.249363173
Scrn1	*Gstm1*	0.116747516
Scrn1	*Hnrnpa2b1*	0.111376491
Scrn1	*Idh1*	0.029821659
Scrn1	*Kpnb1*	0.071539687
Scrn1	*Mapk1*	0.023470139
Scrn1	*Marcks*	0.063487157
Scrn1	*Ncam1*	0.020226391
Scrn1	*Prdx2*	0.117919142
Scrn1	*Prdx6*	0.174435039
Scrn1	*Pygb*	0.152486767
Scrn1	*Scarb2*	0.037631627
Scrn1	*Abca1*	0.117888048
Scrn1	*Adam10*	0.057995271
Scrn1	*Aldh2*	0.068245508
Scrn1	*Apoe*	0.206752288
Scrn1	*Asrgl1*	0.115441169
Scrn1	*Atp1a2*	0.200996322
Scrn1	*Atp1a3*	0.144203345
Scrn1	*Atp1b2*	0.042780968
Scrn1	*Cadm1*	0.099955681

Scrn1	*Cat*	0.035002149
Scrn1	*Clu*	0.03840103
Scrn1	*Cnrip1*	0.045337319
Scrn1	*Cntn1*	0.060546011
Scrn1	*Cpe*	0.074924938
Scrn1	*Crym*	0.093348519
Scrn1	*Ctsd*	0.077164302
Scrn1	*Dlg1*	0.036081081
Scrn1	*Dnajc5*	0.04510338
Scrn1	*Dpysl5*	0.029356211
Scrn1	*Egfr*	0.047598802
Scrn1	*Ehd1*	0.045154885
Scrn1	*Ephb2*	0.09524663
Scrn1	*Ephx1*	0.029661753
Scrn1	*Fhl1*	0.036855819
Scrn1	*Gfap*	0.16211515
Scrn1	*Glud1*	0.034954985
Scrn1	*Glul*	0.17423403
Scrn1	*Gnao1*	0.033779122
Scrn1	*Gpc4*	0.062837675
Scrn1	*Gpm6b*	0.051377459
Scrn1	*Gstm1*	0.103123187
Scrn1	*Hnrnpa2b1*	0.02303874
Scrn1	*Hspa12a*	0.031959159
Scrn1	*Idh1*	0.054851898

Scrn1	*Isoc1*	0.068859726
Scrn1	*Lancl2*	0.048082731
Scrn1	*Lingo1*	0.043338196
Scrn1	*Lsamp*	0.095933837
Scrn1	*Ly6h*	0.048998547
Scrn1	*Mapk1*	0.056353716
Scrn1	*Mcat*	0.024835659
Scrn1	*Myo6*	0.076505564
Scrn1	*Ncstn*	0.026193173
Scrn1	*Negr1*	0.072091188
Scrn1	*Nutf2*	0.057116433
Scarb2	*Apoe*	0.162417965
Scarb2	*App*	0.100277548
Scarb2	*Atp1a2*	0.027979548
Scarb2	*Atp1a3*	0.10622825
Scarb2	*Cd200*	0.025736676
Scarb2	*Clu*	0.049160836
Scarb2	*Cntn1*	0.055529265
Scarb2	*Cpe*	0.104916867
Scarb2	*Dpysl5*	0.050814892
Scarb2	*Egfr*	0.026477527
Scarb2	*Gdi1*	0.145412103
Scarb2	*Gfap*	0.023957088
Scarb2	*Glul*	0.150165406
Scarb2	*Gpm6b*	0.241307797

Scarb2	*Gstm1*	0.126546724
Scarb2	*Hnrnpa2b1*	0.080135362
Scarb2	*Idh1*	0.029277
Scarb2	*Kpnb1*	0.034366374
Scarb2	*Marcks*	0.108702345
Scarb2	*Ncam1*	0.020487269
Scarb2	*Prdx2*	0.068375383
Scarb2	*Prdx6*	0.183446543
Scarb2	*Pygb*	0.126508067
Scarb2	*Abca1*	0.084828454
Scarb2	*Adam10*	0.02706026
Scarb2	*Aldh2*	0.074839577
Scarb2	*Apoe*	0.179937626
Scarb2	*Asrgl1*	0.117335281
Scarb2	*Atp1a2*	0.166358526
Scarb2	*Atp1a3*	0.099795353
Scarb2	*Cadm1*	0.073353435
Scarb2	*Cntn1*	0.073848357
Scarb2	*Cpe*	0.067138542
Scarb2	*Crym*	0.073007257
Scarb2	*Ctsd*	0.044332053
Scarb2	*Dlg1*	0.022570048
Scarb2	*Dnajc5*	0.028952563
Scarb2	*Ephb2*	0.048262919
Scarb2	*Ephx1*	0.021004564

Scarb2	*Gfap*	0.126990996
Scarb2	*Glul*	0.106833197
Scarb2	*Gnao1*	0.030396916
Scarb2	*Gpc4*	0.049346946
Scarb2	*Gpm6b*	0.040469224
Scarb2	*Gstm1*	0.087992786
Scarb2	*Hspa12a*	0.023895876
Scarb2	*Idh1*	0.023402594
Scarb2	*Isoc1*	0.034140553
Scarb2	*Lancl2*	0.0299789
Scarb2	*Lsamp*	0.054656422
Scarb2	*Mapk1*	0.033794828
Scarb2	*Myo6*	0.066914158
Scarb2	*Negr1*	0.030056284
Scarb2	*Olfm1*	0.040360669
Scarb2	*Pygb*	0.082136685
Scarb2	*Rap2b*	0.024586297
Rab6a	*Apoe*	0.141487413
Rab6a	*App*	0.085788096
Rab6a	*Atp1a2*	0.056775283
Rab6a	*Atp1a3*	0.071610006
Rab6a	*Clu*	0.065770406
Rab6a	*Cntn1*	0.030449435
Rab6a	*Cpe*	0.03308719
Rab6a	*Ctsd*	0.061379425

Rab6a	*Dpysl5*	0.042073916
Rab6a	*Egfr*	0.021232299
Rab6a	*Gdi1*	0.104045476
Rab6a	*Glul*	0.048240167
Rab6a	*Gpm6b*	0.13291691
Rab6a	*Gstm1*	0.057947101
Rab6a	*Hnrnpa2b1*	0.041805445
Rab6a	*Idh1*	0.028968126
Rab6a	*Marcks*	0.129031993
Rab6a	*Ncam1*	0.021516615
Rab6a	*Prdx2*	0.056061297
Rab6a	*Prdx6*	0.082443633
Rab6a	*Pygb*	0.094347742
Prdx2	*Apoe*	0.194110673
Prdx2	*App*	0.166348662
Prdx2	*Atp1a2*	0.069273054
Prdx2	*Atp1a3*	0.090469192
Prdx2	*Cd200*	0.02848101
Prdx2	*Clu*	0.063039327
Prdx2	*Cntn1*	0.045681696
Prdx2	*Cpe*	0.156635723
Prdx2	*Crym*	0.029978906
Prdx2	*Dpysl5*	0.084060709
Prdx2	*Eef2*	0.040659656
Prdx2	*Egfr*	0.048277101

Prdx2	*Ehd1*	0.025661407
Prdx2	*Gap43*	0.024837159
Prdx2	*Gdi1*	0.163401888
Prdx2	*Gfap*	0.053924669
Prdx2	*Glud1*	0.033279116
Prdx2	*Glul*	0.118098589
Prdx2	*Gpm6b*	0.271604274
Prdx2	*Gstm1*	0.124798743
Prdx2	*Hnrnpa2b1*	0.104640514
Prdx2	*Idh1*	0.063992957
Prdx2	*Kif2a*	0.027644996
Prdx2	*Kpnb1*	0.135348135
Prdx2	*Mapk1*	0.055432444
Prdx2	*Marcks*	0.110597383
Prdx2	*Ncam1*	0.043742812
Ncam1	*Apoe*	0.148513049
Ncam1	*App*	0.059475701
Ncam1	*Atp1a2*	0.038352077
Ncam1	*Atp1a3*	0.146709857
Ncam1	*Cadm1*	0.035290688
Ncam1	*Cd200*	0.041323076
Ncam1	*Clu*	0.034811534
Ncam1	*Cntn1*	0.080845392
Ncam1	*Cpe*	0.071280189
Ncam1	*Dpysl5*	0.068592038

Ncam1	*Egfr*	0.044041462
Ncam1	*Gap43*	0.033673172
Ncam1	*Gdi1*	0.120321285
Ncam1	*Glud1*	0.028921658
Ncam1	*Glul*	0.137357781
Ncam1	*Gpm6b*	0.235513309
Ncam1	*Gstm1*	0.079016741
Ncam1	*Hnrnpa2b1*	0.035274502
Ncam1	*Idh1*	0.048295233
Ncam1	*Marcks*	0.113164413
Mapk1	*Apoe*	0.167624973
Mapk1	*App*	0.113745577
Mapk1	*Atp1a2*	0.026303368
Mapk1	*Atp1a3*	0.098730636
Mapk1	*Clu*	0.078073437
Mapk1	*Cntn1*	0.041898992
Mapk1	*Cpe*	0.068998337
Mapk1	*Dpysl5*	0.059531361
Mapk1	*Gdi1*	0.113537128
Mapk1	*Gfap*	0.028094973
Mapk1	*Glul*	0.105455595
Mapk1	*Gpm6b*	0.225592848
Mapk1	*Gstm1*	0.097172087
Mapk1	*Hnrnpa2b1*	0.075816993
Mapk1	*Idh1*	0.02392482

Kpnb1	*Apoe*	0.122006401
Kpnb1	*App*	0.141689643
Kpnb1	*Atp1a2*	0.023233054
Kpnb1	*Atp1a3*	0.05299185
Kpnb1	*Clu*	0.042550775
Kpnb1	*Cpe*	0.12729824
Kpnb1	*Dpysl5*	0.044453798
Kpnb1	*Gdi1*	0.130216766
Kpnb1	*Gfap*	0.023605239
Kpnb1	*Glul*	0.076545994
Kpnb1	*Gpm6b*	0.164891426
Kpnb1	*Gstm1*	0.100161403
Kpnb1	*Hnrnpa2b1*	0.122980984
Kpnb1	*Idh1*	0.022435118
Kif2a	*Apoe*	0.147765025
Kif2a	*App*	0.068966817
Kif2a	*Atp1a2*	0.036721449
Kif2a	*Atp1a3*	0.062678775
Kif2a	*Clu*	0.054543276
Kif2a	*Cntn1*	0.032787543
Kif2a	*Cpe*	0.021682397
Kif2a	*Dpysl5*	0.048397161
Kif2a	*Gdi1*	0.057445933
Kif2a	*Glul*	0.039287582
Kif2a	*Gpm6b*	0.108216084

Kif2a	*Gstm1*	0.036977282
Kif2a	*Hnrnpa2b1*	0.033651093
Idh1	*Apoe*	0.192527365
Idh1	*App*	0.112223747
Idh1	*Atp1a2*	0.034854659
Idh1	*Atp1a3*	0.107127139
Idh1	*Cd200*	0.051922157
Idh1	*Clu*	0.06977202
Idh1	*Cntn1*	0.055891396
Idh1	*Cpe*	0.108040274
Idh1	*Crym*	0.021032179
Idh1	*Dpysl5*	0.080826818
Idh1	*Egfr*	0.04711472
Idh1	*Gdi1*	0.173827907
Idh1	*Glud1*	0.094948896
Idh1	*Glul*	0.185314073
Idh1	*Gpm6b*	0.316230216
Idh1	*Gstm1*	0.134979957
Idh1	*Hnrnpa2b1*	0.055528837
Hnrnpa2b1	*Apoe*	0.222672282
Hnrnpa2b1	*App*	0.211632031
Hnrnpa2b1	*Atp1a2*	0.061268882
Hnrnpa2b1	*Atp1a3*	0.089987641
Hnrnpa2b1	*Cd200*	0.027995338
Hnrnpa2b1	*Clu*	0.08716797

Hnrnpa2b1	*Cntn1*	0.049977491
Hnrnpa2b1	*Cpe*	0.133011871
Hnrnpa2b1	*Crym*	0.049297643
Hnrnpa2b1	*Dpysl5*	0.074417821
Hnrnpa2b1	*Eef2*	0.054654018
Hnrnpa2b1	*Egfr*	0.037579433
Hnrnpa2b1	*Gap43*	0.024192584
Hnrnpa2b1	*Gdi1*	0.15644209
Hnrnpa2b1	*Gfap*	0.136740774
Hnrnpa2b1	*Glud1*	0.040651449
Hnrnpa2b1	*Glul*	0.14559511
Hnrnpa2b1	*Gpm6b*	0.303210072
Hnrnpa2b1	*Gstm1*	0.166703663
Sqstm1	*Apoe*	0.051674771
Sqstm1	*App*	0.026264225
Sqstm1	*Atp1a3*	0.027144732
Sqstm1	*Clu*	0.029096645
Sqstm1	*Gpm6b*	0.053632184
Sqstm1	*Gstm1*	0.022223413
Sqstm1	*Marcks*	0.031420514
Sqstm1	*Rps14*	0.056188423
Sqstm1	*Rpl6*	0.056188423
Sqstm1	*Pdia3*	0.056188423
Sqstm1	*Nedd4*	0.056188423
Sqstm1	*Lars*	0.056188423

Sqstm1	*Hspa5*	0.056188423
Sqstm1	*Gstp1*	0.056188423
Sqstm1	*Gmps*	0.056188423
Sqstm1	*Eef2*	0.056188423
Sqstm1	*Eef1d*	0.056188423
Sqstm1	*Ddx6*	0.056188423
Sqstm1	*Calb1*	0.056188423
Sqstm1	*Atxn2*	0.056188423
Gstm1	*Apoe*	0.25171345
Gstm1	*App*	0.182269802
Gstm1	*Atp1a2*	0.1064691
Gstm1	*Atp1a3*	0.149926724
Gstm1	*Cadm1*	0.026760267
Gstm1	*Cd200*	0.080246938
Gstm1	*Clu*	0.167798031
Gstm1	*Cntn1*	0.113868994
Gstm1	*Cpe*	0.168296607
Gstm1	*Crym*	0.071210811
Gstm1	*Dpysl5*	0.126724727
Gstm1	*Eef1d*	0.028682998
Gstm1	*Eef2*	0.053541636
Gstm1	*Egfr*	0.077665522
Gstm1	*Gap43*	0.042283539
Gstm1	*Gdi1*	0.160897377
Gstm1	*Gfap*	0.135171842

Gstm1	*Glud1*	0.129544021
Gstm1	*Glul*	0.203096626
Gstm1	*Gpm6b*	0.408964589
Gpm6b	*Apoe*	0.398958619
Gpm6b	*App*	0.338152383
Gpm6b	*Atp1a2*	0.266898946
Gpm6b	*Atp1a3*	0.389427076
Gpm6b	*Cadm1*	0.076677009
Gpm6b	*Cd200*	0.20605245
Gpm6b	*Clu*	0.342121322
Gpm6b	*Cntn1*	0.337744374
Gpm6b	*Cpe*	0.369820573
Gpm6b	*Crmp1*	0.073273828
Gpm6b	*Crym*	0.215350666
Gpm6b	*Dpysl5*	0.368912966
Gpm6b	*Eef1d*	0.040351485
Gpm6b	*Eef2*	0.092684135
Gpm6b	*Egfr*	0.228433635
Gpm6b	*Ehd1*	0.021903082
Gpm6b	*Gap43*	0.116996792
Gpm6b	*Gdi1*	0.376092891
Gpm6b	*Gfap*	0.207308464
Gpm6b	*Glud1*	0.245243482
Gpm6b	*Glul*	0.43369134
Glul	*Apoe*	0.25679514

Glul	*App*	0.15005839
Glul	*Atp1a2*	0.113134427
Glul	*Atp1a3*	0.199003789
Glul	*Cadm1*	0.066359796
Glul	*Cd200*	0.174144014
Glul	*Clu*	0.151606581
Glul	*Cntn1*	0.204410301
Glul	*Cpe*	0.202220152
Glul	*Crmp1*	0.040077013
Glul	*Crym*	0.119891441
Glul	*Dpysl5*	0.191105039
Glul	*Eef2*	0.026759345
Glul	*Egfr*	0.145829248
Glul	*Gap43*	0.046741089
Glul	*Gdi1*	0.202900267
Glul	*Gfap*	0.105962502
Glul	*Glud1*	0.172740042
Glud1	*Apoe*	0.127260676
Glud1	*App*	0.074198137
Glud1	*Atp1a2*	0.02022562
Glud1	*Atp1a3*	0.078438672
Glud1	*Cd200*	0.043812209
Glud1	*Clu*	0.04645202
Glud1	*Cntn1*	0.042177311
Glud1	*Cpe*	0.081903636

Glud1	*Dpysl5*	0.047434333
Glud1	*Gdi1*	0.127132538
Gfap	*Apoe*	0.186124753
Gfap	*App*	0.196433175
Gfap	*Atp1a3*	0.055903849
Gfap	*Clu*	0.113334203
Gfap	*Cntn1*	0.023905193
Gfap	*Cpe*	0.072388554
Gfap	*Dpysl5*	0.04883831
Gfap	*Gdi1*	0.113249683
Gdi1	*Apoe*	0.263272135
Gdi1	*App*	0.160231486
Gdi1	*Atp1a2*	0.155981225
Gdi1	*Atp1a3*	0.152106539
Gdi1	*Cadm1*	0.035749854
Gdi1	*Cd200*	0.107789479
Gdi1	*Clu*	0.137339343
Gdi1	*Cntn1*	0.143957024
Gdi1	*Cpe*	0.170500144
Gdi1	*Crmp1*	0.060339755
Gdi1	*Crym*	0.101726017
Gdi1	*Dpysl5*	0.169773213
Gdi1	*Eef2*	0.045292924
Gdi1	*Egfr*	0.147774058
Gdi1	*Gap43*	0.064063624

Tnr	*Abca1*	0.104699219
Tnr	*Adam10*	0.091387708
Tnr	*Aldh2*	0.117489035
Tnr	*Apoe*	0.191843073
Tnr	*Asrgl1*	0.118578731
Tnr	*Atp1a2*	0.258291507
Tnr	*Atp1a3*	0.141458258
Tnr	*Atp1b2*	0.097089445
Tnr	*Atp6v0a1*	0.054344267
Tnr	*Cadm1*	0.123447106
Tnr	*Cat*	0.097562981
Tnr	*Clu*	0.037190472
Tnr	*Cnrip1*	0.070302957
Tnr	*Cntn1*	0.134846863
Tnr	*Cpe*	0.141279268
Tnr	*Crym*	0.129250787
Tnr	*Ctsd*	0.091500133
Tnr	*Dlg1*	0.031007152
Tnr	*Dnajc5*	0.044693739
Tnr	*Dpysl5*	0.083464081
Tnr	*Egfr*	0.126583965
Tnr	*Ehd1*	0.100866594
Tnr	*Ephb2*	0.100503007
Tnr	*Ephx1*	0.020034841
Tnr	*Fhl1*	0.056472524

Tnr	*Gdi1*	0.026873416
Tnr	*Gfap*	0.174894298
Tnr	*Glud1*	0.09065647
Tnr	*Glul*	0.22762677
Tnr	*Gnao1*	0.043582946
Tnr	*Gpc4*	0.092117179
Tnr	*Gpm6b*	0.040530031
Tnr	*Gria2*	0.033097739
Tnr	*Gstm1*	0.098625518
Tnr	*Hnrnpa2b1*	0.034922732
Tnr	*Hsd17b10*	0.039609926
Tnr	*Hspa12a*	0.14689686
Tnr	*Idh1*	0.090117058
Tnr	*Isoc1*	0.123611528
Tnr	*Kif2a*	0.069785359
Tnr	*Lancl2*	0.086355565
Tnr	*Lingo1*	0.113080087
Tnr	*Lrp1*	0.034449129
Tnr	*Lsamp*	0.083779859
Tnr	*Ly6h*	0.038221453
Tnr	*Mapk1*	0.102394167
Tnr	*Myo6*	0.116607187
Tnr	*Ncstn*	0.050160234
Tnr	*Negr1*	0.090365337
Tnr	*Nsf*	0.026033693

Tnr	*Olfm1*	0.092129687
Tnr	*Ptpra*	0.082884024
Tnr	*Pygb*	0.130720039
Tnr	*Rap2b*	0.128419978
Tnr	*Scarb2*	0.070542581
Tnr	*Scrn1*	0.08271873
Tnr	*Sirt2*	0.066658251
Tnr	*Slc1a2*	0.206135672
Tnr	*Slc32a1*	0.021884392
Tnr	*Slc44a1*	0.02564276
Tnr	*Slc6a11*	0.148563461
Tnr	*Syn1*	0.094610439
Tnr	*Syt1*	0.081100851
Gap43	*Apoe*	0.117799173
Gap43	*App*	0.040763891
Gap43	*Atp1a2*	0.067164326
Gap43	*Atp1a3*	0.108348856
Gap43	*Clu*	0.029291834
Gap43	*Cntn1*	0.043860495
Gap43	*Cpe*	0.022046754
Gap43	*Dpysl5*	0.039715512
Slc1a2	*Abca1*	0.188548877
Slc1a2	*Adam10*	0.141804606
Slc1a2	*Aldh2*	0.171548903
Slc1a2	*Apoe*	0.195937244

Slc1a2	*Asrgl1*	0.162210529
Slc1a2	*Atp1a2*	0.280262426
Slc1a2	*Atp1a3*	0.19595181
Slc1a2	*Atp1b2*	0.126771661
Slc1a2	*Atp6v0a1*	0.061101122
Slc1a2	*Cadm1*	0.169598609
Slc1a2	*Cat*	0.174679255
Slc1a2	*Clu*	0.06481365
Slc1a2	*Cnrip1*	0.140163158
Slc1a2	*Cntn1*	0.18884765
Slc1a2	*Cpe*	0.192711378
Slc1a2	*Crym*	0.211950487
Slc1a2	*Ctsd*	0.126779079
Slc1a2	*Dlg1*	0.083173325
Slc1a2	*Dnajc5*	0.079748196
Slc1a2	*Dpysl5*	0.122378322
Slc1a2	*Egfr*	0.189078637
Slc1a2	*Ehd1*	0.117144462
Slc1a2	*Ephb2*	0.17084636
Slc1a2	*Ephx1*	0.033317559
Slc1a2	*Fhl1*	0.116840172
Slc1a2	*Gdi1*	0.041435955
Slc1a2	*Gfap*	0.19857622
Slc1a2	*Glud1*	0.159171899
Slc1a2	*Glul*	0.261419538

Slc1a2	*Gnao1*	0.096054715
Slc1a2	*Gpc4*	0.125270476
Slc1a2	*Gpm6b*	0.062592809
Slc1a2	*Gria2*	0.049295504
Slc1a2	*Gstm1*	0.138943264
Slc1a2	*Hnrnpa2b1*	0.077983639
Slc1a2	*Hsd17b10*	0.032730333
Slc1a2	*Hspa12a*	0.162422906
Slc1a2	*Idh1*	0.135893776
Slc1a2	*Isoc1*	0.174098238
Slc1a2	*Kif2a*	0.072358671
Slc1a2	*Lancl2*	0.112107863
Slc1a2	*Lingo1*	0.112799117
Slc1a2	*Lrp1*	0.056951215
Slc1a2	*Lsamp*	0.131788601
Slc1a2	*Ly6h*	0.076611607
Slc1a2	*Mapk1*	0.114023865
Slc1a2	*Mcat*	0.030261862
Slc1a2	*Myo6*	0.192462489
Slc1a2	*Ncstn*	0.064732402
Slc1a2	*Negr1*	0.117225218
Slc1a2	*Nsf*	0.028866299
Slc1a2	*Olfm1*	0.134361718
Slc1a2	*Prdx6*	0.03490757
Slc1a2	*Ptpra*	0.089825094

Slc1a2	*Pygb*	0.182546526
Slc1a2	*Rap2b*	0.184576455
Slc1a2	*Scarb2*	0.093941779
Slc1a2	*Scrn1*	0.134809029
Slc1a2	*Sirt2*	0.119220179
Pygb	*Apoe*	0.24759205
Pygb	*App*	0.172192611
Pygb	*Atp1a2*	0.117080003
Pygb	*Atp1a3*	0.123489951
Pygb	*Cadm1*	0.023648666
Pygb	*Cd200*	0.074755574
Pygb	*Clu*	0.120003231
Pygb	*Cntn1*	0.108675091
Pygb	*Cpe*	0.162767732
Pygb	*Crmp1*	0.033512153
Pygb	*Crym*	0.072341788
Pygb	*Dpysl5*	0.137837681
Pygb	*Eef2*	0.044100506
Pygb	*Egfr*	0.107680029
Pygb	*Ehd1*	0.024707928
Pygb	*Gap43*	0.040531381
Pygb	*Gdi1*	0.197067207
Pygb	*Gfap*	0.101415894
Pygb	*Glud1*	0.086292823
Pygb	*Glul*	0.181007669

Pygb	*Gpm6b*	0.361217901
Pygb	*Gstm1*	0.157542054
Pygb	*Hnrnpa2b1*	0.144810059
Pygb	*Idh1*	0.141646453
Pygb	*Kif2a*	0.050545498
Pygb	*Kpnb1*	0.145816386
Pygb	*Mapk1*	0.113913765
Pygb	*Marcks*	0.137875048
Pygb	*Ncam1*	0.094556928
Pygb	*Prdx2*	0.172348919
Pygb	*Prdx6*	0.2207281
Prdx6	*Apoe*	0.254551448
Prdx6	*App*	0.1570516
Prdx6	*Atp1a2*	0.143904647
Prdx6	*Atp1a3*	0.212003809
Prdx6	*Cadm1*	0.06529251
Prdx6	*Cd200*	0.184457431
Prdx6	*Clu*	0.147216255
Prdx6	*Cntn1*	0.215516196
Prdx6	*Cpe*	0.220458814
Prdx6	*Crmp1*	0.044887816
Prdx6	*Crym*	0.104676473
Prdx6	*Dpysl5*	0.198157569
Prdx6	*Eef2*	0.030141915
Prdx6	*Egfr*	0.187258516

Prdx6	*Ehd1*	0.022346498
Prdx6	*Gap43*	0.060831379
Prdx6	*Gdi1*	0.226674833
Prdx6	*Gfap*	0.105058481
Prdx6	*Glud1*	0.160870032
Prdx6	*Glul*	0.245956695
Prdx6	*Gpm6b*	0.415190599
Prdx6	*Gstm1*	0.195103596
Prdx6	*Hnrnpa2b1*	0.158798212
Prdx6	*Idh1*	0.205400241
Prdx6	*Kif2a*	0.051404178
Prdx6	*Kpnb1*	0.118587346
Prdx6	*Mapk1*	0.135194991
Prdx6	*Marcks*	0.179666947
Prdx6	*Ncam1*	0.161319023
Prdx6	*Prdx2*	0.166899521
Marcks	*Apoe*	0.290594721
Marcks	*App*	0.154248916
Marcks	*Atp1a2*	0.184151194
Marcks	*Atp1a3*	0.160370815
Marcks	*Cadm1*	0.028313701
Marcks	*Cd200*	0.059188311
Marcks	*Clu*	0.144209279
Marcks	*Cntn1*	0.143935727
Marcks	*Cpe*	0.100858116

Marcks	*Crmp1*	0.059272977
Marcks	*Crym*	0.078680696
Marcks	*Ctsd*	0.020543977
Marcks	*Dpysl5*	0.133726993
Marcks	*Eef1d*	0.043225199
Marcks	*Eef2*	0.052779619
Marcks	*Egfr*	0.140083231
Marcks	*Gap43*	0.119806319
Marcks	*Gdi1*	0.16766803
Marcks	*Gfap*	0.092908674
Marcks	*Glud1*	0.068723023
Marcks	*Glul*	0.16168305
Marcks	*Gpm6b*	0.350131653
Marcks	*Gstm1*	0.151015031
Marcks	*Hnrnpa2b1*	0.117123095
Marcks	*Idh1*	0.108340974
Marcks	*Kif2a*	0.104742025
Marcks	*Kpnb1*	0.078572036
Marcks	*Mapk1*	0.098102164
Sirt2	*Marcks*	0.041601899
Sirt2	*Prdx6*	0.066429458
Sirt2	*Pygb*	0.027840419
Sirt2	*Apoe*	0.071326986
Sirt2	*App*	0.033354098
Sirt2	*Atp1a3*	0.053038879

Sirt2	*Clu*	0.02981546
Sirt2	*Cntn1*	0.026670444
Sirt2	*Cpe*	0.033881068
Sirt2	*Dpysl5*	0.027257069
Sirt2	*Gdi1*	0.041695909
Sirt2	*Glul*	0.105049614
Sirt2	*Gpm6b*	0.128628391
Sirt2	*Gstm1*	0.056366994
Sirt2	*Hnrnpa2b1*	0.023379289
Sirt2	*Abca1*	0.103559505
Sirt2	*Adam10*	0.041126854
Sirt2	*Aldh2*	0.086171388
Sirt2	*Apoe*	0.171531241
Sirt2	*Asrgl1*	0.099584887
Sirt2	*Atp1a2*	0.184963293
Sirt2	*Atp1a3*	0.099562181
Sirt2	*Atp6v0a1*	0.020063612
Sirt2	*Cadm1*	0.070208608
Sirt2	*Cnrip1*	0.022466628
Sirt2	*Cntn1*	0.062212052
Sirt2	*Cpe*	0.060734668
Sirt2	*Crym*	0.072069639
Sirt2	*Ctsd*	0.042682522
Sirt2	*Dlg1*	0.046814068
Sirt2	*Dnajc5*	0.04112233

Sirt2	*Egfr*	0.026588383
Sirt2	*Ehd1*	0.024734472
Sirt2	*Ephb2*	0.043698188
Sirt2	*Gfap*	0.120638174
Sirt2	*Glul*	0.126205581
Sirt2	*Gnao1*	0.047173606
Sirt2	*Gpc4*	0.036592577
Sirt2	*Gpm6b*	0.059228611
Sirt2	*Gstm1*	0.105826079
Sirt2	*Hspa12a*	0.021291821
Sirt2	*Idh1*	0.02992285
Sirt2	*Isoc1*	0.021117885
Sirt2	*Lancl2*	0.035382348
Sirt2	*Lrp1*	0.021694551
Sirt2	*Lsamp*	0.05252087
Sirt2	*Ly6h*	0.020273389
Sirt2	*Mapk1*	0.031004239
Sirt2	*Myo6*	0.07744051
Sirt2	*Negr1*	0.025169413
Sirt2	*Olfm1*	0.031100624
Sirt2	*Pygb*	0.091494992
Sirt2	*Rap2b*	0.035387856
Sirt2	*Scarb2*	0.042449369
Sirt2	*Scrn1*	0.07049247
Txnl1	*Lars*	0.056188423

Txnl1	*Hspa5*	0.056188423
Txnl1	*Eef2*	0.056188423
Rps6	*Rps14*	0.056188423
Rps6	*Rpl6*	0.056188423
Rps6	*Atxn2*	0.056188423

Other works:

1. **Kumar, R**., et. al., *FGF2 affects Parkinson's disease associated molecular networks through exosomal Rab8b/Rab31*. Front. Genet. 2020, doi: 10.3389/fgene.2020.572058 (accepted manuscript).
2. Pigoni, M., **Kumar, R.**, et. al., *Seizure protein 6 controls glycosylation and trafficking of kainate receptor subunits GluK2 and GluK3*. The EMBO Journal, 2020. 39(15): p. e103457.
3. Rudan Njavro, J., **Kumar, R.**, et. al., *Mouse brain proteomics establishes MDGA1 and CACHD1 as in vivo substrates of the Alzheimer protease BACE1*. The FASEB Journal, 2020. 34(2): p. 2465-2482.
4. Mayer, S., **Kumar, R.**, et. al., *Collybistin activation by GTP-TC10 enhances postsynaptic gephyrin clustering and hippocampal GABAergic neurotransmission*. Proceedings of the National Academy of Sciences, 2013. 110(51): p. 20795.
5. Hsia, H.-E., **Kumar, R.**, et. al., *Ubiquitin E3 ligase Nedd4-1 acts as a downstream target of PI3K/PTEN-mTORC1 signaling to promote neurite growth*. Proceedings of the National Academy of Sciences, 2014. 111(36): p. 13205.
6. Kurz, A$^{\Psi}$. & **Kumar, R**$^{\Psi}$., et. al., *miRNA sequencing from routine colonic biopsies reveals an enrichment of mucosal hsa-miRNA-486-5p in Parkinson's disease*. 2020. (Submitted).

ψ – shared first authorship.

Posters:

1. **Kumar, R.**, et al. *Weighted protein network analysis (WPCNA) decrypt Rab8b and Rab31 as key affiliates of exosomal secretion; extending their role in Parkinson's disease pathology seeding and spreading.* [version1; not peer reviewed].F1000Research 2019, 8(ISCB Comm J):2127 (poster) (https://doi.org/10.7490/f1000research.1117783.1).
2. **Kumar, R.**, G.U. Höglinger, and T. Koeglsperger, *Decoding Parkinson Disorder (PD) Pathophysiology: α-Synuclein over-expression enhances inward calcium influx and exosome release in LUHMES cells*. ScienceOpen Posters. (doi: 10.14293/S2199-1006.1.SOR-.PPYUSNN.v1).
3. **Kumar, R.**, et al., *Abundant -Synuclein expression triggers the release of exosomes and inward calcium influx in LUHMES cells.* Extracellular vesicles: From biology to biomedical application, Heidelberg, Germany.

Author information:

The author was born in a western-Himalayan village of Himachal (in English it would roughly translates to ‘snow-lap’) Pradesh, a Himalayan state in India. Author was a preeminent student during his school for twelve consecutive years and received state scholarship of merit, until 10th years of his school. After concluding the final year of the school in 2000, he jointly completed his Bachelor of Science in Biological Sciences (B.Sc.) (Zoology) with a special focus to chordate and non-chordate nervous systems from Punjab University Chandigarh and Himachal Pradesh University, Summerhill, Shimla. He continued to pursue a Master of Science (M.Sc.) degree in Biotechnology at Bangalore University, India in 2003-05. At Bangalore university author was among the top students of Biophysics department. The learning process took him to Auckland University of Technology (AUT), New Zealand (NZ) where he received another post-graduate qualification majoring in Molecular Genetics (Mol. Gen.). In later phase of studies at AUT, author had an opportunity to pursue a research project at Knowledge Engineering and Discovery Research Institute (KEDRI), AUT and at KEDRI author got exposed to the field of Computational-Neuroscience, where he worked on extraction of gene regulatory networks (GRN) using machine-learning tools and methods from a microarray-dataset collected from a long-term-potentiation (LTP)-induced hippocampal tissue. The authors work on GRN led him to be among the top five students in the course *Data Mining and Decision Support* by implementation of machine learning tools, that was offered as a part of the AUT curriculum. After GRN-project author started working on the computational-neurogenetic modelling of Huntington's disease using machine learning methods. Later, author spent contributing to the proposals of investigating the molecular mechanisms of synaptic-elimination in an inner-ear pertaining to establish Cochlea as a research model to study synaptic elimination process at Liggin’s Institute, University of Auckland (UoA). Later in 2012, author moved to Germany and joined Max Planck Institute for Experimental medicine (MPIEM) in Gottingen, Germany and contributed to the understanding of the molecular mechanisms of synaptic plasticity and investigated the roles of pre/post-synaptic proteins in different research models. After MPIEM author joined German Center for Neurodegenerative Diseases (DZNE) and Technical University of Munich (TUM) as a doctoral candidate and investigated the correlates of stimulus responsive exosome release and its implications to neurodegenerative diseases with a special emphasis to LBP. During the PhD, author was awarded a travel grant from European Society of Pharmacology in 2019 and one of his paper published in *Advanced Science* was acclaimed as the “Paper of the Month” by German Physiological Society. Author received Max Planck Scholarship for 2-years during 2012-14 and was considered for the Coursera financial assistance award for the course in “Light Emitting Diodes and Semiconductor Lasers”, 2020 by University of Colorado Boulder, USA. Apart from his academic accomplishments, at the age of 14-years author commanded a fleet of 120 junior-division cadets as a Sergeant in Norther-western-zone of National Cadet Corps, followed by a two-year social service under National Social Service scheme. Author is a state-level boxer and had won Bronze medal in the state level boxing championship held in Himachal Pradesh, India during 2003.